UPCONVERTING LUMINESCENT MATERIALS FOR SOLAR ENERGY CONVERSION

Minnea Tuomisto

TURUN YLIOPISTON JULKAISUJA – ANNALES UNIVERSITATIS TURKUENSIS
SARJA - SER. AI OSA - TOM. 621 | ASTRONOMICA - CHEMICA - PHYSICA - MATHEMATICA | TURKU 2019

TURUN YLIOPISTO

UPCONVERTING LUMINESCENT MATERIALS FOR SOLAR ENERGY CONVERSION

Minnea Tuomisto

TURUN YLIOPISTON JULKAISUJA – ANNALES UNIVERSITATIS TURKUENSIS
SARJA - SER. AI OSA - TOM. 621 | ASTRONOMICA - CHEMICA - PHYSICA - MATHEMATICA | TURKU 2019

University of Turku

Faculty of Science and Engineering
Department of Chemistry
Laboratory of Materials Chemistry and Chemical Analysis
University of Turku Graduate School
Doctoral Programme in Physical and Chemical Sciences

Supervised by

Adjunct Professor Mika Lastusaari
Department of Chemistry
Laboratory of Materials Chemistry and
Chemical Analysis
University of Turku
FI-20014 Turku, Finland

Reviewed by

Professor Graziella Malandrino
University of Catania
Department of Chemical Sciences
Catania, Italy

Docent Anatolijs Sarakovskis
University of Latvia
Institute of Solid State Physics
Riga, Latvia

Opponent

Associate Professor Sarah Mc Cormack
The University of Dublin
Trinity College Dublin
Department of Civil, Structural and Environmental Engineering
Dublin, Ireland

The originality of this thesis has been checked in accordance with the University of Turku quality assurance system using the Turnitin OriginalityCheck service.

ISBN 978-951-29-7877-9 (PRINT)
ISBN 978-951-29-7878-6 (PDF)
ISSN 0082-7002 (Painettu/Print)
ISSN 2343-3175 (Sähköinen/Online)
Punamusta Oy, Finland 2019

‘’Life would be tragic if it weren’t funny.’’

- Stephen Hawking

‘’What I love about science is that as you learn,
you don’t really get answers.
You just get better questions.’’

- John Green

ABSTRACT

UNIVERSITY OF TURKU
Faculty of Science and Engineering, Department of Chemistry, Laboratory of Materials Chemistry and Chemical Analysis

TUOMISTO, MINNEA: Upconverting luminescent materials for solar energy conversion
Doctoral thesis, 134 p.
December 2019

As attractive energy converters, solar cells are considered to play a vital role in covering the constantly increasing energy demands in the future. Despite the strong success in the field, a variety of solar cells including the commercially available ones are utilizing mainly the visible region of the solar spectrum, and thus are lacking the capacity to exploit effectively the infrared region. This issue gives a possibility to improve the solar cell efficiencies by using the unutilized energy of the infrared radiation. One solution to overcome this issue is to use upconverting luminescent materials which are capable of converting infrared radiation to visible by stacking photons. However, despite the potential, the rather weak conversion efficiency still limits the use of these materials. On the other hand, even small portions of this converted radiation would have significant effect on the solar cell efficiency which is why the development of these materials is desirable.

The main aims of this thesis work were to investigate and develop different fabrication methods and properties of the upconverting materials that could be used in solar cells. These methods included the co-precipitation method to prepare crystalline inorganic upconverting fluoride materials, the atomic and the molecular layer deposition techniques to fabricate upconverting oxide and hybrid thin films, and the direct particles doping method for preparation of upconverting luminescent glasses. In addition, another goal was to study the possibilities to enhance the upconversion luminescence which was done by adding transition metal ions (Cr^{3+} or Mn^{n+}) into the Yb^{3+} and Er^{3+} doped fluoride material. Improvement in the upconversion luminescence intensity was obtained by using Cr^{3+} ions.

Another enhancement possibility is to use efficient NIR absorbers together with a strong upconverting lanthanide ion. The combined ALD/MLD technique was shown to enable the combination of NIR harvesting organic moiety and upconverting lanthanide ions to form a hybrid thin film. The ALD and the combined ALD/MLD techniques were demonstrated to be well suitable for upconverting thin film fabrication. Moreover, the direct particles doping method was shown to offer a promising way to introduce a variety of crystalline luminescent materials into different glass matrices.

TIIVISTELMÄ

TURUN YLIOPISTO
Luonnontieteiden ja tekniikan tiedekunta, Kemian laitos, Materiaalikemian ja kemiallisen analyysin laboratorio

TUOMISTO, MINNEA: Käänteisvirritteiset luminoivat materiaalit aurinkoenergian hyödyntämisessä
Väitöskirja, 134 s.
Joulukuu 2019

Aurinkoenergian tarjoamia mahdollisuuksia pidetään yhtenä lupaavimmista vaihtoehdoista kasvavien energiatarpeiden täyttämisessä tulevaisuudessa. Aurinkokennot ovat kehittyneet paljon viime aikoina, mutta silti suurin osa tutkituista ja kaupallisesti saatavilla olevista aurinkokennoista pystyy hyödyntämään auringon spektristä vain näkyvän valon alueen jättäen infrapuna-alueen lähes kokonaan hyödyntämättä. Tämä ongelma tarjoaa mahdollisuuden parantaa aurinkokennojen tehokkuutta. Yksi tapa hyödyntää infrapunasäteilyn energiaa on käyttää käänteisvirritteisiä luminoivia materiaaleja, jotka pystyvät muuntamaan infrapunasäteilyä näkyväksi valoksi pinoamalla fotoneja. Tämän prosessin heikko teho rajoittaa toistaiseksi materiaalien käyttöä. Toisaalta, jopa pienellä IR-säteilyn muuntomäärällä on mahdollisuus vaikuttaa merkittävästi aurinkokennon tehokkuuteen, minkä vuoksi materiaalien kehittäminen on herättänyt kiinnostusta.

Väitöskirjatyön tavoitteena oli tutkia ja kehittää aurinkokennoissa mahdollisesti käytettävien käänteisvirritteisten materiaalien ominaisuuksia ja valmistusmenetelmiä. Menetelmiin kuului kerasaostusmenetelmä, jolla valmistettiin kiteisiä fluoridimateriaaleja; atomi- ja molekyylikerroskasvatusmenetelmät, joilla valmistettiin kiteisiä oksidi ja amorfisia hybridiohutkalvoja; sekä seostusmetelemä luminoivien lasien valmistukseen. Lisäksi tavoitteena oli tutkia mahdollisuuksia parantaa käänteisvirritteistä luminesenssia käyttämällä siirtymämetalli-ioneja (Cr^{3+} ja Mn^{n+}). Käänteisvirritteisen luminesenssin intensiteettiä kasvatettiin lisäämällä Cr^{3+} -ioneja fluoridimateriaaliin, joka oli seostettu Yb^{3+} ja Er^{3+} -ioneilla.

Käänteisvirritteisen luminesenssin tehostamisessa voidaan hyödyntää myös tehokkaasti NIR-säteilyä absorboivan orgaanisen osan yhdistämistä käänteisvirritteisesti luminoivaan lantanidi-ioniin. Näiden osien yhdistäminen todettiin olevan mahdollista yhdistetyllä ALD/MLD -tekniikalla, jolla valmistettiin hybridikalvoja. Tämän yhdistetyn tekniikan ja ALD-tekniikan osoitettiin olevan hyvin käyttökelpoisia käänteisvirritteisten kalvojen valmistuksessa. Lasimateriaaleilla tutkitun seostusmenetelmän osoitettiin olevan lupaava menetelmä erilaisten luminoivien kiteisten materiaalien lisäämisessä lasiin.

TABLE OF CONTENTS

Preface

Now that I am finishing the thesis work it is the time to thank all the people who have made it possible. One of the best aspects of working has definitely been the possibility to work with all the fantastic people. At this point, I have a lot of learned things and good memories to take with me to my future journey.

The PhD research was carried out in the Inorganic Materials Chemistry Group of the Department of Chemistry at the University of Turku. The work started with the Academy of Finland project NOMSEC (Novel Optical Materials for Solar Energy Conversion) and was continued with the financial support from the Fortum Foundation, the Magnus Ehrnrooth Foundation and the Finnish Cultural Foundation. All the financial support is gratefully acknowledged.

I wish to express my sincere gratitude for Professor Graziella Malandrino and Assoc. Prof. Anatolijs Šarakovskis for reviewing this thesis and for their valuable comments. I am very thankful for Associate Professor Sarah Mc Cormack for agreeing to be my opponent.

I am very grateful for my supervisor Adj. Prof. Mika Lastusaari for the guidance and sharing of knowledge. I am grateful for the opportunity to work on interesting topics and your efforts to make all the co-operation possible.

I wish to express my deep gratitude for my research director Professor Carita Kvarnström for all the support, guidance and encouragement you have given me during these years.

I also want to thank Dr. Pia Damlin and Dr. Mikko Salomäki for your guidance and nice discussions. In addition, all the students who have participated in the perovskite research, especially Esa-Pekka Mattila, Bo Peng and Eerik Salonen earn thanks.

This thesis work would not been the same without all the collaboration. I wish to thank Professor Maarit Karppinen and Dr. Zivile Giedraityte from Aalto University for your valuable contribution and sharing of knowledge on atomic and molecular layer deposition techniques.

I wish to thank all the collaborators in Tampere Technical University, especially Assistant Professor Laeticia Petit and Nirajan Ojha for introducing me to the glass materials and for your valuable contribution. The time I spent in your laboratory was very interesting and I liked working with you.

In addition to the mentioned collaborators, I would like to thank all the other co-authors: Dr. Emilia Palo, Dr. Tero Laihinen, Dr. Iko Hyppänen, Professor Hendrik Swart, Professor Jorma Hölsä, Hoang Nguyen, Jaakko Oksa, and Dr. Turkka Salminen. Your contribution has been vital to the publications. I also wish to thank Professor Tero Soukka.

At the Laboratory of Materials Chemistry and Chemical Analysis we have had an excellent working atmosphere. This is all thanks to the wonderful current and former staff and students and their effort to lift the spirit. I wish to thank Dr. Ari Lehtonen, Dr. Antti Viinikanoja, Dr. Iko Hyppänen, Dr. Hellen Santos, Dr. Milla Suominen, Dr. Leena Mattsson, Esko Salojärvi, Pasi Salonen, Rahul Yewale, Lauri Marttila, Sachin Kochrekar, Ville Eskonen, Sami Vuori and all the others for nice discussions and good humor. I also wish to thank the visiting researchers Dr. Liana Namakura and Dr. Jose Carvalho.

Kari Loikas and Mauri Nauma earn special thanks for the technical support during my thesis work. The Laboratory would not have been functional without Kirsi Laaksonen who also earns special thanks. I wish to thank Kaisa Ketomäki and Hanna-Leena Partanen for administrative support.

I would like to extend my warm thanks to Dr. Emilia Palo and Dr. Isabella Norrbo with whom I have had a pleasure to share an office during my thesis work. I have really enjoyed our time together at and outside the office and during the conference trips. All the support you have given me have been essential for the thesis work. It has been wonderful to share the journey with you.

As much as I enjoyed working with this thesis, it would not have been possible without the good balance in life. For this, I want to thank my family and friends. I begin to thank my friends I got during the university time: Hanna-Mari, Marica, Jasmin, Olli and Tero. You all have been there since the early states of my chemistry studies and without your support I would not have reached this point. We have had a lot of great time together and I hope we will also have in the future!

Among the friends outside the academic world, first of all, I want to thank Pihla, Emmi, Miia, Janita and Emilia for sharing many good memories with me during all the years we have known each other. We all have had a lot of fun together. I wish to have more time to spend with you in the future!

My friend whom I have known for the longest time, Susanna, you are like a sister to me. Thank you for your support and good company. The trips I made with you and your daughter, Vanessa, have been important breaks and they brought me a lot of good energy that helped me during the thesis work. I hope we are heading for a new trip soon!

Finally, I would have not reached this point without the love and support of my family. Suunnaton kiitos äidilleni Merville ja isälleni Raimolle kaikesta siitä tuesta ja kannustuksesta, jota olen saanut päästäkseni tähän pisteeseen. Suuret kiitokset myös veljelleni Mikalle. Haluan kiittää myös kaikkia niitä sukulaisia, jotka ovat osoittaneet tukea ja kannustusta opiskelulleni ja väitöskirjaprojektilleni.

Turku 17.10.2019
Minnea Tuomisto

LIST OF ORIGINAL PUBLICATIONS

This thesis is based on the following original publications and supplementary unpublished results, referred to in the text by the Roman numerals.

I Tuomisto, M., Palo, E., Laihinen, T., Hyppänen, I., Lastusaari, M., Swart, H.C., Hölsä, J., Effect of Mn and Cr doping on the up-conversion luminescence from $NaYF_4:Yb^{3+},Er^{3+}$, *Opt. Mater*. **59** (2016) 115–119.

II Tuomisto, M., Giedraityte, Z., Karppinen, M., Lastusaari, M., Photon up-converting $(Yb,Er)_2O_3$ thin films by Atomic Layer Deposition, *Phys. Status Solidi-R* **11** (2017) e201700076.

III Giedraityte, Z., Tuomisto, M., Lastusaari, M., Karppinen, M., Three- and two-photon NIR-to-vis Yb,Er up-conversion from ALD/MLD deposited molecular hybrid thin films, *ACS Appl. Mater. Inter.* **10** (2018) 8845–8852. https://pubs.acs.org/doi/10.1021/acsami.7b19303

IV Nguyen, H., Tuomisto, M., Oksa, J., Salminen, T., Lastusaari, M., Petit, L., Upconversion in low rare-earth concentrated phosphate glasses using direct $NaYF_4:Er^{3+}$, Yb^{3+} nanoparticles doping, *Scripta Materialia* **139** (2017) 130–133.

V Ojha, N., Tuomisto, M., Lastusaari, M., Petit, L., Upconversion from fluorophosphate glasses prepared with $NaYF_4:Er^{3+},Yb^{3+}$ nanocrystals, *RSC Adv.* **8** (2018) 19226.

Article **III** was first included in the PhD thesis: Zivile Giedraityte, Novel Inorganic–Organic Luminescent Materials by Atomic/Molecular Layer Deposition, 2018, Aalto University

LIST OF OTHER RELATED PUBLICATIONS

Ojha, N., **Tuomisto, M**., Lastusaari, M., Petit, L., Phosphate glasses with blue persistent luminescence prepared using the direct doping method, *Opt. Mater.* **87** (2019) 151–156.

Tuomisto, M., Giedraityte, Z., Mai, L., Devi, A., Boiko, V., Grzeszkiewicz, K., Hreniak, D., Karppinen, M., Lastusaari, M., Up-converting ALD/MLD thin films with Yb^{3+}, Er^{3+} in amorphous organic framework, *J. Lumin.* **213** (2019) 310–315.

ABBREVIATIONS AND SYMBOLS

A	activator
AFM	atomic force microscopy
ALD	atomic layer deposition
ALE	atomic layer epitaxy
APTE	addition de photons par transfers d'energie
a-Si	amorphous silicon
BBV	beam-bending viscometer
BTC	1,3,5-benzenedicarboxylic acid
CTAB	cetyltrimethylammonium bromide
c-Si	crystalline silicon
CSU	co-operative sensitization
CVD	chemical vapor deposition
DMF	N,N-dimethylformamide
DSSC	dye-sensitized solar cell
EDTA	Na_2-ethylenediaminetetraacetic acid
EMU	energy migration-mediated upconversion
EQE	external quantum efficiency
EQE_{UC}	external quantum efficiency due to upconversion
ETU	energy transfer upconversion
ESA	exited state absorption
ESR	electron spin-resonance spectroscopy
FRET	Förster resonance energy transfer
FTIR	Fourier transform infrared spectroscopy
GC	glass ceramic
GIXRD	grazing incident X-ray diffraction
GPC	growth-per-cycle
GSA	ground state absorption
IR	infrared radiation
L	ligand
MLD	molecular layer deposition
MOF	metal organic frameworks
NDC	1,4-naphthalenedicarboxylic acid
NIR	near infrared radiation
PA	photon avalanche
R	rare earth
RET	resonance energy transfer
SEM	scanning electron microscopy
S	sensitizer

SPR	surface plasmon resonance
TEM	transmission electron microscopy
thd	2,2,6,6-tetramethyl-3,5-heptanedione
TTA	triplet-triplet annihilation
UC	upconversion luminescence
UCQY	quantum yield of upconversion luminescence
VDP	vapor deposition polymerization
XPD	X-ray powder diffraction
XPS	X-ray photoelectron spectroscopy
XRF	X-ray fluorescence spectroscopy
XRR	X-ray reflectivity

1. INTRODUCTION

The conventional fluorescence involves one high-energy excitation photon to produce one emitted photon with lower energy. Therefore, it differs from the upconversion luminescence (UC) in which two or more low-energy photons are absorbed and subsequently one high-energy photon is emitted (Fig. 1). The UC is often described as a photon stacking process. This unique luminescence property of UC materials enables the utilization of infrared radiation (IR) energy in solar cells which are currently incapable of exploiting effectively this region of the solar spectrum (Fig. 1).[1–3]

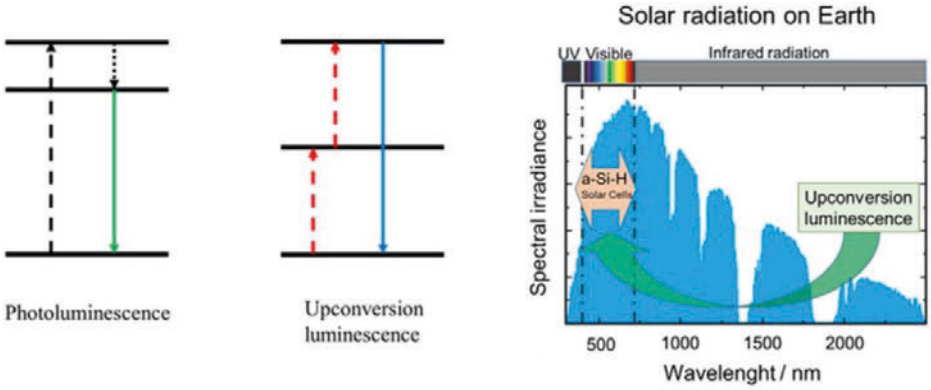

Fig. 1. Schematic representation of the conventional photoluminescence and the upconversion luminescence processes (left) and the solar radiation on Earth (right).

The use of UC materials in solar cells was first reported in 1996 when a vitroceramic material doped with lanthanide ions capable of the UC process was incorporated into a GaAs solar cell.[4] The following research has focused on a variety of different solar cells including organic solar cells, perovskite and dye sensitized solar cells (DSSC), amorphous silicon (a-Si) solar cells, and crystalline silicon (c-Si) solar cells that represents the majority of commercially available solar cells. The type of the solar cell sets limits to the UC materials which can be designed to absorb in a different radiation region.

The materials capable of generating upconversion luminescence are mainly divided into two groups. First are the materials that consists of inorganic host doped with lanthanide ions or transition metals that work as an emitter of the UC, and second

are the organic chromophores capable of showing triplet-triplet annihilation (TTA)-based upconversion. In addition, it is possible to combine different materials into hybrid materials in which organic molecules harvest excitation radiation and transfer the absorbed energy to the upconverting ion. The basic requirement for the upconversion luminescence is the existence of the intermediate energy states with relatively long lifetimes. The lanthanide ion based upconversion rely on the abundant 4f electronic energy levels while the TTA- upconversion is based on the triplet states of the chromophore molecules.[1,2,5] Nevertheless, this thesis work discusses only the lanthanide ion based upconversion luminescence.

The UC materials can be introduced into the solar cells in several ways. For example, the inorganic crystalline materials can be doped into a glass layer or they can be synthetized as powders that are subsequently attached on a surface to form a film. The UC material may also be prepared directly as a film, for instance, by using vapor deposition techniques. In this thesis work, one of the aims has been to study different fabrication methods for UC layers. The selected methods were the atomic layer deposition and the combined atomic and molecular layer deposition techniques, as well as the direct particles doping method for preparation of luminescent glasses.

One of the major reasons why UC materials have not reached success in the commercial solar cell field is the challenge with the low efficiency of the UC process. In the literature, a variety of enhancement possibilities have been suggested including the manipulation of the crystal lattice and combination of a strong lanthanide upconverter with an effective IR absorber molecule. Another aim of this thesis work has been to investigate the possibilities to enhance the upconversion luminescence. The main results of this thesis research will be shown at the experimental part, but first the literature review will give an introduction to the upconversion luminescence and the enhancement possibilities, as well as to the materials that have been essential in this research.

2. LITERATURE REVIEW

2.1. Upconverting crystalline materials

2.1.1. Composition and electronic energy scheme

The UC-materials generally contain inorganic host and dopant ions which are usually trivalent lanthanide ions (e.g. Er^{3+}, Tm^{3+}, Ho^{3+} and Tb^{3+}) but some transition metals (e.g. Cr^{3+}, Ni^{2+} and Mo^{3+}) have additionally showed upconversion luminescence. A single ion or multiple ions can be used as dopants. For example, when two ions are used, one of them will work as an activator (emitter) and the other as a sensitizer (absorber). The upconversion luminescence can be enhanced by selecting a sensitizer with a large absorption cross-section. The studied host materials have mainly been halides such as fluorides, bromides, chlorides and iodides. In addition, oxides, vanadates and phosphates have been studied. The ideal properties for a crystalline host material are chemical and thermal stability, optical transparency, high tolerance for luminescence centers and low phonon energy. When compared to the molecular hosts, inorganic hosts such as glasses and crystals have less effective non-radiative deactivation routes for excited lanthanide ions.[1,6,7]

The effect of the host lattice on the upconversion luminescence efficiency is often described by the phonon dynamics and the local crystal field. These should be taken under consideration when selecting the host in particular for nanomaterials. The main loss mechanism for UC emissions is the phonon-induced non-radiative process which involves the multiphonon-assisted relaxations. During these relaxations, the energy difference between the higher energy level and the lower energy level is converted non-radiatively to the lattice phonons. The number of phonons needed for this process can be indicated by the cutoff phonon energy of the host lattice. In general, the phonon energy of the host lattice should be low enough to ensure the efficient UC emissions. The optical properties of the upconverting lanthanide ion are influenced by the local crystal symmetry surrounding the ion. Generally, a less symmetric crystal phase favors a strong UC. For instance, monoclinic ZrO_2 nanoparticles show stronger upconversion emissions than the tetragonal phase nanoparticles.[6,8]

One of the best host materials for upconversion has been the rare earth fluoride $NaYF_4$ which has a hexagonal (β) and a cubic (α) phase structure. When the material is heated, the cubic phase will first transform to the hexagonal and further back to

the cubic while the phase transformations are irreversible.[9] In general, the cubic phase is indicated as a low-temperature or a high temperature cubic. In both cubic and hexagonal phase, Na^+ and Y^{3+} are statistically distributed over the same lattice site with space groups Fm-3m and $P6_3/m$, respectively.[10] The cubic $NaYF_4$ phase has a fluorite type (CaF_2) structure in which the symmetry of the cation site occupied with Na^+, Y^{3+} or Ln ions is O_h for the high-temperature structure and C_{3v} for the low-temperature structure. In the hexagonal $NaYF_4$ lattice, the symmetry of the Na site is C_{3h} and the symmetry of Na/Y/Ln –site is C_3.[11] The hexagonal $NaYF_4$ phase, especially doped with Yb^{3+}-Er^{3+} ion-pair, produces strong upconversion luminescence when compared to the cubic form.[12,13] As known, the cubic phase of $NaYF_4$ is about an order of magnitude less efficient than the corresponding hexagonal phase.[14] The strong UC of the hexagonal phase is explained by the low phonon energy of the $NaYF_4$ lattice and the symmetry differences between the two phases.[15,16]

In addition to the fluoride hosts, the rare earth oxides are well studied due to their good chemical stability. Y_2O_3 have three different structures: hexagonal, monoclinic and cubic.[17] The cubic Y_2O_3 has coordination number 6 and it contains two non-equivalent yttrium S_6 and C_2 symmetry sites.[18,19] Moreover, ZrO_2 host doped with Er or Yb-Er have shown upconversion.[20] Some examples of another studied hosts are $CaMoO_4$ co-doped with Er^{3+}/Yb^{3+},[21] Gd_2O_2S:10%Er^{3+},[22] and other M_2O_2S:Er (M=Y, Gd, La)[23].

The upconversion luminescence requires existence of multiple metastable energy levels which makes lanthanides ideal for this purpose. Trivalent lanthanide ions with partly filled 4f-orbitals have electronic energy states that enable the excitation of the material and finally the luminescent emission. Each lanthanide ion has unique electronic configuration (Fig. 2). The 4f-electrons are well shielded by the outer complete 5s and 5p shells which minimize the impact of the surrounding environment. Therefore, the 4f electrons do not take part in chemical bonding which makes the chemical properties of lanthanides very similar. This also makes the separation of the ions very difficult.[5,7,16]

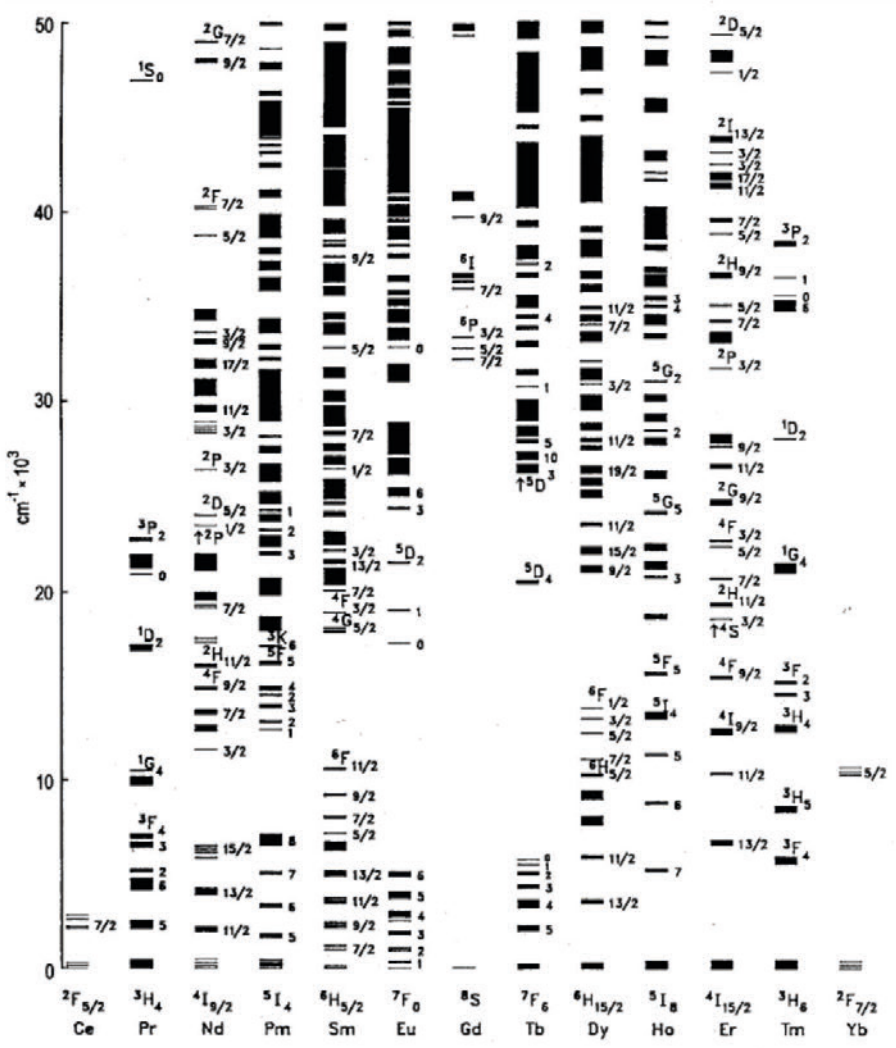

Fig. 2. Energy levels scheme of lanthanides (Dieke diagram).[5,24,25]

The luminescence of lanthanides originates from the electronic transitions between 4f levels that are formed due to several interactions within the ion (Fig.3). The largest interaction is the Coulombic interaction which represents the electron-electron repulsion within the 4f orbitals. This interaction induces terms which are further split into several J-levels by spin-orbit coupling. These free ion levels are indicated by Russel-Saunders notation of $^{2S+1}L_J$, where 2S+1 represents the total spin multiplicity, L the total orbital angular momentum and J the total angular momentum of the f electrons. The f-f transitions are parity forbidden according to the Laporte rule but

become partly allowed when lanthanides are placed in a coordinating environment such as an inorganic crystal or an organic ligand. This is due to the crystal field splitting, which causes the further splitting of the electronic energy levels.[5,7,16,26]

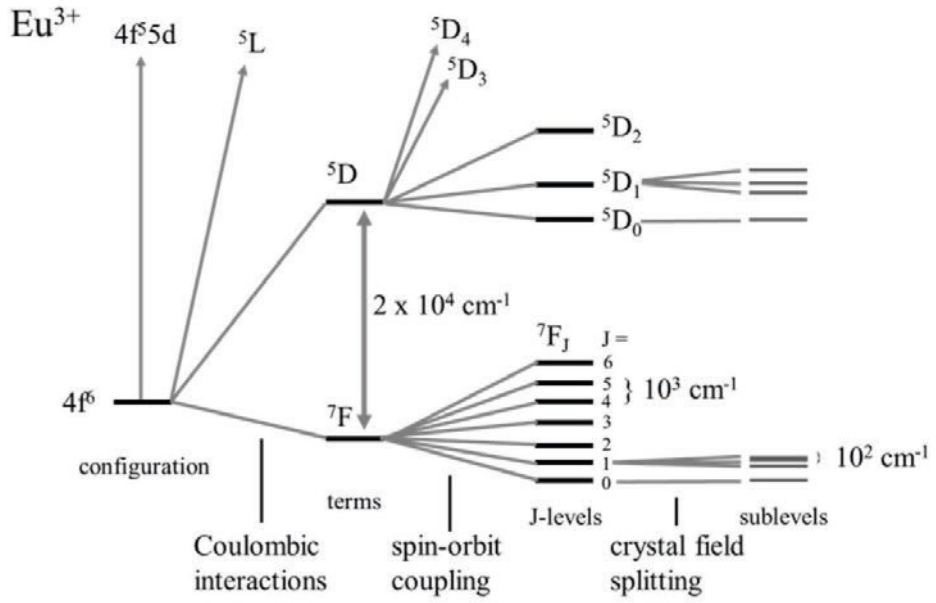

Fig. 3. The interactions inducing the formation of the different electronic energy levels of Eu^{3+} with [Xe] $4f^6$ $5d^0$ configuration. Based on a figure by Werts.[7]

The activators capable of generating useful upconversion luminescence emissions have equally spaced intermediate states in which the spacing is large enough to reduce the probability of non-radiative multiphonon relaxations. Such latter-like arrangement of the energy levels appears with Er^{3+}, Tm^{3+}, and Ho^{3+}, which are frequently used as activators. In addition, all trivalent lanthanides, excluding La^{3+} ($4f^0$), Ce^{3+} ($4f^1$) and Lu^{3+} ($4f^{14}$), are able to show upconversion luminescence. However, most of the ions will produce rather low UC-efficiency.[16,26,27]

The materials doped only with an activator have two major parameters that effect to the UC-efficiency. First, the distance between two neighboring activator ions, and second, the absorption cross-section of the ions. The distance between the ions becomes shorter when higher doping levels are used, which can lead to increasing cross-relaxation processes and quenching of the excitation energy. The activator concentration has an upper limit which depends on the host but in most upconversion materials the limit is 3 mol-% for Er^{3+} and 0.5 for Tm^{3+}.[28] The absorption cross-

sections of most lanthanide activator ions are quite low which makes the UC-efficiencies of singly doped materials relatively low.[16,26,27]

To enhance the UC, it is possible to use an activator-sensitizer ion-pair in which the sensitizer with a large absorption cross-section will effectively absorb the excitation radiation. One frequently used sensitizer is the trivalent Yb that possesses only one exited 4f level of $^2F_{5/2}$. The absorption cross-section of Yb^{3+} at 980 nm is relatively large and the $^2F_{7/2} \rightarrow {}^2F_{5/2}$ transition of Yb^{3+} matches well with the f-f transitions of the commonly used upconverting ions. The sensitizer concentration is typically kept high (around 20 mol-%) in doubly or triply doped materials.[16,27]

2.1.2. Upconversion mechanisms

The upconversion emissions can result from various energy transfer processes that may occur among the abundant energy levels of trivalent lanthanide ions. The basic energy transfer processes between two ions are the resonant radiative energy transfer, resonant nonradiative energy transfer, phonon-assisted nonradiative energy transfer and the cross-relaxation (Fig. 4). Moreover, the mechanisms generating the upconversion emissions are generally divided up into five classes (Fig. 5). The most straightforward mechanism is the ground state absorption (GSA) followed by exited state absorption (ESA). Other main mechanisms are energy transfer upconversion (ETU), co-operative sensitization upconversion (CSU), photon avalanche (PA) and energy migration-mediated upconversion (EMU).[1,16,27]

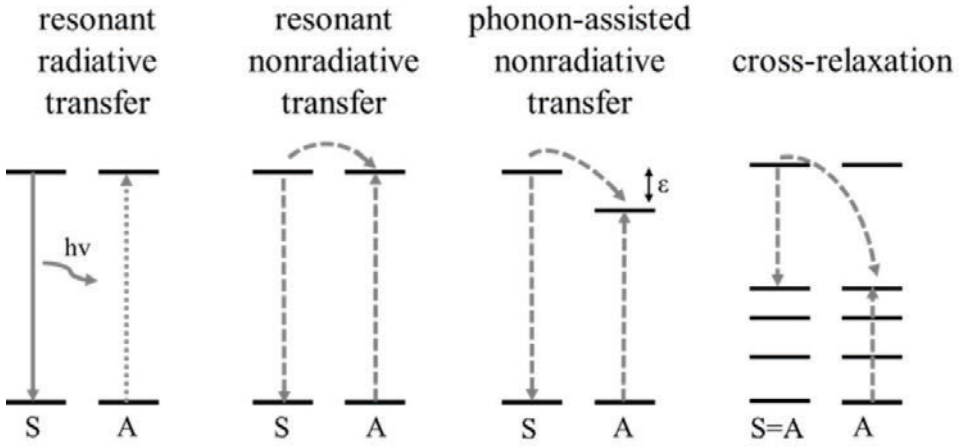

Fig. 4. Schematic representation of the basic energy transfer processes between two ions. In the scheme, ε is the energy mismatch. Based on a figure by Auzel.[1]

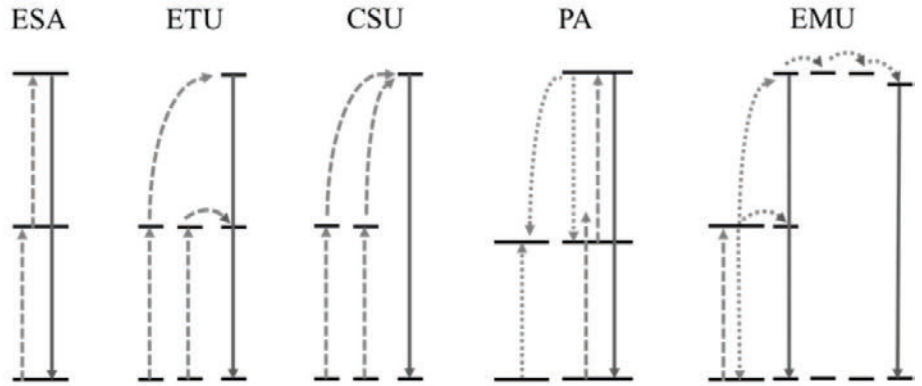

Fig. 5. Schematic principles of the general upconversion processes including exited state absorption (ESA), energy transfer upconversion (ETU), co-operative sensitization upconversion (CSU), photon avalanche (PA) and energy migration-mediated upconversion (EMU).

In exited-state absorption, a single ion absorbs two (or more) pump photons by utilizing a ladder-like structure of energy levels (Fig. 5). The sequential absorption by the single ion requires multiple energy levels with intermediate levels that are stable enough for adequate electron populations. The excited state of the ion may relax back to ground state and generate upconversion emission.[1,16,27]

Energy transfer upconversion, also called as APTE (addition de photon par transferts d'énergie), is the most efficient energy transfer mechanism for upconversion. ETU mechanism is similar to ESA, both processes need absorption of two or more photons, but ETU involves neighboring ions instead of a single ion (Fig.5). The neighboring ions are called a sensitizer and an activator. In the process, each sensitizer ion is excited from the ground state to the metastable state. Subsequently, the sensitizer ions transfer the absorbed energy to the activator that is exited stepwise starting from the ground state and ending to the energy state with higher energy than the excitation energy. Finally, the excited state of the activator may relax to the ground state by resulting in upconversion emission.[1,16,27]

Co-operative sensitization is for the Ln^{3+} ions without the metastable states capable of working as an energy storage reservoir. For instance, the ion can be Tb^{3+} or Eu^{3+}. Otherwise this mechanism has similar principle than the ETU mechanism, both involve neighbor ions, but in the co-operative sensitization mechanism the two sensitizers transfer their excited state energy simultaneously to the activator (Fig. 5). This enables the excitation of the activator to the energy state which corresponds to

the energy of two excitation photons. The excited state of the activator may relax to the ground state with upconversion emission.[1,16,27]

Photon avalanche effect was first discovered by Chivian et al. (1979) in Pr^{3+} doped $LaCl_3$ and $LaBr_3$. In this process, the excitation energy does not match the energy gap between the intermediate and ground state of the ion, and thus higher pump intensity is required (Fig. 5). The process starts with ground state absorption which results in population of the intermediate state. This is followed by excited state absorption which populates the higher-lying emitting state. A cross-relaxation occurs between the ion in the exited state and the neighboring ion in the ground state leading to situation in which both ions are at the intermediate state. The repetition of this cycle results in increased population of the intermediate state and luminescent state which finally enables the PA upconversion emission. Nevertheless, PA has limitations such as the high pump power threshold and delayed emission response.[1,16,27]

In the energy migration-mediated upconversion process, four types of ions are embedded in the different layers of the UC-material: sensitizers, accumulators, migrators and activators (Fig. 5). The sensitizer absorbs the excitation energy and transfers it to the accumulator by ETU mechanism. This populates the higher excited energy level of the accumulator which transfers the energy to the migrator. The energy might migrate between migrators until it is finally trapped by the activator resulting in upconversion luminescence.[27]

2.1.3. Lifetime

The rare earth ions possess the unique energy level schemes with the necessary intermediate states for the upconversion luminescence. These intermediate states need also sufficiently long lifetimes to ensure the high population of the excited energy states. The lifetime of an excited state is based on the rates of both radiative and nonradiative depopulation processes. The radiative rate is particularly dependent on the electronic structure of the lanthanide ion. Thus, the importance of the coordination geometry and the chemical nature of the coordination is considered to be minor.[29]

Unlike the radiative rate, the rate of the nonradiative depopulation is dependent on the energies of the participating phonon modes, and an energy gap law for the multiphonon-relaxation rate constant, w_0, has been defined as (Equation 1)[29]

$$w_0 = \beta e^{-\alpha p} \quad (1)$$

where α and β are parameters characteristic of the host material, $p = \Delta E/\hbar\omega$ is the number of phonons that are needed for filling the energy gap ΔE while each phonon has the energy ħω. The multiphonon relaxation in lanthanides is dominant when $p<5$. Phonon energies of oxides and fluorides are at the highest ~600 cm^{-1} and ~400 cm^{-1}, respectively.[29,30] In the case of Er^{3+} ion, the energy gap between the red upconversion emission level ($^4F_{9/2}$) and the nearest lower lying energy level ($^4I_{9/2}$) is ~2650 cm^{-1} which means that over 6 fluoride and over 4 oxide phonons are needed for filling the energy gap. As follows the radiative rate is dominant with fluorides, whereas with oxides, the multiphonon relaxation is competitive.

The lifetimes of lanthanide-based materials show size dependency in such a way that upconverting nanoparticles exhibit shorter lifetimes than larger crystals. The lifetimes of different emissions may also vary. For example, in Er^{3+} nanomaterials, the red emission lifetime is usually longer than the green emission lifetime. The size dependency has been suggested to be due to the presence of quenchers enhancing the non-radiative relaxation processes. These quenchers present in a solvent or on a surface of a nanoparticle may be molecular vibrations, such as C–H, N–H and O–H.[7,31–33]

2.1.4. Power dependence

The intensity of upconversion luminescence is dependent on the pump excitation power density and it follows the Equation 2[34,35]

$$I \propto P_{exc}^{n} \tag{2}$$

where I is the intensity of the upconversion luminescence, P_{exc} is the pump excitation power and n is the number of photons needed for the upconversion process. The number of the photons can be determined from the plot of the luminescence intensity versus the pump power in double-logarithmic representation where the slope indicates n.[34,35] This dependency applies with material systems without sensitizer, and with activator-sensitizer systems when low excitation power is used.[35] Saturation occurs with high excitation power densities and the slope of the curve becomes one.[35]

2.1.5. Quantum yield

The quantum yield of upconversion luminescence (UCQY) describes the efficiency of the upconversion process. The UCQY is strongly dependent on the excitation power density due to the nonlinear nature of the UC-process.[36] Two different methods have been used to measure the UCQY. First, the internal method defines the ratio of upconverted to absorbed photons (Equation 3)[8]

$$internal\ UCQY = \frac{photons\ emitted}{photons\ absorbed} \propto \frac{emitted\ UC\ intensity}{absorbed\ excitation\ light} = \frac{I_{UC}}{\varepsilon P} \quad (3)$$

where ε is the absorption coefficient and P is the excitation power. The maximum internal UCQY is at 100/n % for n-photon UC-process where at least two photons are needed for upconversion.

The second method, the external method, defines the number of upconverted photons to certain amount of incident photons (Equation 4)[37]

$$external\ UCQY = \frac{upconverted\ photons}{incident\ photons} \quad (4)$$

This method has been used when upconversion is studied for solar applications due to the more relevant information about the actual performance of a solar device and not about the internal processes of the device.[38] It should be noticed that the internal UCQY is always higher than the external UCQY. For example, β-$NaYF_4$: 25% Er^{3+} has showed external (internal) UCQY of 8.6 % (12.0%) at irradiances of 4020 W/m^2, and the external (internal) UCQY for Gd_2O_2S: 10% Er^{3+} has been 8.5 % (15.1 %) at 4070 W/m^2.[37] In addition, the used excitation bandwidth has an effect to the quantum yield. Broadband excitation has enabled as high upconversion photoluminescence quantum yield as 16.2 ± 0.5% at 2270 ± 100 mW mm^{-2} for β-$NaYF_4$: 10% Er^{3+}.[39] The previous quantum yield values have been measured with microcrystalline materials. When the particle size decreases to nanosized the UCQY drops enormously: even dropping about 95 % for internal UCQY have been detected for $NaYF_4$:Yb^{3+},Er^{3+} when particle size has decreased from 30 to 10 nm.[36] The maximum UCQY for nanomaterials have been only about a few percent.[4]

2.1.6. Enhancing the properties of upconverting materials

Use of additional metal ions

One possibility to tailor the upconversion luminescence properties is to use additional metal ion such as alkali metals or transition metals that may act as a sensitizer in the system.[40] These metal ions may also be able to affect the local crystal field of the activator ion.[41] Changes in the crystal field will also change the distances of the dopant ions which will effect to the transition probabilities of the upconversion process. Another possibility is to use noble metals that may generate the plasmon coupling effect to enhance the upconversion luminescence.[42,43] For crystalline materials, doping can stabilize a specific crystallographic phase which may affect to the upconversion luminescence efficiency. For instance, doping $NaYF_4$ host with metal ion that is larger in size than Y^{3+} will favor the hexagonal phase instead of the

cubic phase.[44] Some ionic radii of ions that have been studied for tuning the upconversion luminescence are listed in table 1.

Table 1. Ionic radii of transition metal ions studied for upconversion luminescence enhancement. Collected from table by Shannon.[45]

ion	radii/Å	ion	radii/Å	ion	radii/Å	ion	radii/Å	ion	radii/Å
Bi^{3+}	0.96-1.17	K^{+}	1.37-1.64	Ni^{2+}	0.55-0.690	Sr^{2+}	1.18-1.44	Zn^{2+}	0.60-0.740
Ca^{2+}	1.00-1.34	Li^{+}	0.590-0.92	Sc^{3+}	0.745-0.870	Ti^{4+}	0.42-0.74		
Cr^{3+}	0.615	Mn^{2+}	0.66-0.96	Sn^{4+}	0.55-0.81	Y^{3+}	0.900-1.075		

Alkali and alkaline earth metals

Li^{+} ion has been used to tailor the crystal field of the activator ion Er^{3+} in Y_2O_3 host.[46–48] The co-doping with Li^{+} was observed to enhance the upconversion luminescence intensity. Similar results have been obtained for Li^{+} doped Y_2O_3:Yb^{3+},Ho^{3+} material.[49] Beside the modification of the crystal field also the reduced number of OH groups and the increased lifetime of the intermediate state of Er^{3+} have been proposed to be the reason for the enhancement.[47,49] Improvement of upconversion luminescence by Li^{+} co-doping has been studied also with materials such as $BaTiO_3$:Yb^{3+},Er^{3+},[50] and $CaMoO_4$:Yb^{3+},Er^{3+}.[51]

Co-doping $NaYF_4$:Yb^{3+},Er^{3+} with K^{+},[52] and Sr^{2+} or Ca^{2+} ions[53] have been observed to affect the morphology of the material. Increasing K^{+} concentration changed the shape of the particles from elliptical shape to hexagonal prisms and further to nanorods. Moreover, this ion enhanced the green upconversion emission intensity. Sr^{2+} co-doping resulted in promoted formation of the cubic structure while Ca^{2+} enabled tuning of the crystallite size from smaller to larger when Ca^{2+} concentration was increased.

Transition metals

The blue, green, red and UV upconversion emissions of hexagonal $NaYF_4$:Yb^{3+},Er^{3+} have been enhanced by tridoping with Sc^{3+}.[54] In addition, the decay time was observed to increase with different amounts of Sc^{3+}. It was also concluded that the Sc^{3+} ion was able to tailor the local crystal field of the $NaYF_4$ host lattice. Co-doping Ti^{4+} in $NaYF_4$:Yb^{3+},Er^{3+} has also been observed to enhance the upconversion luminescence of the material and prolong the lifetimes.[55] Moreover, a valence balance was established with Na^{+} that is able to occupy Y^{3+} sites.

$NaYF_4$:Yb^{3+},Er^{3+} microcrystals co-doped with Cr^{3+} and prepared with hydrothermal method have been studied.[41] The concentrations of the studied doping ions were 20 mol-% for Yb, 2 for Er and from 0 to 40 for Cr. The particle size was observed to grow when the Cr concentration increased. The preparation method included the use of sodium citrate which is known to be able efficiently control the particle morphology.[56–58] It was attributed that the selective adsorption of citrate ions was behind the morphology and size changes. The upconversion luminescence was measured in deionized water dispersion of the crystals. The upconversion luminescence was enhanced when Cr^{3+} was used up to the 25 mol-% concentration. The strongest intensity was obtained with 15 mol-% of Cr^{3+}. Moreover, the power dependence results suggested that Cr^{3+} ions have not affected the UC mechanism. X-ray diffraction patterns showed shifts which suggest that Cr^{3+} ion can shrink the crystal lattice.

Cr^{3+} sensitized upconversion emission (at 510-560 nm) from $La_3Ga_5GeO_{14}$:Yb^{3+},Er^{3+},Cr^{3+} using broad-band excitation (590-800 nm) has been demonstrated.[59] The increase in Cr^{3+} concentration (from 5 to 30 %) was observed to quench the upconversion luminescence intensity when excitation at 976 nm was used. Therefore, the Cr^{3+} content was suggested to be kept low when Cr^{3+} sensitized upconversion from Yb^{3+}-Er^{3+} is studied. The broadband excitation studies revealed important features in the upconversion process. These were the efficient energy transfer between Cr^{3+} to Yb^{3+} and inefficient energy transfer from Cr^{3+} to Er^{3+}. This was observed from the decay results where the increase of Yb^{3+} content resulted in prolonged decays. Therefore, the use of Yb^{3+} as a 'bridge' between the ions was essential. Another interesting observation was that the process needed low contents of Cr^{3+} because larger amounts would interfere the energy transfer from Cr^{3+} to Yb^{3+}.

Trivalent chromium has shown broad-band absorption and is therefore used as a sensitizer in upconverting transition metal-lanthanide molecular complexes.[60] Moreover, Cr(III) has been proposed to be a solution to a common inefficiency problem with lanthanide supramolecular compexes.[61] Materials in which the activator is embedded in a molecular complex show typically inefficient upconversion luminescence due to reduced excited state lifetimes caused by increased nonradiative relaxation processes. The proposed possibility to circumvent this problem has been the use of a combination of sensitizers with long-lived excited states such as Cr(III).[61]

In general, doping $NaRF_4$ (R = rare earth) lattice with ions that are larger in size than the R^{3+} ion will favor the formation of hexagonal phase instead of the cubic phase. When using smaller ion such as Mn^{2+} to replace Y^{3+}, the formation of the cubic phase

has shown to be dominant.[62] The reason behind this was proposed to be in the charge differences. The Y^{3+} substitution with Mn^{2+} can generate an extra F^- ion on the grain surface which would induce transient electric dipoles with negative poles pointing outwards. The charge repulsion between the negative poles and F^- ions in the solution would hinder the diffusion of the F^- ions from the solution to the grain surface, and thus result in retardation of the crystal growth. Even Mn^{2+} content reaching 5 % can generate the formation of the single-phase cubic $NaLuF_4$ material during hydrothermal synthesis, and the particle size can be grown larger (up to 19.9 nm) when the content is increased up to 40 %.[63]

It has been shown that Mn^{2+} enables the tuning of upconversion emission of Er^{3+}, Ho^{3+} and Tm^{3+} activators into a single band in $KMnF_3$ host with Yb^{3+} sensitizer.[64] The single band contained red and near-infrared spectral region. Strong red upconversion emission has also been observed with MnF_2:Yb^{3+},Er^{3+} material.[65]

$NaYF_4$:Yb^{3+},Er^{3+} co-doped with Ni^{2+} (10-40 mol-%) has shown enhanced upconversion luminescence when compared to the material without Ni^{2+}.[66] All the materials had the hexagonal structure. Shifts in the diffraction reflections were observed which would indicate changed crystal fields. Strongest enhancement was obtained with 20 mol-% of Ni^{2+} which was proposed to be due to the increased asymmetry in the crystal field. Energy-dispersive X-ray fluorescence showed the presence of all expected elements (F, Na, Y, Ni, Yb and Er) in the nanoparticles. Further increase of the Ni^{2+} amount resulted in decreased upconversion luminescence intensity. The possibility of the smaller Ni^{2+} ion to occupy the sites of Y^{3+} and Na^+ was suggested to be the reason behind the decreased luminescence.

In 2011, Cao et al studied the co-doping Y_2O_3:Er^{3+} with Zn^{2+}, Li^+ and Zn^{2+}-Li^+ using the sol-gel synthesis.[47] Each ion co-doping resulted in enhancement of upconversion luminescence intensity when compared to the Y_2O_3:Er^{3+} material. Doping with these ions was proposed to reduce the defects (OH groups) of the nanocrystals which was pointed out to be the reason behind the UC enhancement. In addition to this, the tailored local environment of the Er^{3+} ion was believed to cause the green emission lifetime to increase.

Post-transition metals

Co-doping of Sn^{4+} (up to 5 mol-%) has resulted in enhancement of the upconversion luminescence of the hexagonal $NaYF_4$:Yb^{3+},Er^{3+} material.[67] The strongest upconversion intensity was observed with 3 mol-% of Sn. The valence of the co-doped tin was investigated using X-ray photoelectron spectroscopy (XPS) and electron spin-resonance spectroscopy (ESR). A change from Sn^{4+} to Sn^{2+} was

observed when Sn-concentration was increased above 3 mol-%. In addition to luminescence enhancement, the increasing Sn-concentration resulted in decreased decay time constant.

The enhancement of the upconversion luminescence of Er^{3+} by using Bi^{3+} co-doping has been studied in Y_2O_3:Er^{3+},[68] and Zn_2SiO_4:Yb^{3+},Er^{3+}.[69] Both materials showed enhanced upconversion luminescence when Bi^{3+} was co-doped in the materials. This was attributed to the modification of the local crystal field around Er^{3+} in the Y_2O_3 host which would enhance the radiative transition rate and favor the enhancement of the upconversion emission intensity. The optimal Bi^{3+} content in the Y_2O_3 host was found to be 1.5 mol% which enhanced the upconversion luminescence intensity by 1.5 times. The Zn_2SiO_4 host can crystallize with a rhombohedral structure in which the Zn^{2+} sites have C_1 symmetry. The rare earth dopants may occupy the Zn site during the used microwave synthesis. The optimal Er^{3+} and Yb^{3+} concentrations were 0.5 mol% and 3, respectively. 1 mol% Bi^{3+} addition resulted in the strongest upconversion intensity which was improved by 20 times. Bi^{3+} has larger ionic radius (0.96 Å) than Zn^{2+} (0.74 Å) and thus it is able to distort the lattice and reduce the local crystal field of Er^{3+} which was suggested to be the reason behind the upconversion enhancement.

Plasmonic enhancement using noble metals

Noble metals (Au, Ag, Cu, Pt) are used to induce the plasmonic enhancement which arises from resonant oscillation of the free electrons on the metal surface when stimulated by light.[42,43] This surface plasmon resonance (SPR) oscillation is able to propagate along a metallic surface and constitute an intense electric field which may result in enhanced efficiency of the energy conversion processes needed for the upconversion luminescence.[42,70] Surface plasmon can influence the upconversion luminescence in three ways:[70,71] 1) enhance the absorption of the sensitizer, 2) improve the radiative decay rate of the activator, and 3) increase the energy transfer from the sensitizer to the activator. The enhancement factors up to 450 have been reported.[71]

SPR is strongly dependent on the size, size distribution, shape, composition and surrounding environment of the metallic nanoparticles or substrate.[43,70] Therefore, the studies about the plasmonic enhancement have been focused on optimization of the plasmonic structure. Moreover, upconverting materials have been introduced to the metallic surfaces using different ways. First way is that UC-particles can be deposited on the metallic surface. The surface may be a specifically engineered film, such as gold island film,[72] gold nanopillars on continuous gold film,[73] or a metallic film and UC-particles may be separated with an additional intervening layer[74]. In

addition, other surfaces, such as silver nanogratings,[75] gold nanoparticles,[76] and 3D plasmonic nanoantenna[77] have been studied. Second way is that the metallic particles can be attached on to the UC-particles' surface.[78,79] The final third way is to use core-shell design. For instance plasmon enhancement of the upconversion luminescence from the $Y_2O_3:Yb^{3+},Er^{3+}$ material in core/spacer/shell design ($Au/SiO_2/Y_2O_3:Yb^{3+},Er^{3+}$) has been studied.[80] Optimization of the spacer thickness resulted in enhancement of the upconversion luminescence up to 9.59 fold.

Surface passivation and broadband sensitization

Upconversion efficiencies of nanoparticles are lower than those of corresponding bulk materials due to the increased surface-to-volume ratio which exposes most of the lanthanide ions to quenching by ligands, solvents, surface defects or impurities.[81–83] Surface passivation is one way to prevent the quenching effects and enhance the upconversion luminescence. This can be done by homogeneous or heterogeneous active core-inert shell design.[84]

The homogeneous core-shell structure refers to the identical host lattice material in the core and shell. For instance, the upconversion luminescence was enhanced by 7 and 29 times in $NaYF_4$:Yb,Er/$NaYF_4$ and $NaYF_4$:Yb,Tm/$NaYF_4$ core/shell materials, respectively.[85] In the heterogeneous core-shell structure, the core and the shell matrix have different compositions. This type of structure have been studied with cubic $NaYF_4$:Yb,Er/CaF_2 core-shell material.[86] Enhancement of 4-5 times stronger than that of $NaYF_4$:Yb,Er/$NaYF_4$ and 300 times stronger than the pristine nanoparticles was obtained. Moreover, the (α- NaYF4:Tm)/CaF_2 core-shell material has shown the high quantum yield of 0.6 ± 0.1 % under low power density excitation (0.3 W/cm^2) and 35-fold increase in the intensity of the upconversion luminescence.[87]

The core-shell design enables the use of different doping ions with inorganic hosts, and also the combination of lanthanides and organic dye molecules. This design offers the possibility to enhance the absorption of the materials, and thus enhance the upconversion luminescence. An active core/active shell approach has been used in the design of the $NaGdF_4$:Yb,Er/$NaGdF_4$:Yb core-shell material which showed significant enhancement of the upconversion luminescence (approximately 13 and 20 fold for the green and red emissions, respectively) when compared to the core-only nanoparticles.[88]

Organic molecules can work as antennas to harvest the excitation energy. This type of 'antenna effect' has been studied using commercial, broadly absorbing infrared dyes (IR-808 and IR-820) that were attached to $NaYbF_4$:Tm/$NaYF_4$:Nd core-shell

nanoparticles.[89] Upconversion quantum efficiency of 19 % was reported. Moreover, a broad NIR excitation response range from 700 to 800 nm was obtained. A commercially available cyanide dye, IR-780, has been carboxylated to form IR-806 dye which was attached to the surface of β-$NaYF_4$:Yb,Er nanoparticles.[90] A significant increase of the overall upconversion luminescence intensity (even by a factor of 3300) was observed.

Core-shell design has been used to study β-$NaYF_4$:Yb,Er crystals for dye sensitized solar cells.[57] The β-$NaYF_4$:Yb,Er crystals of 400 nm in diameter and 470 nm in height were coated first with amorphous SiO_2 as inner shell with 10 nm thickness, and second with anatase TiO_2 grains of 30 nm in thickness as outer shell. SiO_2 shell was designed to create an electrical isolation for the upconversion core to prevent electron trapping caused by the β-$NaYF_4$:Yb,Er crystals. The upconversion luminescence intensity was observed to decrease after SiO_2 coating, and after further TiO_2 coating the intensity remained unchanged. However, the overall change was considered to be minor and a highly crystalline core with strong luminescence and double shells would not result in heavy attenuation of the luminescence intensity.

2.1.7. Preparation methods

Crystalline materials

Coprecipitation

One of the most uncomplicated methods for upconversion material preparation is the coprecipitation method which needs no costly equipment or time consuming, complex procedures. One of the earliest studies based on this method focused on preparation of LaF_3 nanoparticles doped with Ln^{3+} (Ln = Eu, Er, Nd, and Ho).[91] The procedure included mixing of two solutions in which the first contained ammonium di-*n*-octadecyldithiophosphate and NaF, and the other solution was a mixture of the rare earth nitrates in water. This was done at 75 °C for two hours, and followed by cooling, separating with centrifugation, washing and finally drying.

Similar steps were followed when NaF in water, rare earth chlorides, and Na_2-ethylenediaminetetraacetic acid (EDTA) were used to synthetize $NaYF_4$:Yb,Er.[92] Differing from the previous, this synthesis was made in the room temperature. After the synthetization, the materials were annealed under H_2/N_2 atmosphere at 400 – 600 °C for five hours to enhance the upconversion luminescence emissions. The presence of EDTA enabled the control of the particle size in the range of 37 to 166 nm diameter. Coprecipitation method has been used also for oxide materials such as Y_2O_3:Sm and Gd_2O_3:Sm,[93] and Y_2O_3:Er and Y_2O_3:Yb,Er.[94]

Some materials prepared with coprecipitation method need post-annealing process or a calcination step to obtain the desired optical properties. To avoid the extra heating step, a high-temperature coprecipitation method has been developed for the highly uniform particle synthetization.[95,96] This method uses oleic acid as a capping ligand and octadecene as a solvent.[97] The two main steps are the formation of small amorphous $NaYF_4$ coprecipitates at the room temperature and further the growth of the nanoparticles at high temperature such as 300 °C. The coprecipitation synthesis route has been widely used for upconverting nanoparticle preparation.[98–102]

Hydro(solvo)thermal synthesis

Hydro(solvo)thermal syntheses enable the preparation of highly crystalline materials under relatively low temperatures. The hydro(solvo)thermal reactions are performed in a sealed environment in which a high pressure and temperature above the critical point of the solvent promote the reactions between the solid precursors. The needed environment can be created in a specialized reaction vessel called autoclave which has a protective insert such as a teflon or a titanium layer. However, this kind of system excludes the possibility to observe the nanoparticles as they grow. Nevertheless, simultaneous control over the crystallographic phases, sizes and morphologies can be achieved, especially when organic additives are used. Some examples of the used additives are oleic acid, polyethylenimine, EDTA, and cetyltrimethylammonium bromide (CTAB).[16,95,96]

The hydro(solvo)thermal preparation of β-$NaYF_4$:Ln^{3+} (Ln = Eu, Tb, Yb/Er, and Yb/Tm) has been extensively studied by Li et al.[103] The procedure included rare earth chlorides and NaF as precursors, distilled water, ethanol and acetic acid as solvents, and CTAB and EDTA as organic additives to control the crystal morphology and size. The precursor solution was heated in an autoclave at 180 °C for 24 h, and finally the precipitates at room temperature were separated by centrifuging, washed and dried. Similar procedure have been utilized in preparation of β-$NaYF_4$:Yb,Er for perovskite solar cells.[104]

Thermal decomposition

Thermal decomposition is one of the most commonly used methods for the synthetization of the high quality, monodisperse upconversion nanoparticles with controllable particle size. The used precursors are generally organometallic compounds which decompose at an elevated temperature in a high-boiling point solvent in an oxygen free environment. The precursor compound is most commonly metal/Ln-trifluoroacetate and the solvent may be oleic acid, oleylamine, tri-*n*-octylphosphine oxide or 1-octadecene. This method requires well optimized

synthesis parameters such as the reaction time, reaction temperature and the concentration of the reagents to ensure the preparation of the high-quality nanoparticles. In addition, this method has risen some safety concerns due to the air-sensitive and toxic precursors and by-products such as HF. One of the earliest development of this method was done with synthetization of monodisperse LaF_3 nanoplates.[105] Later on this method was used to synthetize upconversion materials such as $NaYF_4$:Yb,Er/Yb,Tm,[106] $NaGdF_4$:Yb,Er[88] and CaF_2:Tb[107]. [95,96,108]

Other methods

Sol-gel process is one example of techniques used for preparation of upconversion nanocrystals for applications such as thin film coatings and glass materials. The process involves hydrolysis and polycondensation of the precursors that are usually metal alkoxides (or halides). For upconversion nanocrystals, typically a calcination is needed to improve the crystallinity.[16] For example, this method has been used to prepare Er-doped sol-gel silica-glasses[109] and Er-doped $Y_2Ti_2O_7$ nanocrystals[110]. The drawback with the process is a long heating time of up to a few days.

In addition to the above-mentioned co-precipitation method, the urea-based homogeneous precipitation method has been used to prepare oxide materials, such as Gd_2O_3:Yb,Ho[111] and Y_2O_3:Yb,Er[112]. The precursors and solvents needed for these precipitations were rare earth nitrates, de-ionized water, nitric acid and urea. The latter study involved also EDTA to control the particle size. Moreover, microwave assisted methods have produced upconverting nanoparticles, such as $NaYF_4$:Yb,Er[113] and GdF_3:Yb,Er[114]. This method typically involves organic precursors, such as trifluoroacetates.

Bridgman method and modified versions of the method have been used to prepare upconverting single crystals. The method uses polycrystalline precursor materials and seed crystal which are heated above the melting point of the crystal for several hours, and finally cooled slowly to the room temperature. Some examples of materials prepared using this method are $LiYF_4$:Yb,Er[115], $LaCl_3$:Er[116], and KPb_2Br_5:Er[117].

Solid state reactions may also be used to prepare upconverting materials. For example, the ground mixture of RF_3, NaF and NaBr have been heated to 550 °C in a HF/Ar gas stream for 20 h to form β-$NaYF_4$:Er –material.[12,118] Moreover, $Y_6W_2O_{15}$:Yb,Er material was obtained when rare earth oxides and tungsten trioxide were ground, and calcined at 1100 °C for six hours.[119]

Upconverting films

Upconverting films have been fabricated either by first synthetizing the particles and then depositing them on substrates or by directly fabricating the upconverting material as a film. Reports can be found on various deposition techniques including spin coating[120,121], dip-coating[122], sol-gel method[123,124], pulsed laser deposition[125] and chemical vapor deposition[126]. In addition, printing technology, such as screen printing, has been used to introduce upconverting particles on a film.[111] Next, the thin film deposition techniques that are based on chemical processes and gaseous precursors are introduced. In this thesis work, the focus is on the atomic layer deposition technique which has been used for luminescent thin film fabrication.[127–129]

Chemical vapor deposition

Chemical vapor deposition (CVD) is a relatively mature vapor phase technique used in research and industry to fabricate a variety of thin films and coatings for applications such as semiconductors for microelectronics, optoelectronics, energy conversion devices and fibers. In the CVD process, the gas-phase precursors are simultaneously in a reaction chamber which is activated (e.g. by heat, light or plasma). The gaseous precursors may dissociate and/or chemically react in the gas phase (homogeneous reactions) or on a surface (heterogeneous reactions) to form a solid stable material that is either a powder or a film. The material can be inorganic or organic. Possible by-products are removed using purging gas. The CVD technique offers composition control and it is used in production of synthetic diamonds, graphene, metals, silicon dioxide, silicon nitrides and polysilicon. CVD technique has many developed variations such as thermally activated CVD, plasma enhanced CVD and photo-assisted CVD.[130,131]

Atomic layer deposition

Atomic layer deposition is based on chemical reactions of gaseous precursors that are introduced on the substrate surface sequentially and separately which enables control over thickness and conformity of the thin films. The history of ALD started at 1960s and 1970s when ALD was developed to grow ZnS thin films for electroluminescent displays. The technique was first termed as atomic layer epitaxy (ALE) but the name was afterwards changed to atomic layer deposition. Since then, ALD has shown its importance in microelectronics industry and in nanotechnology. To date, the ALD has been used in research and industry in areas such as photovoltaics, optoelectronics and supercapacitors, and the technique has been typically used to deposit inorganic binary compounds such as oxides, nitrides and sulfides.[132–134]

The atomic layer deposition technique has exhibited potential advantages, especially when compared to other film deposition techniques such as chemical vapor deposition and physical vapor deposition. ALD offers conformity, thickness and composition control, repeatability, and materials deposition with atomic-level precision. In addition, the deposited films are dense and pinhole-free. All the benefits are obtained due to the cyclic and self-limiting nature of the ALD process.[132–134]

The general ALD process has been described by an ALD cycle in which two precursors are usually presented (Fig. 6). In the process, the gaseous precursors are alternately and sequentially pulsed into a reaction chamber in vacuum. The chamber is in selected temperature to accelerate the chemical reactions between the precursors and the substrate surface. Each precursor pulse leads to self-limiting, gas-solid reaction, which is often called a half-reaction, and is followed by a purge of an inert carrier gas to remove unreacted precursors and possible reaction by-products. Self-limiting growth is ensured when the pulsing and purging steps are optimized to be adequately long. After both half-reactions and purges, the ALD cycle is complete and a monolayer of the desired material has grown. The cycle is repeated until the targeted film thickness is obtained.[132–134]

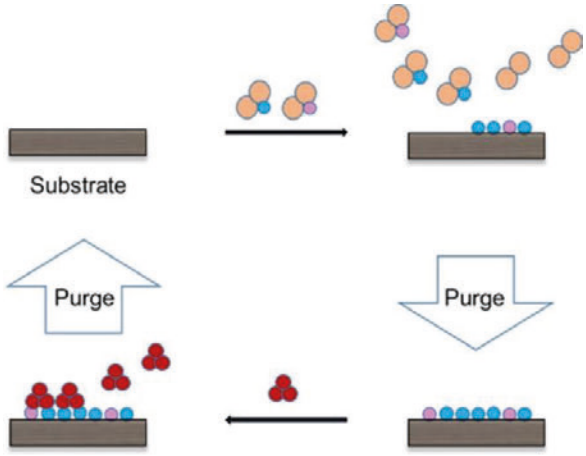

Fig. 6. Schematic representation of an ALD cycle.

The film growth is described with the growth-per-cycle (GPC) value that means the average increase in film thickness during one ALD cycle. An ideal process shows a temperature range in which the GPC value stays constant and does not dependent on parameters such as temperature, gas pressure, pulse and purging times. This specific temperature range, often referred to as an ALD window, enables the self-limiting processes of the ALD (Fig. 7.). All ALD processes do not show ALD window, however, the process may still be highly reproducible. Outside the ALD window, the temperature affects the growth. A relatively low temperature may lead to precursor

condensation and, on the other hand, too high temperature may cause decomposition of the precursor. This sets limitations to the precursors. In addition to thermal stability, the precursors need to have high volatility, high reactivity to co-reactant surface and complete unreactivity towards the surface covered with the precursor.[132–135]

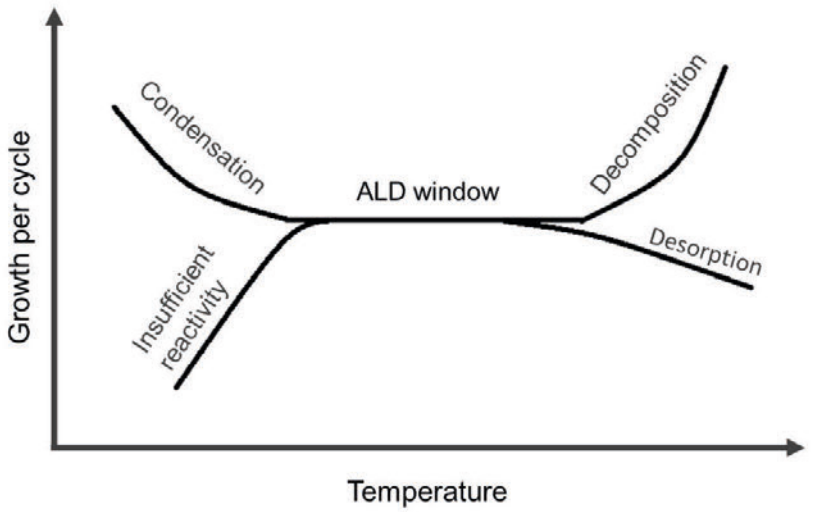

Fig. 7. ALD window. Similar as the figure by Karppinen.[135]

Atomic and molecular layer deposition in preparation of hybrid materials

Whereas ALD was developed to fabricate inorganic thin films, the molecular layer deposition technique can be considered as a counterpart for ALD to prepare organic thin films. The two techniques were developed independently of each other, and consequently MLD technique was first reported in 1990s by several researchers from Japan. This technique was developed from the already existing method known as vapor deposition polymerization (VDP), and it was first referred to as either alternating vapor deposition or layer-by-layer growth and as well as VDP. Today MLD and combination of ALD and MLD is used to preparation of porous films, surface functionalization of ultrafine powders and fabrication of inorganic-organic hybrid materials.[135–138]

MLD process is similar to ALD process where the precursors in gas-phase are separately and sequentially supplied into a reaction chamber where they chemically react with the substrate surface (Fig. 8). The combination of these both techniques enables the fabrication of inorganic-organic hybrid thin films that may not be obtainable by using any other film deposition method. MLD offers the similar

benefits as ALD such as conformity and control over molecular layer and thickness. However, hindered growth may occur when ALD/MLD or MLD are used due to several causes. The organic layer may not grow perpendicular to the surface if the organic molecular chains are long. This kind of molecules may bend and react more than once with the surface which may lower the growth rate. In addition, large molecules may cause steric hindrance.[135–138]

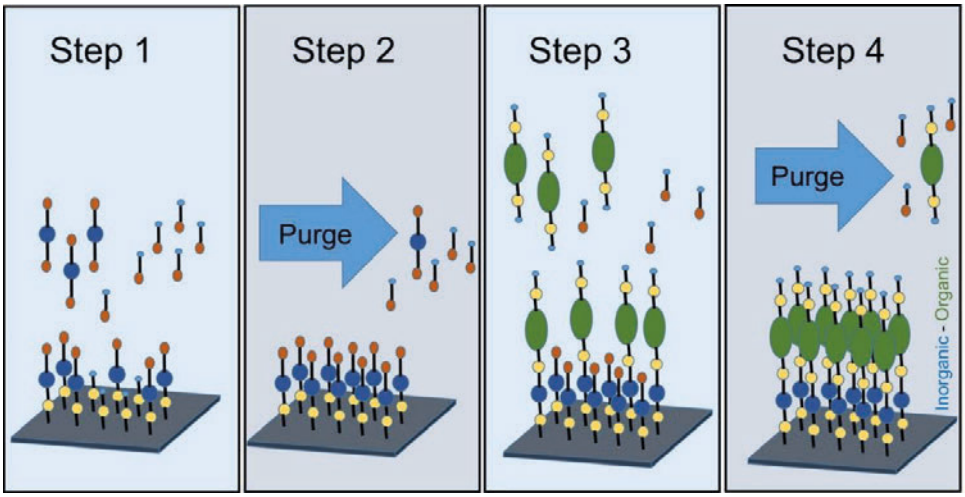

Fig. 8. The ALD/MLD process.

2.2. Other lanthanide based materials

2.2.1. Luminescent lanthanide complexes

Luminescent lanthanide complexes have been studied intensively after the optical properties were discovered in 1942. Ytterbium and neodymium chelates have been studied since 1958 and 1960s, and Yb^{3+}-porphyrin complexes have been studied since 1990s. These materials have shown potential particularly in bioanalytical applications. Combination of a lanthanide ion and certain organic ligands in a complex offers two benefits: the organic ligands may protect the metal ion from vibrational coupling and increase the absorption of the excitation radiation by the antenna effects. Mostly the complexes are studied in aqueous media. However, the lanthanide complexes suffer from poor thermal stability and low mechanical strength which have restrict the practical use of the materials. One studied solution has been to introduce the complexes in a stable rigid matrix, such as a silica- or titania based material.[7,139]

Lanthanide complexes consist of a chromophore moiety (antenna ligand) and a central ion coordinating moiety (lanthanide ion carrier chelate) (Fig.9). The commonly used chromophores consist of groups such as pyridine, bipyridine, terpyridine, β-diketonates and triphenylene. The chelate structures that coordinates the central lanthanide ion are typically composed of polyacid and macrocycle structures. These complexes are also often called lanthanide chelates due to the multiple coordination bonds between the organic structure and the central ion. The lanthanide coordination is mainly due to the ionic bonding interactions and strong coordination can be obtained in aqueous media.[140,141]

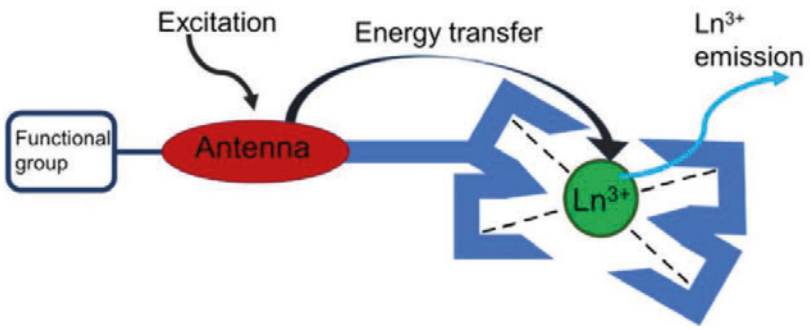

Fig. 9. A schematic representation of a lanthanide complex with luminescence.

The luminescence mechanism of the lanthanide complexes is complicated but it can be described with a simplified three-step model. First, the ligand absorbs the excitation energy, and then transfers it to the lanthanide ion which finally emits light. Three different mechanisms for intramolecular energy transfer in lanthanide complexes have been suggested (Fig.10). In mechanism I, an intersystem crossing occurs between the lowest singlet and triplet excited states of the ligand which is followed by energy transfer from the triplet state to the lower energy state of the lanthanide ion. In mechanism II, the energy transfer from the singlet state to the lower energy state of the ligand is direct. The mechanism III involves also the upper intermediate state of the lanthanide ion where the energy is transferred from the singlet state. After this, the energy is transferred back to the triplet state of the ligand and further to the lower energy state of the lanthanide ion.[142]

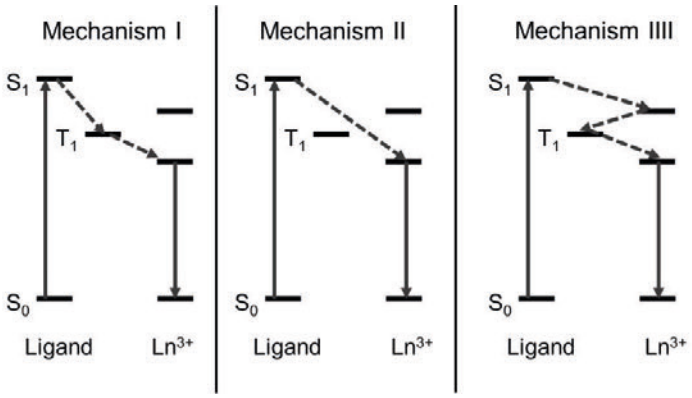

Fig.10. The different mechanisms for intramolecular energy transfer in lanthanide complexes. Similar as in[142]

In general, the intramolecular energy transfer between the organic ligand and the lanthanide ion involves an intersystem crossing from the ligand singlet state (S_1) to the ligand triplet state (T_1). This type of mechanism is usually called as the Dexter exchange mechanism which is a double-electron exchange mechanism that operates with short distances. The luminescence properties of this type of materials depend on two factors. First is the efficiency of the energy transfer between the ligand and the central ion, and second is the concentrations of quenchers surrounding the central ion.[141–145]

While the Dexter mechanism operates with short distances, the resonance energy transfer (RET) occurs with long distances. Instead of RET, sometimes the term Förster resonance energy transfer (FRET) is used. In this kind of process, the energy transfer occurs non-radiatively from the excited luminescent molecule (donor) to the energy receiving molecule (acceptor). The FRET mechanism is a non-radiative dipole-dipole interaction between the transition dipoles of the donor and acceptor. It is highly dependent on the distance between the donor and acceptor and it can operate with long distances up to 10 nm.[141–145]

The number of studies focusing on molecular complexes capable of upconversion luminescence is quite small and they were first introduced not until 2011.[61,146–151] The molecular UC systems are expected to have benefits such as high absorptivity, small size, simple addition of functional groups and less toxic nature when compared to the inorganic upconverting nanoparticles. Nevertheless, observing upconversion with these systems particularly in solutions appears to be a difficult task due to the presence of the quenchers such as OH, NH and CH oscillators.[152]

The UC complexes consist of ligands (L) with sensitizer (S, such as Yb^{3+} or Cr^{3+})[61,151], and activator (A, such as Er^{3+} or Tb^{3+})[147,150] (Fig. 11). The use of two sensitizers per activator is preferable due to the improved intensity of the upconversion luminescence.[61] Two other requirements for the system has also been suggested.[146] First, the sensitizer should have long enough lifetime to enable the sequential energy transfer needed for upconversion luminescence. And second, the activator should be protected from high-frequency vibrations. The studied upconversion luminescence mechanisms in molecular systems are mainly limited to GSA/ESA and ETU mechanisms in which the latter is more efficient.[146] In addition, the CSU has been studied with Tb^{3+} activator.[151]

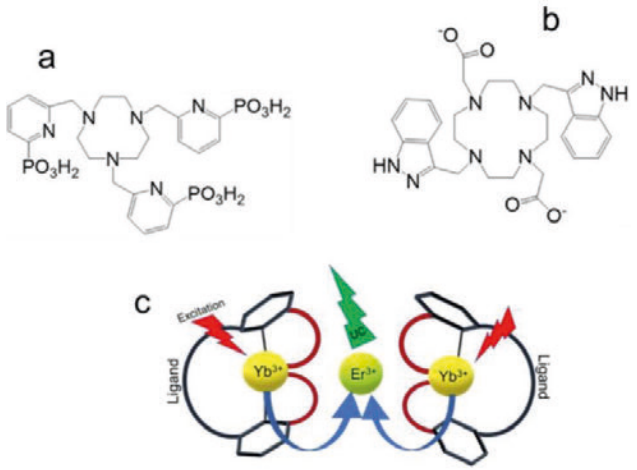

Fig. 11. Ligands used in UC complexes (a and b) and a schematic representation of UC complex with two sensitizers (c).[149,151]

2.2.2. Metal organic frameworks

Metal organic frameworks (MOF) are solid-state materials with hybrid inorganic-organic structure that combines metal ions or clusters and molecular building blocks. These organic ligands link the metal ions or clusters via coordination bonds and form 1-, 2- or 3-dimensional networks. These materials have high porosity, high volume and surface area, and low crystal density. In addition, MOFs have high structural tunability when compared to other solid porous materials such as zeolite or silica. Metal organic frameworks have been studied for applications in areas such as bioimaging, sensing and photocatalysis.[153–156]

The rare earth ions have been studied as the metal source for upconverting MOFs. Nd^{3+} has been coordinated with 1,4-naphthalenedicarboxylate (NDC) linker in DMF

solvent (N,N-dimethylformamide) to form $[Nd_2(NDC)_3(DMF)_4]\cdot H_2O$ material.[157] The material showed UV upconversion emission at 391.6 nm and blue upconversion emission at 449.5 nm under 580 nm excitation. The proposed upconversion mechanism for this system was the ETU. In addition, $[Nd_2\text{-}(H_2O)_4][\{C_5H_3N(COO)_2\}_2\{C_6H_4\text{-}COO)_2\}]$ material has shown UV/VIS emission (at 422 nm with shoulders at 364 and 461 nm) under 580 nm excitation.[158] The upconversion mechanism GSA/ESA was suggested to apply for this system.

Rare earths (R) Er^{3+}, Y^{3+}, Gd^{3+}, Lu^{3+} and Yb^{3+} have been used together with 1,3,5-benzenetricarboxylic acid (BTC) to form $R(BTC)(H_2O)\cdot DMF$ metal organic frameworks.[159] The synthetized materials were 3D porous framework crystalline materials with a rod-like shape. The UC-MOFs with Y^{3+} and Er^{3+} showed the green and red upconversion emissions of Er^{3+} under 980 nm excitation. The optimal Er^{3+} concentration was demonstrated to be 6 %. The upconversion mechanism was studied by preparing MOFs with Y/Yb/Er in which Yb concentration was changed from 30 to 60 and 90 % while Er concentration was kept at 10 %. The upconversion emissions of these materials remained basically at the same level which suggested that ESA would be more probable mechanism with this system than ETU mechanism.

MOF and upconverting nanoparticles have been combined to form upconverting nanocomposite core-shell materials.[153] The upconverting $NaYF_4$:Yb,Er nanoparticles were used as a core and iron(III) terephthalate (MIL-101_NH_2) MOF was used as a shell material. The surface amino groups of the core-shell particles were modified using poly(ethylene glycol)-2-amino ethyl ether acetic acid and folic acid, and the upconversion luminescence were detected from this surface modified material in water. The core-shell material showed the green and red emissions of Er^{3+} with 980 nm excitation.

2.3. Upconversion in glasses and glass-ceramics

2.3.1. Introduction to glasses

Glasses are amorphous solids that differ from crystals in the lack of the long-range atomic order which gives them the ability to be modified to have almost unlimited amount of geometrical structures. Due to the lack of the long-range order a glass have higher configuration entropy and higher free energy than the crystalline material with the same composition. Thermodynamically glasses are in metastable state. Moreover, glasses have high optical transparency and thermochemical strength which makes them useful for optical applications. Glass can be doped with rare earth

ions or microcrystallites or glass can be prepared in such a way that particles are directly crystallized into the glass to form glass ceramics, GCs (Fig. 12).[160–162]

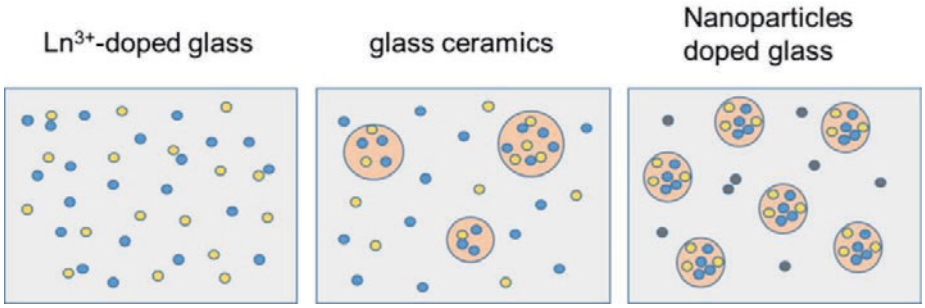

Fig. 12. Schematic representation of the difference in the Ln^{3+} distribution in various glasses. Based on a figure by Zhao.[160]

Glass has a network that composes of single atoms or molecular units. In principle, the constituents that form the glass have no requirement of stoichiometry which facilitates the doping of active elements such as transition metals. All the constituent in a glass are either network formers or network modifiers. Extra network formers may help to increase the chemical durability, suppress the crystallization rate and increase the viscosity of the glass. The network modifiers can introduce ionic bonding to the structure of largely covalent network and thus give more flexibility in the structure. The network modifier may be one of the lanthanide ions which have large sizes that prevent their use as network formers. The 3d transition metals may enter to the glassy network as formers or modifiers.[161,162]

2.3.2. Preparation

Glasses can be prepared by using the conventional melt-quenching technique which is the most commonly used technique for bulk glasses. This method has been used, for example, with glasses having P_2O_5-SrO-Na_2O-Er_2O_3 composition.[163] In the process, precursor chemicals are mixed and heated to 1100 °C for 30 min with a heating rate of 10 °C/min and the melt is poured into a preheated brass mold and annealed at 400 °C for 5 h to decrease the residual stress. Other techniques for bulk glass preparation are the chemical vapor deposition and sol-gel process.[162]

The preparation of glass ceramics can be carried out by melting glass and converting it into ceramic using an appropriate heat treatment which usually includes two step heating.[164] This type of treatment induces the devitrification of the glass where the nucleation and the crystal growth occur during bulk crystallization. For glass ceramics preparation, a phase-separating agent such as magnesium oxide may be needed.[165] Glass ceramics with $NaYF_4$:Yb^{3+},Er^{3+} nanocrystals have been prepared by

using the melt-quenching technique and an appropriate heat treatment to form the glass ceramic.[165–167]

In one example of the glass ceramic procedure, the precursors of the glass with composition $SiO_2 – Al_2O_3 – Na_2CO_3 – CaO – NaF – YF_3 – YbF_3 – ErF_3$ were first heated at 1500 °C for an hour and then poured onto a preheated brass plate and annealed at 500 °C for 10 hours to relinquish the inner stress. The glass ceramics were obtained by heat-treatment at 700 °C for four hours. Other techniques to form glass ceramics have also been used. Combination of modified chemical vapor deposition and solution doping has often been used to prepare rare earth doped fibers.[165] In addition, a new technique where ALD and CVD are combined have been investigated for rare earth doped optical fiber fabrication.[165,167]

2.3.3. Different glass systems

Among various oxides SiO_2, GeO_2, B_2O_3 and P_2O_5 are used as industrial materials for glasses. This is due to their good network forming ability which enables the development of the three-dimensional network and the use as a single component glass able to form a glass itself.[162] Silica glass has been the most commonly used single component glass due to the good properties such as optical transparency in a wide wavelength range and high chemical and mechanical durability.[162] However, this glass has a high melting temperature which may be a drawback for some applications. Upconverting silica glasses have been studied, for example, for optical devices.[109] When rare earths are added to silica, for example in optical fibers, usually co-doping with alumina (Al_2O_3) or phosphorus pentoxide (P_2O_5) is needed to prevent clustering of the rare earths due to the low solubility of rare earths into the silica network.[165]

Nonsilicate glasses such as phosphate, borate, germanate, vanadate or tellurite systems are not generally applied for mass production but they do show some unique properties that cannot be obtained with silicate glasses.[162] Tellurite glasses have received attention due to their potential as an optical glass with high refractive index.[162] Thulium and ytterbium co-doped tellurite glasses with composition $80TeO_2–10K_2O–(9.9 – x)TiO_2– 0.1Tm_2O_3–xYb_2O_3$ (x=0.1–2.0) have showed upconversion luminescence.[168] $Tm^{3+}/Ho^{3+}/Yb^{3+}$ triply doped bismuth tellurite glasses with multicolor upconversion have also been investicated.[169] Moreover, erbium doped zink tellurite glasses with silver nanoparticles[170] and erbium doped germanium-tellurite glasses with gold nanoparticles[171] have showed plasmon enhanced upconversion luminescence. However, tellurite glasses may be toxic due

to the possible leakage that may occur in a corrosive environment due to the disruptive nature of tellurite to the tellurite glass network.[165]

Phosphate glasses are an eco-friendly option for the tellurite glasses.[172] They consist of P-O-P chains that contains four-fold coordinated phosphorous[162] Phosphate glasses have low nonlinear refractive index and a high absorption cross-section which are ideal properties for optical applications. These glasses have also high solubility of noble metals, rare earths and nonoxide semiconductor compounds such as CdS.[162] However, phosphate glasses have high phonon energy which is known to quench the upconversion luminescence.[173] Fluoride glasses have also a very low nonlinear refractive index which would be ideal for some applications but these glasses have not been researched widely due to the high toxicity of the fluoride glasses and the precursors. In addition, they are unstable and expensive.[174]

Oxyfluoride glass-ceramics can be oxides such as silicate, quartz, germinate, phosphate and borate, or they can be chalcogenide, halogenide or mixed nature. GCs are formed when the parent glass is heat treated in such a way that it will first lead to nucleation and further to crystal growth. Oxyfluoride glass-ceramics consists of oxide glass network which contains imbedded fluoride crystals. Therefore, they combine the good mechanical and chemical durability of oxides and low phonon energy of fluorides which makes them ideal for upconversion luminescence. For nanoparticles, the glass phase prevents the agglomeration of the particles and offers a protective layer to prevent the surface related quenching. Moreover, GCs have negligible porosity and great uniformity when compared to sintered ceramics.[174]

Upconversion from oxyfluoride glasses containing LaF_3 and CaF_2 have been studied.[175–178] Such fluorides have low phonon energies and are thus ideal environments for upconverting ions. Oxyfluoride glass ceramics containing $NaYF_4$:Er particles have been prepared by melt-quenching and subsequent heating.[179] The heat treatment enabled the phase transition from cubic to hexagonal, although, pure hexagonal phase was not obtained. $NaYF_4$ nanocrystals have also been investigated to precipitate in glass with composition SiO_2-Al_2O_3-Na_2O-NaF-YF_3-ErF_3-YbF_3 after heat treatment.[180,181] The oxyfluoride glasses with composition of SiO_2-Al_2O_3-AlF_3-Na_2CO_3-NaF-Lu_2O_3-Yb_2O_3-HoF_3-CeF_3 have been prepared using the traditional melting quenching technique route to investigate the effect of Ce^{3+} to the upconversion luminescence of Ho^{3+}.[182] Ce^{3+} addition was found to enable the spectral conversion of Ho^{3+} from pure green to yellow and finally to red under 980 nm excitation.

The GCs approach to prepare Ln^{3+}-containing nanocrystals in glass where nanocrystals are growth in situ in a glass matrix is commonly used method but it is challenging to control the composition and nanostructure of the nanocrystals with it.[160] First, the concentrations are not well-defined and the control of the crystalline sites is limited. Moreover, the obtainable Ln^{3+} concentrations in nanocrystals are limited due to the restricted solubility and short-distance diffusion of Ln^{3+} ions in glass, as well as the large volume fractions (25-35 %) of nanocrystals growth in situ. Second, it is impossible to grow core-shell and heterogeneous structures with this method. Third, it is possible that in situ growth of nanocrystals may occur during post-annealing or reheating process. To overcome these issues the direct doping method where separately synthetized nanocrystals are doped into a glass melt may be used.

2.4. Upconversion for utilization of solar energy

While solar energy offers an abundant energy source to meet the increasing energy consumption demands, the development of efficient and cost-effective solar cells is widely studied. The major problem with effective solar conversion to electricity in conventional solar cells is the lack of ability to absorb radiation in a wide range. The standard solar irradiation spectrum (Air Mass 1.5) consists of wide range photons with wavelengths ranging from ultraviolet to infrared region (300 – 2500 nm)[183]. However, the single-junction PV devices are able to use only a small fraction of the photons and typically NIR and IR range remains non-utilized.[184] This issue can be circumvented by using upconversion luminescence materials.

The conversion efficiency of any traditional single p-n junction solar cell has an upper limit which is determined by the bandgap energy of the semiconductor material that has been used to prepare the cell.[184] With a single bandgap of 2 eV and an ideal upconverter material attached to the rear side of the solar cell a theoretical efficiency limit for the cell has been calculated to be 63.2% for concentrated sunlight and 47.6% for non-concentrated sunlight.[185] The placing of the upconverter material has an effect on the conversion efficiency. The rear side of the solar cell has often been considered to be the optimum place for the upconversion material.[4] Especially when a reflection layer is used together with an upconverter (Fig. 13). An exception for the attachment to the rear side has been the glasses and glass ceramic materials which can be placed on top of a conventional solar cell due to the fairly transparent nature.[4]

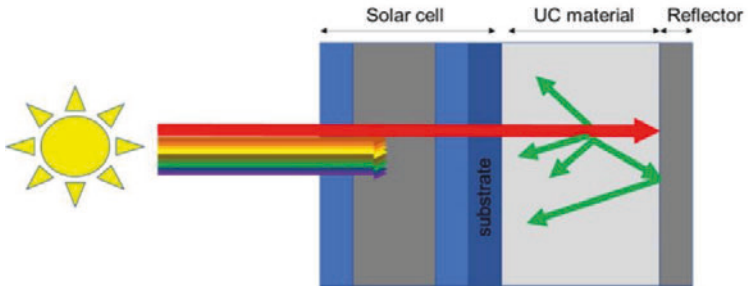

Fig. 13. Representation of an UC solar cell with reflector.

One important figure-of-merit for photovoltaics is the external quantum efficiency (EQE) and for upconversion solar cells the EQE due to upconversion (EQE_{UC}).[4] EQE is the ratio of extracted electron flux (current) of the solar cell to the incident photon flux (ϕ_{in}) onto the solar cell whereas EQE_{UC} is defined as (Equation 5)[4]

$$EQE_{UC} = \frac{\Delta I_{SC,UC}}{q\phi_{in}} \quad (5)$$

where $\Delta I_{SC,UC}$ is the additional short-circuit current due to upconversion and q is the elementary charge.

2.4.1. Crystalline silicon solar cells

The c-Si solar cells have the maximum conversion efficiency as high as 25.6 %[186] which is close to the Schokley-Queisser limit (~30 %). The c-Si solar cells are able to absorb light less than 1100 nm due to the bandgap of crystalline silicon (~1.12 eV)[183]. These limits set limitations to the upconversion materials which need to absorb above 1100 nm. Other desirable properties for the upconversion materials in c-Si cell are good response under low-intensity excitation range (10–100 Wm^{-2}), high conversion efficiency and high transparency towards the upconverted light.[185]

The upconversion materials that are single doped with Er^{3+} have attracted attention in the field. For a bifacial c-Si solar cell with an acrylic adhesive medium layer containing $NaYF_4$:20% Er^{3+} microcrystals on the rear, an external quantum efficiency of 2.5 % was obtained under excitation at 1523 nm.[187] In addition, microcrystalline $NaYF_4$:20% Er^{3+} have been attached to a c-Si solar cell by filling a powder cell and using an index-matching liquid, and an external upconversion efficiency of 0.34 % with 1.09 W cm^{-2} at 1523 nm has been reported.[188] BaY_2F_8:30% Er upconverter material mounted in front of a single-face silicon solar

cell was studied and external quantum yield of upconversion as high as 6.5 % at an irradiance of 8.5 W under 1557 nm excitation was achieved.[189] The same material was also studied in[190]. $Gd_2O_2S:Er^{3+}$ has also been investigated for silicon solar cells[22,118] In addition to monochromatic studies, $NaYF_4$:20% Er^{3+} has been studied also under broad spectrum illumination.[191]

Glasses and glass ceramics can be placed on top of the crystalline solar cells. For example fluoroindate glasses co-doped with Yb^{3+} and Er^{3+} have been studied for c-Si solar cells.[192] The glasses with composition InF_3 - ZnF_2 – SrF_2 – BaF_2 – YbF_3 – ErF_3 were placed on top of a commercial solar cell but the glass samples were not optically coupled with the solar cell that is no index matching oil between the glasses and the solar cell were used. Nevertheless, a glass sample co-doped with 2.25 mol-% of Er^{3+} and 0.1 mol-% of Yb^{3+} produced an EQE of 0.4 % under excitation with 37 mW at 1480 nm.

2.4.2. Amorphous silicon solar cells

Amorphous silicon solar cells have promising properties such as relatively low manufacturing cost, easy preparation and good chemical stability which are reasons behind the wide interest towards these cells in solar industry and research. Hydrogen passivation is often used with a-Si cells to enhance the electrical behavior, and the bandgaps of the a-Si:H solar cells are from 1.7 to 2 eV.[193] Upconversion materials offers even more advantage for a-Si solar cells than for c-Si solar cells due to the higher inability to utilize the IR photons. a-Si solar cells are able to absorb light shorter than 700 nm[183] which makes the upconversion materials with absorption above 700 nm suitable for these cells.

Upconverting $NaYF_4$:18% Yb^{3+},2% Er^{3+} nanocrystals have been attached to amorphous solar cells by using solidified mixture of polydimethylsiloxane and the upconversion powder, and enhancement of short circuit density from 16 to 17 $mAcm^{-2}$ (6.25 %) has been reported.[194] Another way to use the $NaYF_4:Yb^{3+},Er^{3+}$ powder in amorphous solar cells has been to first dissolve it to polymethylmethacrylate (PMMA) in chloroform and after use spin coating to form a film with thickness of 200–300 µm.[195] This type of coating showed an external quantum efficiency of 0.02 % at 980 nm.[195]

In addition to crystalline materials research, upconverting glasses and glass ceramics have also been studied for amorphous silicon solar cells. Triwavelength excitation (808, 980, 1530 nm) for germanate oxyfluoride glasses containing $LaF_3:Er^{3+}$ crystals resulted in significant enhancement of the upconversion luminescence intensity.[175]

Other studied glass ceramics have been the oxyfluoride borosilicates containing $NaYF_4$:Yb^{3+},Er^{3+},[196] and $NaGdF_4$:Er^{3+}.[197] Moreover, Er^{3+}-Yb^{3+} co-doped TeO_2-PbF_2 oxyfluoride tellurite glasses have been attached at the back of amorphous silicon solar cells in combination with a rear reflector and a 0.45 % improvement in efficiency was obtained under co-excitation of AM1.5 and 400 mW 980 nm laser radiation.[198]

2.4.3. GaAs solar cells

The first solar cell with upconversion material was reported in 1996.[4] In the study, Yb^{3+} and Er^{3+} was used to harvest IR radiation by coupling a substrate-free GaAs cell to a 100 µm thick vitroceramic material doped with the lanthanide ions. The efficiency of 2.5 % for an input excitation of 1 W at 1.39 eV (0.039 cm^2 cell) was reported. Furthermore, Yb-Er has been investigated with $Y_6W_2O_{15}$ host material in GaAs solar cell and the maximum output power of 0.339 x 10^{-6} with a 973 nm laser excitation at 145.65 W/cm^2.[119]

2.4.4. Dye-sensitized solar cells

Dye-sensitized solar cells were first reported by Grätzel in 1991.[199] DSSCs offer low cost, simple fabrication methods and environmentally friendly option to common solar cells. Usually the band-gap of the dyes are higher than 1.8 eV.[183]. These cells are able to absorb wavelengths shorter than 700 nm which makes them ideal for enhancement by upconversion. The first reported DSSC with rare-earth-doped upconversion material (LaF_3:Yb^{3+}/Er^{3+}-TiO_2 nanocomposites) was reported in 2010.[200]

Ho^{3+}/Yb^{3+} co-doped Gd_2O_3 nanoparticles have been introduced into a TiO_2 layer of a DSSC solar cell.[111] Enhancement of the power conversion efficiency from 6.701 % to 7.403 % was reported. YOF:Yb^{3+}/Er^{3+} particles have been doped into a TiO_2 photoanode layer and an efficiency increasement of 23 % was reported when 7 wt.% of the YOF material was used.[201] $NaYF_4$:Yb^{3+},Er^{3+}@TiO_2 core-shell nanoparticles were used to prepare the photoelectrode of the DSSC which resulted in 23.1 % enhancement of the energy conversion efficiency.[202]

2.4.5. Perovskite solar cells

Lead halide perovskite ($CH_3NH_3PbX_3$; X = I, Br, Cl) solar cells were introduced in 2009 and since then they have been highly studied due to the promising properties such as low-cost and relatively easy fabrication, unique optical and electrical properties, and high efficiency.[203] In the few recent years, the power conversion

efficiency of the cells has increased from 3.8 % to 22.1 %.[204] Perovskite solar cells have absorption range of 300–800 nm.[205,206] UC rare earth materials have been used in organic-inorganic lead halide perovskite solar cells to expand the absorption range and improve the stability.

A single crystal $LiYF_4:Yb^{3+},Er^{3+}$ has been used as an independent upconverter to enhance the power conversion efficiency of perovskite solar cell.[115] Enhancement of 7.9 % under the irradiation of simulated sunlight by 7–8 solar constants was reported. β-$NaYF_4:Yb^{3+},Er^{3+}$ nanoprisms incorporated in $CH_3NH_3PbI_3$ perovskite solar cell as a mesoporous layer resulted in a power conversion efficiency of 16 % which was 13.7 % increase when compared to a cell only with a common TiO_2 layer and without the upconverter.[104] $NaYF_4$:Yb,Er nanoparticles have also been used as a replacement of m-TiO_2 mesoporous layer in $CH_3NH_3PbI_3$ perovskite solar cells.[207] The power conversion efficiency of the perovskite cell with the upconversion material was reported to be 17.8 % and a power conversion efficiency of 0.35 % was reported when the solar cell was under 980 nm laser irradiation. Core-shell nanoparticles (β-$NaYF_4:Yb^{3+},Tm^{3+}$ at TiO_2 core) have been incorporated into a mesoporous layer of perovskite solar cells ($CH_3NH_3PbI_3$).[208] The efficiency of the solar cell was 16.38 % with the upconversion material and 13.98 % without it.

Upconverting fluorotellurite glasses in combination with perovskite solar cell have been investigated.[209] The glass was composed of $65TeO_2–15Al_2O_3–15CaF_2–5NaF$ with addition of $10YbF_3–xErF_3$ (x = 0.5, 1.0, 1.5, 2.0) and was placed in front of a $MAPbI_{3-x}Cl_x$-based perovskite solar cell. The upconversion luminescence of the glasses showed good stability in temperatures up to 100 °C. An open circuit voltage of 0.83 V and a short circuit current of 0.32 mA/cm^2 under 980 nm NIR irradiation was measured.

2.4.6. Organic solar cells

Organic solar cells have promising advantages such as flexibility, low cost, light-weight and easy fabrication when compared to the Si-based cells. However, the organic solar cells mainly absorb at the visible range. Consequently, a major enhancement of the organic solar cells could be obtained by using upconverting materials.[183]

Er^{3+} and Yb^{3+} doped MoO_3 material has been incorporated in organic solar cell having poly-3-hexylthiophene and phenyl C_{61} butyric acid methyl ester in an active layer.[210] Less than 1 % improvement of short-circuit current under one-sun (AM 1.5) illumination was reported.

3. AIMS OF THE STUDY

The general goals of the research were to optimize and improve the properties of upconverting materials to make them more functional in the field of solar conversion, especially in solar cells. The upconversion luminescence from $NaYF_4$-powders, oxide thin films, hybrid thin films, and fluorophosphate glasses were studied. The main aims were to test the fabrication methods, optimize the parameters needed for efficient upconversion luminescence and enhance the upconversion luminescence by doping metal ions or widen the absorption range of the materials.

The more specific aims in each publication were:

I. To investigate the possibility to enhance the the upconversion luminescence from $NaYF_4$:Yb,Er material by transition metal ion doping and study the effect of this doping on the properties of the materials, such as the composition, phase and the thermal behavior.

II. To test the feasibility of the atomic layer deposition as upconverting film deposition technique by depositing oxide thin films.

III. To evaluate the potential of pyrazine to work as a precursor for an organic moiety in the upconverting hybrid thin film. To study the upconversion luminescence properties of the hybrid material fabricated by using the combined atomic and molecular layer deposition technique.

IV. To test the direct particle doping method for preparation of $NaYF_4$:Yb,Er doped fluorophosphate glasses with the composition $(90NaPO_3 – (10 – x)Na_2O – xNaF)$ (mol%) with x = 0 and 10. To study the survival of the particles and the upconversion luminescence of the glasses.

V. To further improve and optimize the direct particle doping method for preparation of $NaYF_4$:Yb,Er doped fluorophosphate glasses with the composition $(90NaPO_3 – (10 – x)Na_2O – xNaF)$ (mol%) with x = 0 and 10.

4. MATERIALS AND METHODS

4.1. Materials and films preparation

4.1.1. Particles preparation

The upconversion luminescence materials ($NaYF_4$:Yb^{3+},Er^{3+} and $NaYF_4$:Yb^{3+},Er^{3+}, Cr^{3+}/Mn^{2+}) were synthetized with the low-temperature co-precipitation method (**I, IV and V**).[92] The RCl_3 (R: Y, Yb or Er) water solutions used in the synthesis were first prepared by dissolving R_2O_3 (99.99 %) in hydrochloric acid (pro analysi, 37 %), vaporizing the excess acid and finally diluting the remained solutions with distilled water to prepare RCl_3 solutions with 0.2 $moldm^{-3}$ concentration (Equation 6). The pH of the final solutions was adjusted to ca. 2. The $MnCl_2$ (pro analysi) and $CrCl_3$ (96 %) were dissolved directly to distilled water to produce solutions with 0.2 $moldm^{-3}$ Mn^{2+}/Cr^{3+} concentration (**I**).

$$R_2O_3(s) + 6\ HCl(aq) \rightarrow 2RCl_3(aq) + 3H_2O(l) \quad (6)$$

In the synthesis of the upconverting particles, NaF (2.1 g, 12.5 Na/R ratio) was first dissolved in 60 cm^3 of distilled water. The solution was stirred with a mixture of prepared chloride solutions with selected dopant concentrations (Yb:17 %; Er:3/0.3; Mn:0.1–0.2 and Cr:0.05–0.2) for 1 h at room temperature (Equation 7). The precipitates formed were centrifuged (8 min, 3766 g) and washed either with distilled water (one time 60 cm^3) and ethanol (99.5 %, three times 20 cm^3) (**I**) or only once with ethanol (**IV and V).** After each washing the solution was centrifuged. The as-formed low temperature cubic form was dried in a vacuum desiccator. The synthetized materials were annealed at 500 ºC for 5 h under a reducing static N_2 + 10 % H_2 gas sphere to obtain the final product with hexagonal form.

$$RCl_3(aq) + 4NaF(aq) \rightarrow NaRF_4(s) + 3NaCl(aq) \quad (7)$$

4.1.2. Films preparation

The thin films were fabricated using ALD (**II**) or ALD/MLD (**III**) techniques. The used ALD reactor was a commercial F-120 (ASM Microchemistry Ltd.) and precursors were a mixed $(Yb,Er)(thd)_3$ (**II**) or $(Y,Yb,Er)(thd)_3$ (**III**) metal precursors

(synthetized as in [211,212]), and ozone (**II**) or pyrazine carboxylate (**III**). Ozone was generated from oxygen (>99.999 %) in an ozone generator (Fischer model 502). The organic precursor was commercial 2,3-pyrazinedicarboxylic acid powder (Sigma Aldrich) (**III**). During the depositions, the precursors were kept in a glass crucible inside the reactor at 130 °C (the metal precursors) and 145 °C (the organic precursor). The reactants were alternately introduced on a substrate in the reactor while nitrogen (>99.999%; Schmidilin UHPN 3000 N_2 generator) worked as a carrier and purging gas. Inside the reactor, a pressure of 2–4 mbar was maintained during the film depositions. The substrates used were Si(100), DuPont polyimide, quartz and nanocellulose. The depositions took place in temperatures of 300 °C (**II**) and 160–275 °C (**III**). The precursor pulse/purge cycles were: 1.5 s $(Yb,Er)(thd)_3$ / 2s N_2 / 2.5 s O_3 /3 s N_2 (**II**) and 1.5 s $(Y,Yb,Er)(thd)_3$ / 2 s N_2 / 2 s pyrazine / 4 s N_2 (**III**).

4.1.3. Glass materials

Upconverting glasses were prepared by a direct particle doping method in which first the glasses were prepared and after the $NaYF_4$:Yb^{3+},Er^{3+} particles were added to the melted glass (**IV,V**). For the preparation of the glasses with the composition $(90NaPO_3 - (10 - x)Na_2O - xNaF)$ (mol%) with x = 0 and 10, a standard melting process was used. In the process, $Na_6O_{18}P_6$ (Alfa-Aesar, technical grade), Na_2CO_3 (Sigma-Aldrich, >99.5%) or NaF (Sigma-Aldrich, 99.99%) were mixed in a quartz crucible and melted at 750 °C for 5 min. Prior to the melting of the glass with x = 0, a heat treatments at 400 °C (**IV**) and 300 °C (**V**) for 30 min were carried out to decompose Na_2CO_3 and evaporate CO_2. After melting the glasses, the upconverting particles were added at lower temperatures. Doping temperatures of 525, 550 and 575 °C and dwell times of 3 and 5 min were tested. 3.75 wgt% (**IV**) and 5 wgt% (**V**) of $NaYF_4$:Yb^{3+},Er^{3+} particles were used. After the dwell time, the glasses were poured onto a brass mold. All the glasses were annealed at 40 °C below the glass transition temperature for 8h in air.

4.2. Characterization

4.2.1. Microscopy techniques

Atomic force microscopy (AFM) was used to investigate the surface morphology of the ALD deposited thin films (**III**). The used AFM instrument was composed of Veeco Dimension 51000 Scanning Probe Microscope, Nanoscope Controller, Digital Instruments, and Nanoscope Analysis 1.5 Software.

The surface morphology and elemental distribution of the thin films (**II**) and the composition of the glasses (**IV**) were analyzed with scanning electron microscopy (SEM). Two setups were used. First included Leo 1530 Gemini microscope equipped with a Thermo Scientific UltraDry SDD EDSsystem (**II**) and the second consisted of Carl Zeiss Crossbeam 540 microscope equipped with Oxford Instruments X-MaxN 80 EDS detector (**IV**). Prior to imaging the glasses, they were polished and coated with a thin carbon layer.

The particle size and shape were studied with transmission electron microscopy (TEM) (**I**). The apparatus had a JEM-1400 Plus Transmission Electron Microscope with a maximum acceleration voltage of 120 kV and 0.38 nm resolution.

4.2.2. X-ray powder diffraction

The phase purities and crystal structures of the $NaYF_4$:Yb,Er-materials (**I**) were analyzed with the X-ray powder diffraction (XPD) measurements. The XPD-patterns were collected using a Huber G670 image plate Guinier camera (2θ range: 4–100°, data interval: 0.005°). The measurement was carried out at room temperature and the monocromatic copper $K_{\alpha 1}$ radiation (λ: 1.5406 Å) was used. The time for data collection was 30 min.

4.2.3. X-ray reflectivity and grazing incident x-ray diffraction

The film thickness, density and roughness values were determined from X-ray reflectivity (XRR) and the crystallinity of the thin films were studied with grazing incident X-ray diffraction (GIXRD) (**II, III**). The instrument was Panalytical X'Pert MPD Pro Alfa 1 with the XPERT HighScore Plus-reflectivity software for the data analysis.

4.2.4. X-ray fluorescence

The materials compositions were studied with X-ray fluorescence spectroscopy (XRF) (**I, II and III**) using two different instrumentations. The $NaYF_4$:Yb,Er-materials (**I**) were measured with the PANalytical epsilon 1 apparatus (Ag tube with Εκα: 22.1 keV) with its internal Omnian calibration. The thin films were characterized with PANalytical AxiosmmAX with Rh tube (K_α: 20.2 keV), 3 kW model (**II, III**).

4.2.5. Thermal analysis

The thermal analysis of the $NaYF_4$-materials (**I** and additional data for **IV** and **V**) was carried out with a TA instruments SDT Q600 Simultaneous thermogravimetry and differential scanning calorimetry (TGA-DSC) apparatus between 25 and 720 °C in a flowing N_2 gas sphere with a flow rate 100 cm^3min^{-1} and a heating rate 5 °$Cmin^{-1}$. The sample pan was made of aluminium oxide and a similar empty pan was used as a reference.

The thermal behavior of the glasses **(IV, V**) were studied using differential thermal analysis, DTA with Netzch Jupiter F1 apparatus at a heating rate of 10 °$Cmin^{-1}$. The samples were measured in Pt crucibles. The first derivative of the DTA curve was used as the inflection point of the endotherm which was used to determine the glass transition temperature T_g. The onset of the crystallization temperature T_x was ascertained from the beginning of the crystallization feature, and peak of the exotherm, respectively. The temperature accuracy was ±3 °C.

4.2.6. FT-IR spectroscopy

Fourier transform infrared spectroscopy (FTIR) was used to confirm the organic content of the hybrid thin films and to study the bonding scheme (**III**). Nicolet Magna-IR Spectrometer 750 was used with an average of 32 scans and 4 cm^{-1} resolution.

The IR spectra of the glasses were measured with Perkin Elmer Spectrum One FTIR Spectrophotometer in Attenuated Total Reflectance (ATR) mode in the range of 600–1600 cm^{-1} (**V**). Corrections for Fresnel losses were made for the spectra along with normalization to the band having maximum intensity. An average of 8 scans and a resolution of 1 cm^{-1} was used.

4.2.7. Raman spectroscopy

The Raman spectra of the glasses was measured using a 532 nm wavelength laser (Cobolt Samba), a 300 mm spectrograph (Andor Shamrock 303) and a cooled CCD camera (Andor Newton 940P) (**V**). All the spectra were normalized to the band showing the maximum intensity.

4.2.8. Reflection, absorption and transmission

Illumination from a 60 W incandescent light bulb was used with the reflectance measurements of the $NaYF_4$-materials (**I**). The bulb was located 20 cm above the sample and the reflectance of the light was collected with an optical fiber with diameter of 600 µm. The reflectance spectra were recorded with an Avantes AvaSpec-2084x14 spectrometer using a data collection time of 400 ms.

UV-visible absorption spectroscopy was used for the hybrid thin films characterization (**III**). The UV/VIS/NIR absorption spectrometer was PerkinElmer Lambda 950.

The transmission spectra of the polished glasses were recorded in the range of 200–700 nm (**IV**) and 200–1600 nm (**V**) at room temperature. The latter range was used also for the collection of the absorption spectra (**V**). A Shimadzu UV-3600 Plus UV-VIS-NIR Spectrophotometer was used.

4.2.9. Density and viscosity measurements

Archimedes principle was utilized with the density measurements of the glasses (**V**). Ethanol was used as the immersion liquid. The accuracy of the measurement is ±0.02 g/cm^3.

The viscosity of the glasses was measured with a beam-bending viscometer (BBV) in the (Log11–Log13 Pa s) range (**V**). The measurement was conducted under the test protocol ASTM C-1351M. 4 x 5 x 50 mm bars of the glass with x = 0 was used. A parallel-plate viscometer (Model PPV-1000 following the test protocol ASTM C-1351M) was used to measure the glass viscosity in the softening range (Log5–Log 8 Pa s). The measured glasses with x = 0 and x = 10 were prepared in disk with diameter of 10 mm and a thickness of 5 mm.

4.2.10. Upconversion luminescence and lifetimes

The upconversion luminescence of the $NaYF_4$-materials (**I**) was measured with an Ocean Optics PC2000-CCD spectrometer at room temperature. A capillary tube filled partially with the studied material was placed in a sample holder in which the excitation and the emission paths had a 90° angle. A Hamamatsu L9418-04 NIR laser diode (λ_{exc}: 976 nm; V: 0,246 cm^{-1}) was used for the excitation. The emission was directed to the detector using an optical fiber with diameter of 200 µm. A long-pass filter with a cutoff at 850 nm (RG850, Edmund Optics) was used in the excitation path. In the emission light path, a short-pass filter (an extended hot mirror,

Edmund Optics) was used to exclude the scattered excitation radiation. The excitation and emission radiation were focused with lenses.

The upconversion luminescence of the thin films (**II**, **III**) were measured with an Avaspec-HS-TEC CCD spectrometer at room temperature. The materials were excited with an Optical Fiber Systems IFC-975-008 NIR laser (6 W; λ_{exc} = 974 nm). The angle between the excitation and the emission paths was 90° and different angles between the laser beam and the film was tested. The spectra of the oxide film (**II**) was measured at 60° and the power dependency of the same film at 20° angle. An optical fiber (diameter: 600 µm) was used to direct the emission to the detector. In the excitation path, a long-pass filter (Newport 10LWF-850-B) was used, and in the emission path, a short-pass filter (Newport, 10SWF-900-B) was used. Lenses were used to focus the excitation and emission radiation.

Two different set ups were used to measure the upconversion luminescence of the glasses. First, the glasses (**IV**) were ground and placed in a capillary tube and the upconversion luminescence was measured with an Avantes AvaSpec-2048 × 14 CCD spectrometer and an Optical Fiber Systems IFC-975-008 NIR laser (6 W; λ_{exc} = 974 nm). The optical fiber (diameter: 600 µm) directing the emission to the detector was attached to the sample container at 90° angle to the excitation. The system had a long-pass filter (Newport 10LWF-850-B) and a short-pass filter (Newport, 10SWF-900-B) in the excitation and emission paths, respectively. Focusing lenses were also used in both paths. All the materials were measured at room temperature.

The other set up used for the upconversion measurements contained of a monochromator (Digikrom, DK480) and a lock-in amplifier (Stanford Research Systems, SR830) equipped with a TEC-cooled silicon photodiode. The glasses (**V**) were excited with a TEC-cooled fiber coupled multimode laser (II-VI Laser Enterprise, λ_{exc}: ~980 nm, incident power on sample 23.5 mW). The materials were measured at room temperature. A short-pass filter (Thorlabs, FES800) was used in the emission path. The excitation spot size was estimated to be at least 100 mm in diameter.

The upconversion luminescence lifetimes of the glasses (**V**) were measured at room temperature with a Newport 5060 laser driver and Optical Fiber Systems IFC-975-008 laser (6 W; λ_{exc} = 974 nm). A long-pass filter (Newport 10LWF-850-B) and a short-pass filter (Newport 10SWF-850-B) were used in the excitation and emission paths, respectively. The excitation and the emission paths had a 90° angle. The emission was directed into a photomultiplier tube (Hamamatsu R1465) and collected

at 544 nm and 650 nm by using band-pass filters (Thorlabs band-pass filter FL543.5-10 and Thorlabs band-pass filter FB650-10). The excitation power range was from 1000 mV to 9000 mV. The excitation pulse duration was 50 ms and a delay of 50 ms was used before the next excitation pulse. One measurement contained 1000 pulse-delay cycles.

5. RESULTS AND DISCUSSION

5.1. Effect of transition metal doping on upconversion luminescence

The use of UC materials in solar cells have one major drawback which is the efficiency issue. The first aim of this research was to investigate the possibility to enhance the upconversion luminescence by an additional ion doping. The effect of transition metal (Mn and Cr) doping on the properties of upconversion materials were studied (**I**). As the host material, $NaYF_4$ was chosen due to the excellent properties for upconversion luminescence. As the emitter, the Er^{3+} activator was used together with the Yb^{3+} sensitizer. The materials were synthetized using the co-precipitation method at room temperature as described above, in sections 2.1.5 and 4.1.1. The simplicity of the method and the relatively cheap and fast procedure were the reasons for the choice of the synthesis.

5.1.1. Crystal structure, phase purity and morphology

As discussed in section 2.1.1., the $NaYF_4$ host lattice has three possible crystal structures which are the low-temperature cubic (the α-form), the hexagonal (β) and the high-temperature cubic. To study the possible effect of transition metal doping on the phase transition temperature of the material, thermal analysis was carried out. The DSC curves of the prepared materials show the irreversible phase transitions at 350–450 °C and 670 °C (Fig. 14.). The temperature of the transition from the low-temperature cubic to the hexagonal phase is about 70 °C lower with the Cr or Mn co-doped materials than with the $NaYF_4$:Yb,Er material. Thus, the decrease in the transition temperatures suggest that co-doping with either Mn or Cr enables the preparation of the hexagonal material with lower temperature. The Cr and Mn co-doped materials have very similar phase transition temperatures, therefore, the crystallinity can be assumed to be very similar between the materials.

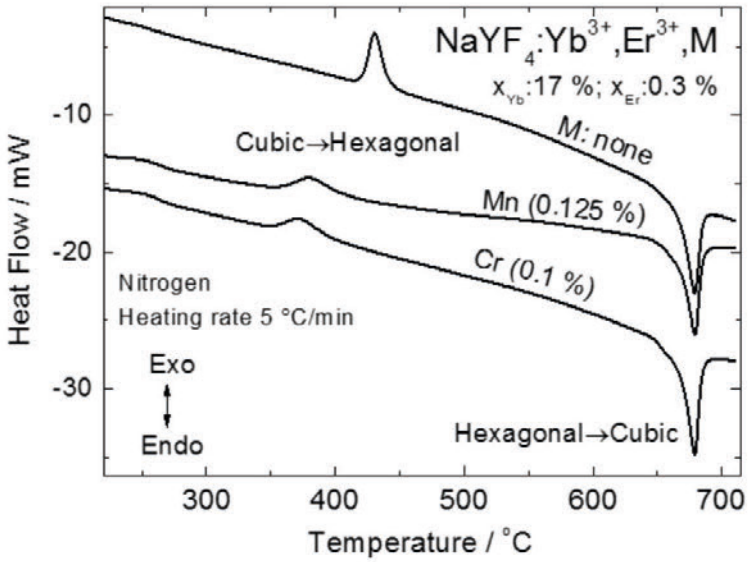

Fig. 14. The DSC curves of the Mn and Cr co-doped and non-co-doped $NaYF_4$:Yb,Er materials. [**I**]

The XPD patterns show that the studied materials have the hexagonal structure without detectable impurities, such as NaF and RF_3 (strongest reflections at 2θ: 39° and 27-34°, respectively) (Fig. 15). The crystallite size could not be estimated from the XPD patterns with the common Scherrer equations which indicates that the sizes are larger than 150 nm. Therefore, TEM images were used to estimate the sizes to rule out the possible size effect on the upconversion luminescence intensity. All materials have very similar morphology and sizes (ca. 250 nm) (Fig. 15). In addition, the crystallites are aggregated in all of the materials. The presence of Mn and Cr was confirmed with XRF measurements and the results of the best upconverting materials are listed in Table 2. The results reveal that the Mn co-doped material has less Er^{3+} than the others which indicates weaker upconversion luminescence.

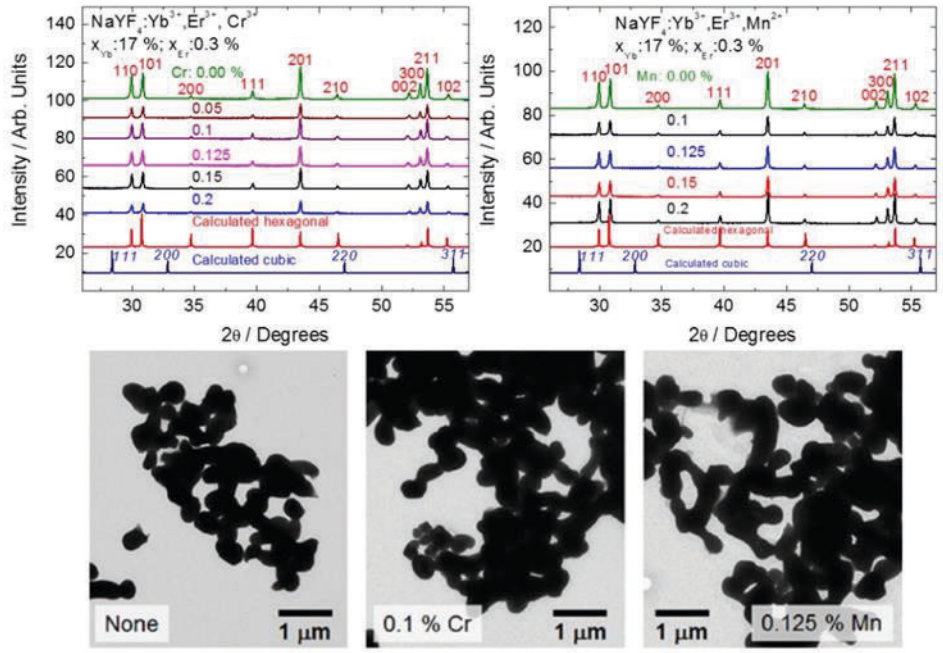

Fig. 15. XPD patterns for materials with Cr (top, left) and Mn (top, right) and TEM images (bottom) of the selected materials. [**I**]

Table. 2. XRF results showing the rare earth and d transition metal contents (mol-%) of the best upconverting materials. [**I**]

Material	Y	Yb	Er	Cr or Mn
$NaYF_4:Yb^{3+},Er^{3+}$	76.9	22.2	0.8	-
$NaYF_4:Yb^{3+},Er^{3+}$,Cr (0.1%)	77.0	21.9	0.7	0.3
$NaYF_4:Yb^{3+},Er^{3+}$,Mn (0.125%)	78.3	20.9	0.4	0.3

5.1.2. Upconversion luminescence

The typical green and red emissions of Er^{3+} are obtained with 976 nm excitation (Fig. 16). The significantly strongest upconversion luminescence intensity is observed with the material co-doped with 0.1 % of Cr. The other studied Cr concentrations result in weaker upconversion luminescence when compared to the non-co-doped material. All tested Mn concentrations clearly weakens the upconversion luminescence intensity. As mentioned above, the XRF results show that the Mn-doped material contains less Er^{3+} than the other materials which is the probable cause of the weak upconversion luminescence.

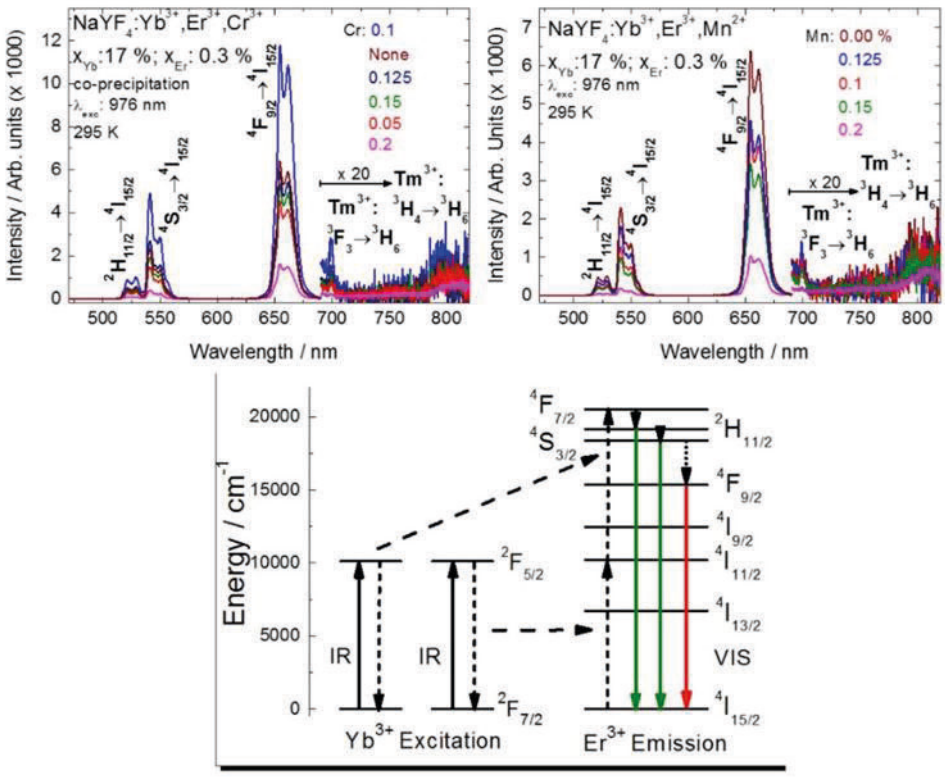

Fig. 16. Upconversion luminescence spectra of the Cr/Mn co-doped materials (above [**I**]) and the UC mechanism (below).

The excitation power densities have no effect on the relative upconversion luminescence enhancement or suppression that appear with the Cr and Mn co-doped materials. This means that the effect strengthens when the power density increases. The pump excitation power density measurements suggested that the upconversion luminescence may be obtained with lower power densities when Cr doping is used. However, the absolute lower limit for obtaining upconversion could not be determined due to the limitation of the measurement system. The materials capable of upconversion luminescence with low excitation power densities are highly desirable because the power of solar radiation on Earth is only about 0.1 W/cm^2.[213]

5.1.3. Reflectance

The obvious reason behind the enhancement of the upconversion luminescence intensity with the Cr co-doped material would be the ability of chromium to absorb the excitation energy and transfer it to either Er^{3+} or Yb^{3+}. However, Cr is expected to be in the trivalent form because in the $NaYF_4$ lattice it will probably replace Y^{3+}. Moreover, the lattice has similar structure than the CaF_2 which suggest that the $NaYF_4$ is strong enough not to allow Cr to have any levels below 12500 cm^{-1} (800 nm). This means that the reason for the enhanced upconversion luminescence is in somewhere else than in the absorption of Cr. The reflectance spectra of $NaYF_4$ materials either tridoped (Y, Er, Cr) or single doped (Cr) shows that the single doped materials have only absorption below 750 nm (Fig. 17). This confirms the absence of the energy levels close to 1000 nm. This means that the mechanism behind the enhancement of the upconversion luminescence caused by Cr co-doping needs further investigations which are beyond this PhD research.

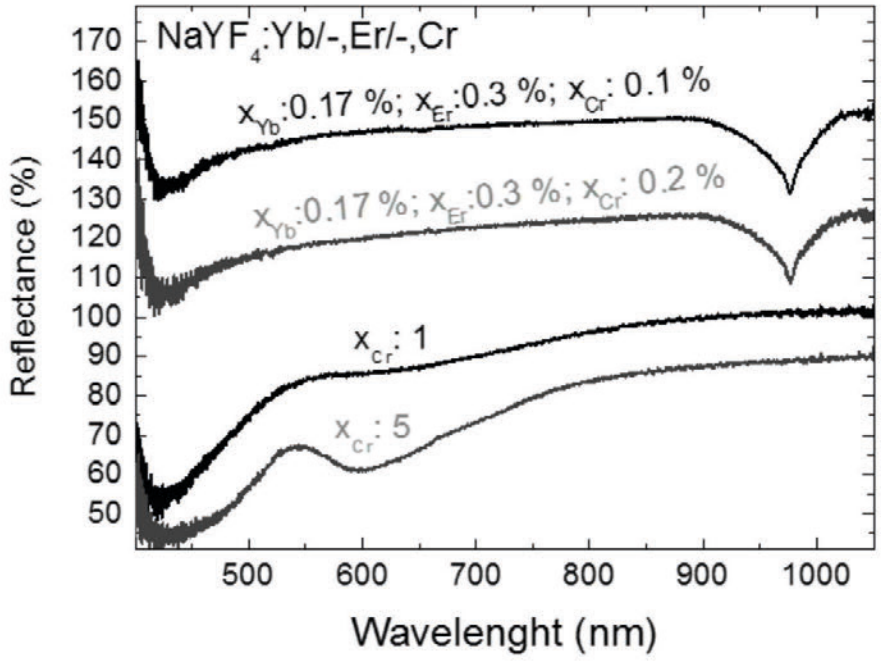

Fig.17. Reflectance spectra of selected Cr co-doped materials [**I**].

5.2. Upconverting thin films

UC thin films in solar cells have been constructed either by using UC powder materials or preparing the UC materials directly as films, as discussed in section 2.1.5. Nevertheless, no single method seems to be superior. ALD and MLD techniques have excellent properties such as conformity, thickness and composition control and repeatability which are ideal for larger scale production. One aim of this study (**II, III**) was to investigate the possibility to use the ALD and the combination of ALD and MLD techniques in upconverting film fabrication.

5.2.1. $(Yb,Er)_2O_3$ thin films

The procedure for oxide film fabrication with ALD has been known for some time, but the luminescence properties of these films have rarely been studied. In this research (**II**), the upconversion luminescence of oxides co-doped with Yb and Er was investigated. The idea behind the dopant choice was to maximize the absorption in the NIR range and thus the yttrium was not incorporated.

The oxide film deposited with 2000 ALD cycles was polycrystalline material based on the grazing incidence x-ray diffraction pattern (Fig. 18). The GIXRD pattern shows also the cubic C-Ln_2O_3 structure. The XRR pattern was used to characterize the film thickness (39 nm), roughness (1 nm) and density (9.2 gcm^{-3}). The growth-per-cycle (GPC) value is 0.195 Å and it was calculated from the film thickness value.

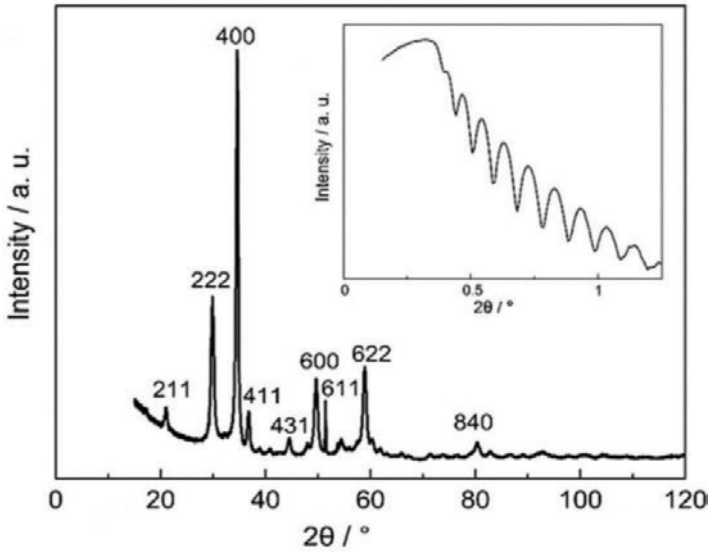

Fig. 18. Indexed GIXRD and XRR patterns [**II**].

The Er/(Yb + Er) ratio for the studied thin film is 0.018 and it was calculated from XRF results. Similar ratio can be calculated for the $(Yb_{0.97}Er_{0.03})(thd)_3$ precursor which suggests that the Er-to-Yb substitution level is close to the desired 3 % level. The SEM-EDX elemental maps show that the elemental distribution of Yb, Er, O and Si is quite homogeneous (Fig. 19 a) and the combined map for Yb and Er reveals that the Er occupies areas with lowered Yb content (Fig. 19 b).

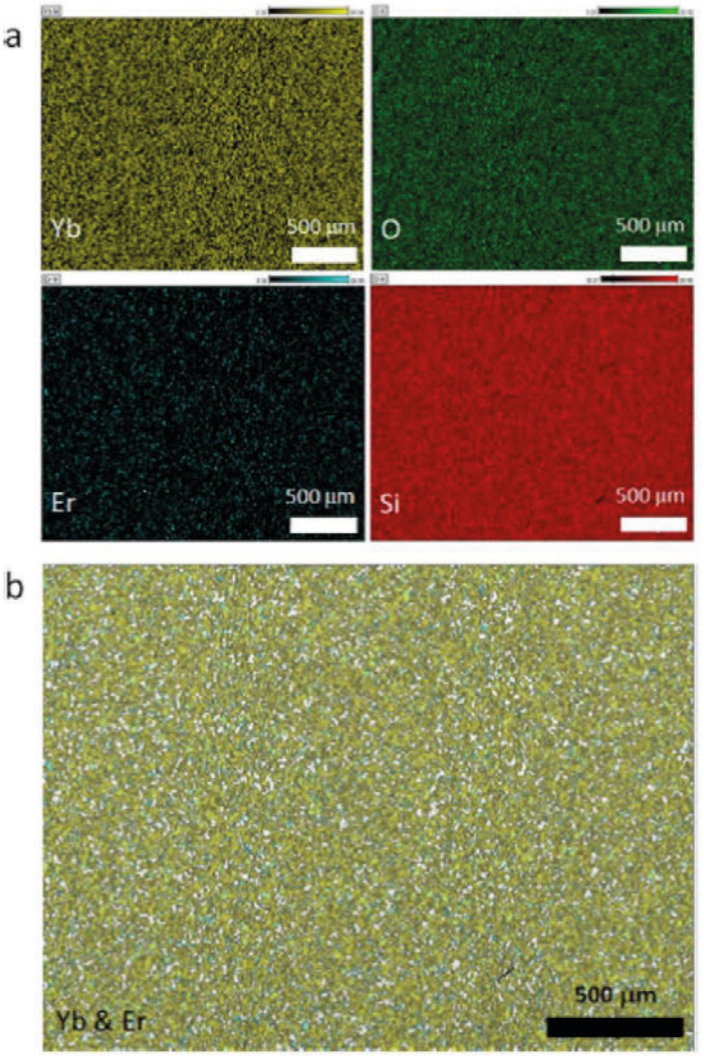

Fig. 19. SEM-EDX elemental maps for Yb, Er, O and Si (a) and combiner elemental maps for Yb and Er (b). [**II**]

The 39 nm thick $(Yb_{0.97}Er_{0.03})_2O_3$ thin film shows the strongest upconversion luminescence intensity (Fig. 20) and is therefore selected for the further characterization. The film with 0 % Er stands for the thin film which was prepared only with Yb. The weak emission detected from this material is due to ppm level impurity concentration of Er always present in materials containing Yb. The selected film shows the green and red upconversion emissions of Er^{3+} with 974 nm excitation (Fig. 20). The pump power dependence of the upconversion luminescence intensity is represented in the log-log graph (Fig. 20) and the slope of the lines are close to 2 which indicates that the both processes need two photons.

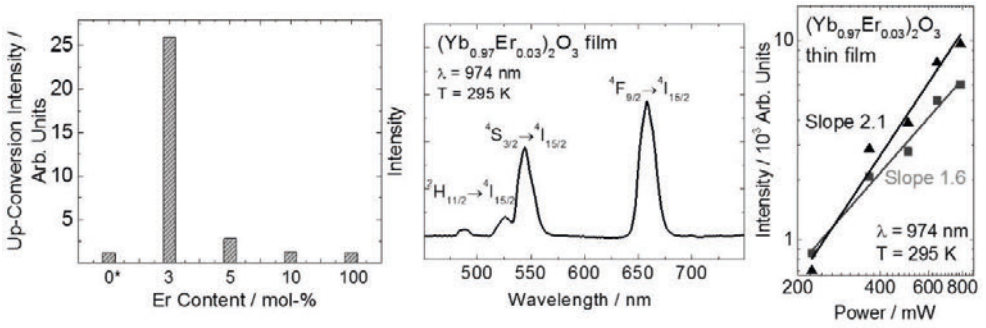

Fig.20. Upconversion luminescence characterizations. The total upconversion intensity with different Er content (left), the upconversion luminescence spectrum of the selected $(Yb_{0.97}Er_{0.03})_2O_3$ thin film (middle) and the pump power dependence of the green and red upconversion emissions of the studied thin film (right). [**II**]

5.2.2. Molecular hybrid thin films with upconversion luminescence

The combination of ALD and MLD techniques enables the fabrication of completely new kind of materials which cannot be made by using any other method. This possibility offers a way to prepare new type of inorganic-organic hybrid materials capable of upconversion luminescence. Combining strong lanthanide emitter with efficient organic absorber could also enable the upconversion luminescence enhancement. Moreover, thin film structure may prevent luminescence quenching effects detected with complexes in aqueous media.

Combining the ALD with the MLD technique enabled the formation of the hybrid inorganic-organic thin films of the complex in which Y^{3+}, Yb^{3+} and Er^{3+} ions were used together with pyrazine (**III**). The pyrazine has shown to form stable complexes[214] and metal-organic frameworks[148] with lanthanides. Therefore, it was selected as the ligand for the (Y,Yb,Er) complex. The films were mainly prepared on silicon substrates but also deposition on quartz, and flexible polyimide and nanocellulose substrates were studied.

The (Y,Yb,Er)-pyrazine thin films were grown using (Y,Yb,Er)(thd)$_3$ (thd: 2,2,6,6-tetramethyl-3,5-heptanedione; Fig. 21) and pyrazinedicarboxylic acid as precursors. The ALD/MLD process worked ideally with deposition temperature of 160 °C and the growth-per-cycle remained constant and independent of the precursor pulse lengths, and the increase of the film thickness was linear when ALD/MLD cycles were increased. In addition, deposition temperatures up to 280 °C were investigated. GIXRD results suggested that the films were amorphous up to 250 °C and some crystallinity could be observed when the deposition temperature was raised up to 275 °C. With GPC value of 3.4 Å/cycle ca. 20–50 nm thick films were deposited and these films were further investigated. The chemical state of the hybrid thin films was studied using FTIR and the data was used to propose a possible bonding scheme which is represented in Fig. 21.

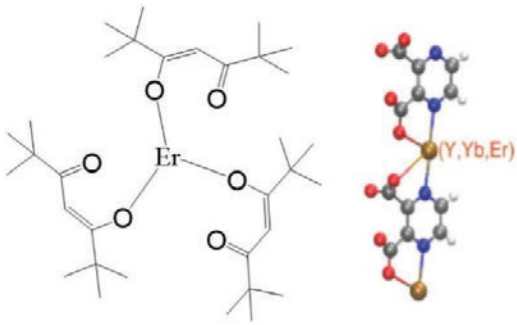

Fig. 21. Schematic representation of the precursor Er(thd)$_3$ (left) and the possible bonding of the (Y,Yb,Er) – pyrazine -thin film (right) [**III**].

The upconversion luminescence efficiency of the complexes depends on the amount of the quenchers surrounding the emitter. Thus, the upconverting material needs to be placed in an environment free of quenchers or the emitter ions needs to be protected from the quenchers. In addition, the upconversion luminescence with sensitizer requires a close-distance between the sensitizer and activator (or i.e. donor and acceptor, respectively) and long enough lifetimes of the sensitizers' excited states to ensure the efficient energy transfer. These basic requirements for upconversion luminescence appears to be fulfilled with the deposited thin films of the (Y,Yb,Er) complex that showed the green, red and blue upconversion emission colors under 974 nm excitation (Fig. 22). The emissions are due to the $^2H_{11/2}$,$^4S_{3/2}\rightarrow{}^4I_{15/2}$; $^4F_{9/2}\rightarrow{}^4I_{15/2}$; $^2H_{9/2}\rightarrow{}^4I_{15/2}$ transitions of Er^{3+}, respectively.

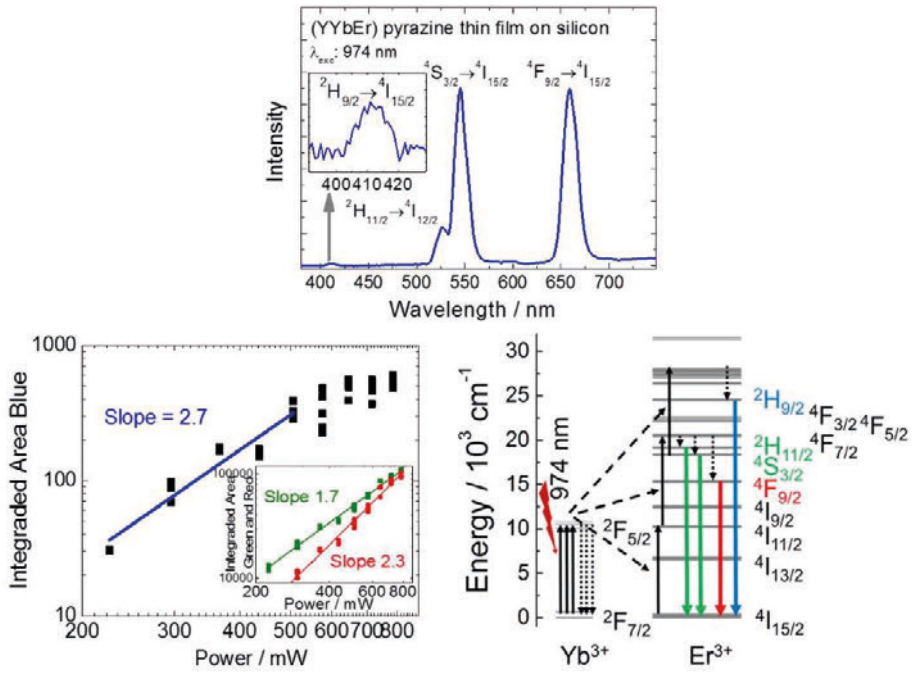

Fig.22. The upconversion luminescence of the (Y,Yb,Er) – pyrazine -thin film (top), the log-log dependency between the intensity and the pump power (bottom, left) and the upconversion mechanism for Yb-Er (bottom, right). [Adapted from **III**]

The upconversion emission requiring the stacking of three photons of hybrid inorganic-organic materials is rarely reported, and therefore, the appearance of the blue emission with the (Y,Yb,Er)-pyrazine thin films is a unique feature. The reason for the infrequency of the blue emission is probably that the blue emission is a three-phonon process, thus, the probability of the blue emission is lower than the two-phonon processes such as the green and red emissions. In addition, molecular complexes have ligands that may act as quenchers in the system.

Thin films with different thicknesses from 20 to 50 nm were deposited on silicon substrate and the effect of the film thickness on the upconversion luminescence was studied. All the films showed the green and red upconversion luminescence under 974 nm excitation and the upconversion intensity was found to be independent of the film thickness between the studied thickness range.

As discussed in the section 2.1.3, upconversion luminescence intensity has an exponential dependency on excitation pump power which enables the study the upconversion process. The upconversion intensity of the hybrid thin films was

measured using different pump excitation powers. In addition, a few spectra per each pump power was measured using different cooling powers for the laser due to the temperature dependence of the excitation wavelength. The log-log dependence between the intensity and the pump power is represented in the Fig.20. The slope of the blue emission (2.7) indicates three photon process, as expected. The slope for the green emission (1.7) indicates two photon process and the slope for the red emission (2.3) may refer to two or three photon process.

5.3. Upconversion from fluorophosphate glasses

As a host for upconverting material, glasses offer flexibility to the UC solar cell design as they can be placed on the top of the cell due to the transparent nature. Properties such as high solubility for rare earth ions and relatively low glass transition temperature make phosphate glasses ideal hosts for upconverting rare earth ions.

Before selecting the glass composition, the suitable doping temperature for the $NaYF_4$:Yb,Er particles was investigated. In the literature, the evaporation of the $NaYF_4$ particles and the melting of NaF has been reported to occur above 750 °C[215] which indicates that the suitable doping temperature is below this temperature. To confirm the convenient doping temperature, thermal analysis was carried out for the β-$NaYF_4$:Yb,Er material used for doping the glasses (Fig. 23.). The DSC curve shows the endothermic signal at ca. 675 °C which is due to the structural change from hexagonal to high temperature cubic phase. Because the hexagonal phase of the $NaYF_4$:Yb,Er material show extremely stronger upconversion luminescence than the cubic phase, the particles doping temperature needs to be lower than 675 °C to avoid the phase change. The DSC curve shows also an endothermic signal around 600 °C which has remained unidentified. However, the presence of amorphous NaF and/or its reaction with non-stoichiometric $NaRF_4$ have been suggested as tentative attributions for the signal.[216]

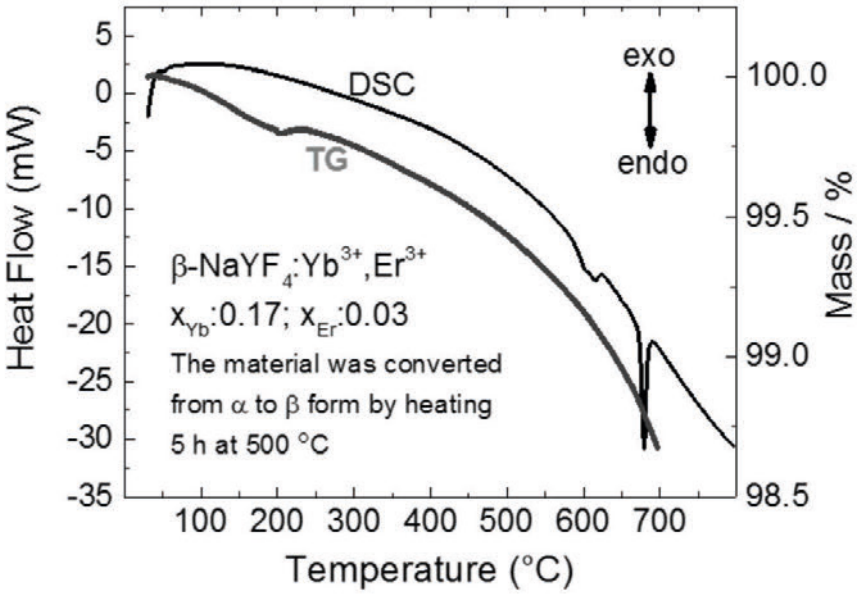

Fig.23. Thermal analysis of beta-$NaYF_4$:Yb,Er.

The fluorophosphates glasses with the composition ($90NaPO_3$ – $(10 – x)Na_2O$ – xNaF) (mol%) with x = 0 and 10 were chosen as the glass host for the $NaYF_4:Yb^{3+},Er^{3+}$ particles due to low melting temperature (750 °C) and good thermal properties, such as stability against crystallization (Table 3). After finding the good host glass, different parameters for particles doping were investigated starting with the doping temperature of 575 °C (T_d) and the dwell time of 3 min (**IV**), and continuing the optimization with different doping temperatures and dwell times (**V**) (Table 4).

Tabale 3. Thermal properties of the fluorophosphate glasses ($90NaPO_3$ – $(10 – x)Na_2O$ – xNaF) (mol%).

x	T_g (°C) (± 3 °C)	T_x (°C) (± 3 °C)	$\Delta T = T_x – T_g$ (°C) (± 6 °C)
0	284	374	90
10	246	356	110

Table 4. Investigated parameters for the preparation of the fluorophosphate glass ($90NaPO_3 – (10 – x)Na_2O – xNaF$) (mol%) doped with $NaYF_4$:Yb^{3+},Er^{3+} particles (NP).

x	NP wt%	doping temperature, T_d / °C	dwell time / min	publication
0	3.75	575	3	IV
0	5	525	3	V
0	5	525	5	V
0	5	550	3	V
0	5	550	5	V
0	5	575	3	V
0	5	575	5	V
10	3.75	575	3	IV
10	5	525	3	V
10	5	525	5	V
10	5	550	3	V
10	5	550	5	V
10	5	575	3	V
10	5	575	5	V

Former studies[217,218] suggested that elements of the particles can diffuse from the particles into the glass during the glass preparation. Thus, the survival of the upconverting particles was investigated by first measuring the upconversion luminescence spectra of the $NaYF_4$:Yb,Er containing glasses with x = 0 and 10 (**IV**). The glasses showed the green and red emissions of Er^{3+} due to the $^2H_{11/2}$,$^4S_{3/2}\rightarrow{}^4I_{15/2}$ and $^4F_{9/2}\rightarrow{}^4I_{15/2}$ transitions, respectively (Fig. 24). The upconversion luminescence intensity of the glass with x = 10 was stronger than of the glass with x = 0. Next, samples with known concentrations of $NaYF_4$:Yb,Er particles were prepared and the upconversion spectra were measured. Finally, the upconversion intensities of the green emission at 550 nm of the prepared samples (Fig. 24) was compared with the intensities of the glasses. This indicated that only 5 and 20 % of the particles survive in the glass with x = 0 and 10. Such low percentages of survived particles clearly brought out the importance of further optimization of the direct particles doping method.

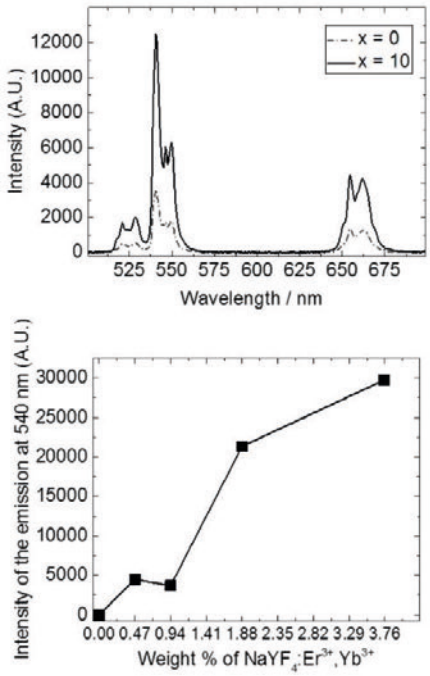

Fig. 24. UC-spectra (top) and UC intensities of green emission at 550 nm of the samples with known $NaYF_4$:Yb,Er concentration (bottom). [**IV**]

5 wt% of $NaYF_4$:Yb,Er material was added in the glasses and different doping parameters were tested (Table 4) (**V**). The glasses are labelled as (T_d - dwell time). During the glass preparation, the glass with x = 0 had too high viscosity at the doping temperature of 525 °C and it could not be quenched. The pictures of the glasses (x = 0 or 10) under daylight and excitation (980 nm) revealed that the upconversion luminescence was obtained with higher doping temperatures with x = 0 than with x = 10 (Fig. 25 and 26). This is in agreement with the changes in the thermal properties of the glasses when Na_2O is replaced by NaF. Such changes are decrease in glass transition (T_g), the onset of crystallization (T_x) and the peak of crystallization (T_p) temperatures as well as the shift of the viscosity to the lower temperatures. In addition, the upconversion luminescence intensity seems to decrease in both glass systems with longer dwell time and increasing doping temperature. The pictures show also that some of the glasses have agglomerates of the particles which reduce the degree of dispersed particles in the glass. However, the (550 - 3) glass with x = 10 appears to be agglomerate-free.

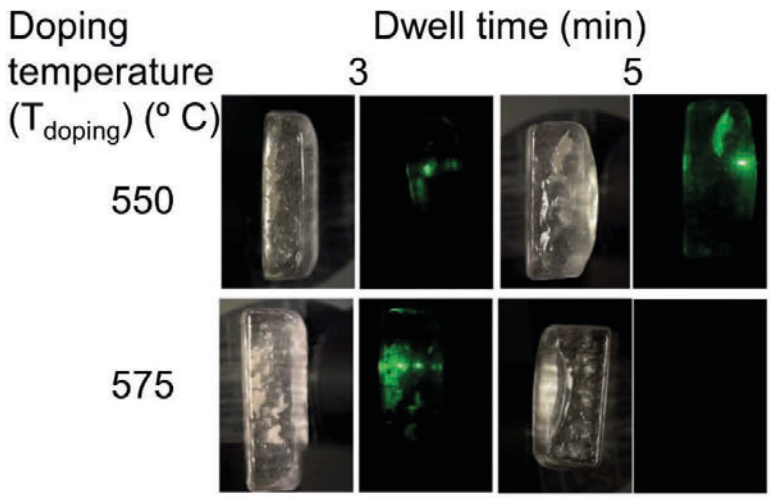

Fig. 25. Pictures of the glasses doped with $NaYF_4$:Yb^{3+},Er^{3+} material in daylight and under excitation at 980 nm. The composition of the glasses were ($90NaPO_3$ – $(10 – x)Na_2O$ – xNaF) with x = 0. [**V**]

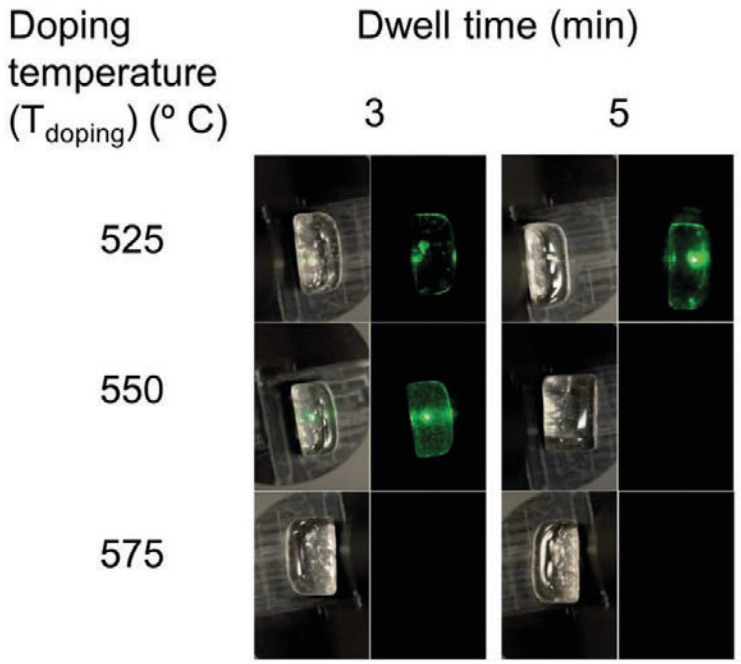

Fig. 26. Pictures of the glasses doped with $NaYF_4$:Yb^{3+},Er^{3+} material in daylight and under excitation at 980 nm. The composition of the glasses were ($90NaPO_3$ – $(10 – x)Na_2O$ – xNaF) with x = 10. [**V**]

In the publication (**V**), four main factors influencing the upconversion luminescence intensity are discussed. Those factors are 1) the thermal stability of the $NaYF_4$:Yb,Er particles, 2) the temperature of the glass melt at the point of adding the particles, 3) the viscosity of the glass melt, and 4) the homogeneity of the dispersion of the particles in the glass. These factors may account for the differences between the upconversion luminescence results of the investigated glasses. The glasses showed the green and red emissions of Er^{3+} (Fig 27). The spectra of the glasses exhibit distinct fine structure which indicates the presence of crystalline $NaYF_4$:Yb,Er. Moreover, the spectra show that an increase in doping temperature and dwell time leads to decreased upconversion luminescence intensity of both green and red emissions. This may due to the lack of the thermal stability of the $NaYF_4$:Yb,Er particles (factor 1) when increasing the T_d and dwell time. This lack is caused by the change from the hexagonal to the high temperature cubic form of the $NaYF_4$:Yb,Er.

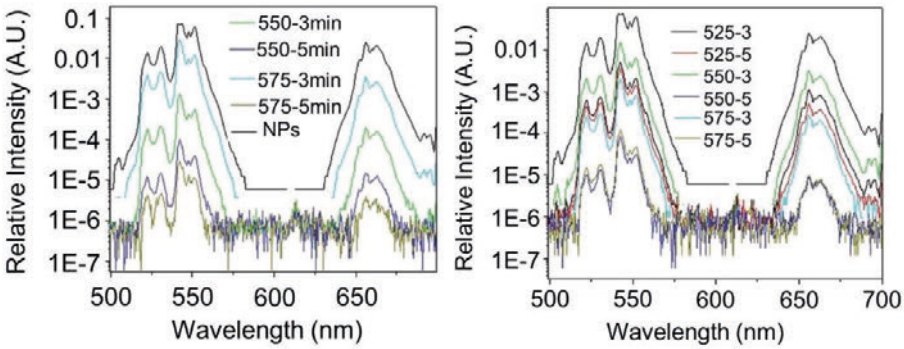

Fig. 27. The upconversion luminescence spectra of the glasses with x = 0 (left) and x = 10 (right). The glasses with composition ($90NaPO_3 – (10 – x)Na_2O – xNaF$) were doped with $NaYF_4$:Yb^{3+},Er^{3+} material. [**V**]

The upconversion luminescence lifetimes of the green and red emissions show indications of the corrosion of the $NaYF_4$:Yb,Er particles (Fig.28). During the heating, the corrosion of the nanoparticles may either occur uniformly or change the composition of the particles. For the x = 0 glass, the green emission lifetime decreases when the T_d and dwell time increase which suggests the occurrence of the homogeneous corrosion. For the x = 10 glass with 3 min dwell time, the green emission lifetime increases when the T_d increases from 525 to 550 °C which indicates that the Er^{3+} concentration decreases. The lifetimes of the red emissions were more difficult to explain. Nevertheless, the lifetimes seem to decrease when the particles are incorporated into the glass.

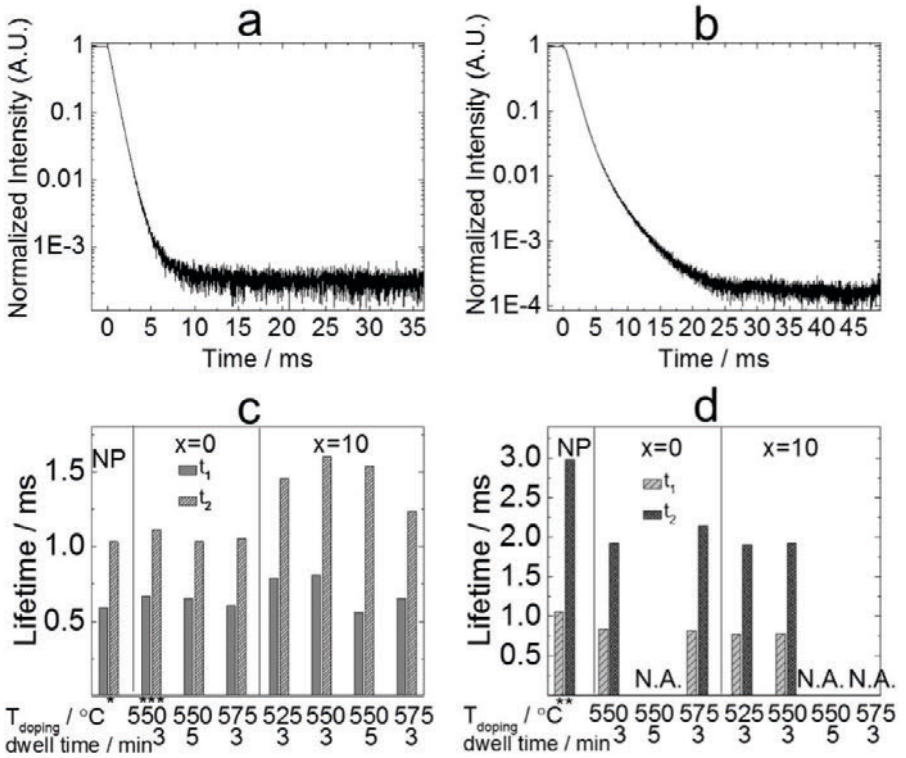

Fig. 28. Decay curves of the $NaYF_4:Yb^{3+},Er^{3+}$ material for green (a) and red (b) emissions, and the lifetimes of the green (c) and red (d) upconversion emissions of the material (NP) and the glasses. All materials were excited at 975 nm with a 0.9 V voltage (except *0.1 V, **0.2 V and ***0.5 V). N.A. refers to cases in which the signal intensity was too low to be measured.

6. CONCLUSIONS AND OUTLOOK

Due to the possibility to exploit the IR region, the upconverting materials offer a promising alternative to solar cell enhancement. These materials can be used in many different solar cells from amorphous and crystalline silicon to organic solar cells. The materials may be introduced into the solar cells in different ways. They can be added into the glass layer which can be placed on the top of the cell or they can be added as an extra layer on the r side of the cell. However, no upconverting layer fabrication method has shown to be superior. The direct particle doping method for luminescent glasses offers the possibility to use the efficient crystalline upconverting materials in solar cells. Alternatively, the atomic layer deposition technique enables the fabrication of thin films with high quality and this technique has already proven its potential in industry and research field. Both methods were studied in this thesis work.

Another challenge in utilizing the whole potential of the upconverting materials is in the rather weak efficiency of the IR conversion to visible especially when considering the use of upconverting thin films or nanomaterials. For crystalline materials, the change in the crystal field around the doped lanthanide may lead to enhancement of the upconversion luminescence. The possibility to improve the upconversion luminescence intensity of crystalline fluoride material by an addition of metal ions were studied in this research. Moreover, a combination of an efficient IR harvester and a strong upconverting ion can enhance the upconversion efficiency. This harvester may be an organic moiety which can be combined with lanthanide upconverter ions by using the combination of atomic and molecular layer deposition techniques. This possibility was also investigated.

The main conclusions based on the publications are:

First, the possibility to improve the upconversion luminescence intensity of Yb/Er -doped fluoride material was studied by transition metal (Cr and Mn) co-doping (**I**). Cr co-doping improved the upconversion luminescence intensity whereas the Mn co-doping was observed to weaken the luminescence. The upconversion luminescence measurements with different power densities suggested that upconversion may be obtained with lower power densities when Cr doping is used. The most possible cause for the weaker luminescence with Mn addition was the lack of Er in the materials when compared to the material doped with only Yb and Er. The results gave no hint for the mechanism behind the enhancement by Cr co-doping and the more detailed research of the mechanism remained beyond this thesis work.

Nevertheless, the future investigations could focus on discovering the possibility of Cr to introduce into the lattice which would be easier to detect with higher concentration of Cr.

Second, the possibility to use ALD (**II**) and ALD/MLD (**III**) techniques for fabrication of upconverting thin films was studied. The upconversion luminescence was clearly detected from the ALD-prepared, crystalline (Yb,Er)oxide thin films and the ALD/MLD-prepared, amorphous hybrid (Y,Yb, Er) -pyrazine thin films. These techniques were demonstrated to be well suited for upconverting film fabrication. The techniques allow the preparation of highly uniform and conformal thin films on different substrates in varying geometries which is an attractive feature when considering different applications including the solar cells. In the future, the NIR harvesting properties of these thin films may be improved by systematically mapping various organic constituents.

Last, the direct doping method for preparation of upconverting phosphate glasses was investigated (**IV,V**). First important conclusion was that the thermal stability of the upconverting particles is not the only parameter to bear in mind when preparing the particles doped glasses. Another parameter to be considered was the corrosion effect of glass melt on the upconverting particles. The doping temperature and the quenching time after the doping were further optimized. Strong upconversion luminescence was observed with the upconverting particles doped phosphate glass containing NaF and prepared with 550 °C doping temperature and 3 min dwell time. In the future, this effect could be avoided by coating the upconverting particles with a protective layer.

Altogether, this thesis work has provided more information on alternative fabrication methods for upconverting layers that could be used in solar cells. The unique possibilities that the atomic layer deposition techniques can offer was demonstrated to apply also for upconversion films. The use of combined ALD/MLD technique was pointed out to enable the combination of organic NIR harvester and upconverting lanthanide ions which could be one solution to the efficiency issue of the upconversion. The direct particles doping method for luminescent glass preparation was shown to be a promising method in introducing efficient upconverting crystalline materials into glasses. In addition, transition metal ion doping of crystalline fluoride material was proved to improve the upconversion luminescence properties.

Although the new insight gained in this thesis work appeared to be promising, it introduces solutions only to a small part of the problems with the upconversion luminescent materials in solar cells. The field has still a variety of issues to overcome before the upconversion materials can be considered as commercially attractive, and the future steps in the upconversion research will reveal the development of this interesting research field.

REFERENCES

(1) Auzel, F. Upconversion and Anti-Stokes Processes with f and d Ions in Solids. *Chem. Rev.* **2004**, *104*, 139–173.

(2) Zhou, J.; Liu, Q.; Feng, W.; Sun, Y.; Li, F. Upconversion Luminescent Materials: Advances and Applications. *Chem. Rev.* **2015**, *115* (1), 395–465.

(3) Baluschev, S.; Miteva, T.; Yakutkin, V.; Nelles, G.; Yasuda, A.; Wegner, G. Up-Conversion Fluorescence: Noncoherent Excitation by Sunlight. *Phys. Rev. Lett.* **2006**, *97* (14), 7–9.

(4) Goldschmidt, J. C.; Fischer, S. Upconversion for Photovoltaics - a Review of Materials, Devices and Concepts for Performance Enhancement. *Adv. Opt. Mater.* **2015**, *3* (4), 510–535.

(5) Kano, T. *Principal Phosphor Materials and Their Optical Properties, Phosphor Handbook*, second edi.; Yen, W., Shionoya, S., Yamamoto, H., Eds.; CRC Press, 2006.

(6) Prasad, P. N.; Chen, G.; Yang, C. Nanophotonics and Nanochemistry: Controlling the Excitation Dynamics for Frequency Up- and Down-Conversion in Lanthanide-Doped Nanoparticles. *Acc. Chem. Res.* **2013**, *46* (7), 1474–1486.

(7) Werts, M. H. *Making Sense of Lanthanide Luminescence*; Science Progress, 2005; Vol. 88.

(8) Chen, G.; Qiu, H.; Prasad, P. N.; Chen, X. Upconversion Nanoparticles: Design, Nanochemistry, and Applications in Theranostics. *Chem. Rev.* **2014**, *114* (10), 5161–5214.

(9) Mathews, M. D.; Ambekar, B. R.; Tyagi, A. K.; Köhler, J. High Temperature X-Ray Diffraction Studies on Sodium Yttrium Fluoride. *J. Alloys Compd.* **2004**, *377* (1–2), 162–166.

(10) You, W.; Tu, D.; Zheng, W.; Huang, P.; Chen, X. Lanthanide-Doped Disordered Crystals : Site Symmetry and Optical Properties. *J. Lumin.* **2018**, *201* (May), 255–264.

(11) Harju, E.; Hyppänen, I.; Hölsä, J.; Kankare, J.; Lahtinen, M.; Lastusaari, M.; Pihlgren, L.; Soukka, T. Polymorphism of NaYF4:Yb3+, Er3+ Up-Conversion Luminescence Materials. *Z. Krist. Proc.* **2011**, *1*, 381–387.

(12) Krämer, K. W.; Biner, D.; Frei, G.; Güdel, H. U.; Hehlen, M. P.; Lüthi, S. R. Hexagonal Sodium Yttrium Fluoride Based Green and Blue Emitting Upconversion Phosphors. *Chem. Mater.* **2004**, *16* (7), 1244–1251.

(13) Zhao, J.; Sun, Y.; Kong, X.; Tian, L.; Wang, Y.; Tu, L.; Zhao, J.; Zhang, H. Controlled Synthesis, Formation Mechanism, and Great Enhancement of Red Upconversion Luminescence of $NaYF_4$:Yb^{3+},Er^{3+} Nanocrystals/ Submicroplates at Low Doping Level. *J. Phys. Chem. B* **2008**, *112* (49), 15666–15672.

(14) Suyver, J. F.; Grimm, J.; Krämer, K. W.; Güdel, H. U. Highly Efficient Near-Infrared to Visible up-Conversion Process in $NaYF_4$:Er^{3+};Yb^{3+}. *J. Lumin.* **2005**, *114*, 53–59.

(15) Suyver, J. F.; Grimm, J.; Van Veen, M. K.; Biner, D.; Krämer, K. W.; Güdel, H. U. Upconversion Spectroscopy and Properties of $NaYF_4$ Doped with Er^{3+}, Tm^{3+} and/or Yb^{3+}. *J. Lumin.* **2006**, *117* (1), 1–12.

(16) Wang, F.; Liu, X. Recent Advances in the Chemistry of Lanthanide-Doped Upconversion Nanocrystals. *Chem. Soc. Rev.* **2009**, *38* (4), 976–989.

(17) Davolos, M. R.; Feliciano, Ã. S.; Pires, A. M.; Marques, R. F. C.; Jr, M. J. Solvothermal Method to Obtain Europium-Doped Yttrium Oxide. **2003**, *171*, 268–272.

(18) Rai, V.; Pandey, S.; Pandey, A. Synthesis and Characterization of Sm-Yb Codoped YO Phosphor. *J. Disp. Technol.* **2013**, *9* (12), 989–994.

(19) Ekambaram, S. Effect of Host-Structure on the Charge of Europium Ion. *J. Alloys Compd.* **2005**, *390* (1–2), 4–6.

(20) Diaz-Torres, L. A.; Meza, O.; Solis, D.; Salas, P.; De La Rosa, E. Visible Upconversion Emission and Non-Radiative Direct Yb^{3+} to Er^{3+} energy Transfer Processes in Nanocrystalline ZrO_2:Yb^{3+},Er^{3+}. *Opt. Lasers Eng.* **2011**, *49* (6), 703–708.

(21) Chung, J. H.; Ryu, J. H.; Eun, J. W.; Lee, J. H.; Lee, S. Y.; Heo, T. H.; Choi, B. G.; Shim, K. B. Green Upconversion Luminescence from Poly-Crystalline Yb^{3+}, Er^{3+} Co-Doped $CaMoO_4$. *J. Alloys Compd.* **2012**, *522*, 30–34.

(22) Martín-Rodríguez, R.; Rabouw, F. T.; Trevisani, M.; Bettinelli, M.; Meijerink, A. Upconversion Dynamics in Er^{3+}-Doped Gd_2O_2S: Influence of Excitation Power, Er^{3+} Concentration, and Defects. *Adv. Opt. Mater.* **2015**, *3* (4), 558–567.

(23) Kumar, G. A.; Pokhrel, M.; Sardar, D. K. Intense Visible and near Infrared Upconversion in M_2O_2S:Er (M = Y, Gd, La) Phosphor under 1550 nm Excitation. *Mater. Lett.* **2012**, *68*, 395–398.

(24) Carnall, W. T.; Goodman, G. L.; Rajnak, K.; Rana, R. S. A Systematic Analysis of the Spectra of the Lanthanides Doped into Single Crystal LaF_3. *J. Chem. Phys.* **1989**, *90* (90), 3443–3457.

(25) Blasse, G.; Grabmaier, B. . *How Does a Luminescent Material Absorb Its Excitation Energy?. In: Luminescent Materials.*; Springer, Berlin, Heidelberg, 1994.

(26) Liu, G. Advances in the Theoretical Understanding of Photon Upconversion in Rare-Earth Activated Nanophosphors. *Chem. Soc. Rev.* **2015**, *44*, 1635–1652.

(27) Dong, H.; Sun, L.; Yan, C. Energy Transfer in Lanthanide Upconversion Studies for Extended Optical Applications. *Chem. Soc. Rev.* **2015**, *44* (2001), 1608–1634.

(28) Haase, M.; Schäfer, H. Upconverting Nanoparticles. *Angew. Chemie - Int. Ed.* **2011**, *50* (26), 5808–5829.

(29) Wermuth, M.; Riedener, T.; Güdel, H. U. Spectroscopy and Upconversion Mechanisms of $CsCdBr_3:Dy^{3+}$. *Phys. Rev. B - Condens. Matter Mater. Phys.* **1998**, *57* (8), 4369–4376.

(30) Riseberg, L. A.; Moos, H. W. Multiphonon Orbit-Lattice Relaxation of Excited States of Rare-Earth Ions in Crystals. *Phys. Rev.* **1968**, *174* (2), 429–438.

(31) Lim, S. F.; Ryu, W. S.; Austin, R. H. Particle Size Dependence of the Dynamic Photophysical Properties of $NaYF_4$:Yb,Er Nanocrystals. *Opt. Express* **2010**, *18* (3), 2309.

(32) Shan, B. J.; Uddi, M.; Yao, N.; Ju, Y. Anomalous Raman Scattering of Colloidal Yb^{3+},Er^{3+} Codoped $NaYF_4$ Nanophosphors and Dynamic Probing of the Upconversion Luminescence. **2010**, 3530–3537.

(33) Mai, H. X.; Zhang, Y. W.; Sun, L. D.; Yan, C. H. Highly Efficient Multicolor Up-Conversion Emissions and Their Mechanisms of Monodisperse $NaYF_4$:Yb,Er Core and Core/Shell-Structured Nanocrystals. *J. Phys. Chem. C* **2007**, *111* (37), 13721–13729.

(34) Pollnau, M.; Gamelin, D.; Lüthi, S.; Güdel, H.; Hehlen, M. Power Dependence of Upconversion Luminescence in Lanthanide and Transition-Metal-Ion Systems. *Phys. Rev. B - Condens. Matter Mater. Phys.* **2000**, *61* (5), 3337–3346.

(35) Suyver, J. F.; Aebischer, A.; García-Revilla, S.; Gerner, P.; Güdel, H. U. Anomalous Power Dependence of Sensitized Upconversion Luminescence. *Phys. Rev. B - Condens. Matter Mater. Phys.* **2005**, *71* (12), 1–9.

(36) Boyer, J. C.; Van Veggel, F. C. J. M. Absolute Quantum Yield Measurements of Colloidal $NaYF_4:Er^{3+},Yb^{3+}$ upconverting Nanoparticles. *Nanoscale* **2010**, *2* (8), 1417–1419.

(37) Fischer, S.; Martín-Rodríguez, R.; Fröhlich, B.; Krämer, K. W.; Meijerink, A.; Goldschmidt, J. C. Upconversion Quantum Yield of Er^{3+}-Doped β-$NaYF_4$ and Gd_2O_2S: The Effects of Host Lattice, Er^{3+} doping, and Excitation Spectrum Bandwidth. *J. Lumin.* **2014**, *153*, 281–287.

(38) Fischer, S.; Fröhlich, B.; Steinkemper, H.; Krämer, K. W.; Goldschmidt, J. C. Absolute Upconversion Quantum Yield of β-$NaYF_4$ doped with Er^{3+} and External Quantum Efficiency of Upconverter Solar Cell Devices under Broad-Band Excitation Considering Spectral Mismatch Corrections. *Sol. Energy Mater. Sol. Cells* **2014**, *122*, 197–207.

(39) MacDougall, S. K. W.; Ivaturi, A.; Marques-Hueso, J.; Krämer, K. W.; Richards, B. S. Ultra-High Photoluminescent Quantum Yield of β-$NaYF_4$: 10% Er^{3+} via Broadband Excitation of Upconversion for Photovoltaic Devices. *Opt. Express* **2012**, *20* (S6), A879.

(40) Ye, S.; Song, E. H.; Zhang, Q. Y. Transition Metal-Involved Photon Upconversion. *Adv. Sci.* **2016**, *3* (12).

(41) Wang, C.; Cheng, X. Influence of Cr^{3+} Ions Doping on Growth and Upconversion Luminescence Properties of β-$NaYF_4$:Yb^{3+}/Er^{3+} Microcrystals. *J. Alloys Compd.* **2015**, *649*, 196–203.

(42) Jain, P. K.; Huang, X.; El-Sayed, I.; El-Sayed, M. Noble Metals on the Nanoscale: Optical and Photothermal Properties and Some Applications in Imaging, Sensing, Biology, and Medicine. *Acc. Chem. Res.* **2008**, *41* (12), 1578–1586.

(43) Hutter, E.; Fendler, J. H. Exploitation of Localized Surface Plasmon Resonance. *Adv. Mater.* **2004**, *16* (19), 1685–1706.

(44) Wang, F.; Han, Y.; Lim, C. S.; Lu, Y.; Wang, J.; Xu, J.; Chen, H.; Zhang, C.; Hong, M.; Liu, X. Simultaneous Phase and Size Control of Upconversion Nanocrystals through Lanthanide Doping. *Nature* **2010**, *463* (7284), 1061–1065.

(45) Shannon, R. D. Revised Effective Ionic Radii and Systematic Studies of Interatomic Distances in Halides and Chalcogenides. *Acta Crystallogr. Sect. A* **1976**, *32* (5), 751–767.

(46) Chen, G.; Liu, H.; Liang, H.; Somesfalean, G.; Zhang, Z. Upconversion Emission Enhancement in Yb^{3+}/Er^{3+} -Codoped Y_2O_3 Nanocrystals by Tridoping with Li^+ Ions. *J. Phys. Chem. C* **2008**, *112* (31), 12030–12036.

(47) Liang, H.; Zheng, Y.; Chen, G.; Wu, L.; Zhang, Z.; Cao, W. Enhancement of Upconversion Luminescence of Y_2O_3:Er^{3+} Nanocrystals by Codoping Li^+-Zn^{2+}. *J. Alloys Compd.* **2011**, *509* (2), 409–413.

(48) Fan, T.; Lü, J. Enhanced 1.5 mm and Green Upconversion Emissions in Y_2O_3:Er^{3+} nanoparticles Codoped with Li^+ ions. *Opt. Commun.* **2013**, *300*, 5–7.

(49) Bai, Y.; Wang, Y.; Peng, G.; Yang, K.; Zhang, X.; Song, Y. Enhance Upconversion Photoluminescence Intensity by Doping Li^+ in Ho^{3+} and Yb^{3+} codoped Y_2O_3 nanocrystals. *J. Alloys Compd.* **2009**, *478* (1–2), 676–678.

(50) Chen, X.; Liu, Z.; Sun, Q.; Ye, M.; Wang, F. Upconversion Emission Enhancement in Er^{3+}/Yb^{3+}- Codoped $BaTiO_3$ nanocrystals by Tridoping with Li^+ ions. *Opt. Commun.* **2011**, *284* (7), 2046–2049.

(51) Chung, J. H.; Ryu, J. H.; Eun, J. W.; Lee, J. H.; Lee, S. Y.; Heo, T. H.; Shim, K. B. High Enhancement of Green Upconversion Luminescence of Li^+/Er^{3+}/Yb^{3+} tri-Doped $CaMoO_4$. *Mater. Chem. Phys.* **2012**, *134* (2–3), 695–699.

(52) Dou, Q.; Zhang, Y. Tuning of the Structure and Emission Spectra of Upconversion Nanocrystals by Alkali Ion Doping. *Langmuir* **2011**, *27* (21), 13236–13241.

(53) Chen, X.; Peng, D.; Wang, F. Tuning $NaYF_4$ Nanoparticles through Alkaline Earth Doping. *Nanomaterials* **2013**, *3*, 583–591.

(54) Huang, Q.; Yu, J.; Ma, E.; Lin, K. Synthesis and Characterization of Highly Efficient Near-Infrared Upconversion Sc^{3+}/Er^{3+}/Yb^{3+} Tridoped $NaYF_4$. **2010**, 4719–4724.

(55) Yu, H.; Huang, Q.; Ma, E.; Zhang, X.; Yu, J. Tuning Crystal Field Symmetry of Hexagonal $NaY_{0.92}Yb_{0.05}Er_{0.03}F_4$ by Ti^{4+} codoping for High-Performance Upconversion. *J. Alloys Compd.* **2014**, *613*, 253–259.

(56) Li, A. H.; Sun, Z. J.; Lu, Q. Laser Heating Effect on the Power Dependence of Upconversion Luminescence in Er^{3+} -Doped Nanopowders. *J Nanopart Res* **2013**, *15*, 1377.

(57) Liang, L.; Liu, Y.; Bu, C.; Guo, K.; Sun, W.; Huang, N.; Peng, T.; Sebo, B.; Pan, M.; Liu, W.; et al. Highly Uniform, Bifunctional Core/Double-Shell-Structured β-$NaYF_4$:Er^{3+},Yb^{3+} @ SiO_2 @TiO_2 Hexagonal Sub-Microprisms for High-Performance Dye Sensitized Solar Cells. *Adv. Mater.* **2013**, *25* (15), 2174–2180.

(58) Li, C.; Quan, Z.; Yang, P.; Huang, S.; Lian, H.; Lin, J. Shape-Controllable Synthesis and Upconversion Properties of Lutetium Fluoride (Doped with Yb^{3+}/Er^{3+}) Microcrystals by Hydrothermal Process. *J. Phys. Chem. C* **2008**, *112*, 13395–13404.

(59) Ye, S.; Song, E. H.; Ma, E.; Zhang, S. J.; Wang, J.; Chen, X. Y.; Zhang, Q. Y.; Qiu, J. R. Broadband Cr^{3+}-Sensitized Upconversion Luminescence in $La_3Ga_5GeO_{14}$:Cr^{3+},Yb^{3+},Er^{3+}. *Opt. Mater. Express* **2014**, *4* (4), 638.

(60) Aboshyan-Sorgho, L.; Cantuel, M.; Petoud, S.; Hauser, A.; Piguet, C. Optical Sensitization and Upconversion in Discrete Polynuclear Chromium-Lanthanide Complexes. *Coord. Chem. Rev.* **2012**, *256* (15–16), 1644–1663.

(61) Suffren, Y.; Zare, D.; Eliseeva, S. V.; Guénée, L.; Nozary, H.; Lathion, T.; Aboshyan-Sorgho, L.; Petoud, S.; Hauser, A.; Piguet, C. Near-Infrared to Visible Light-Upconversion in Molecules: From Dream to Reality. *J. Phys. Chem. C* **2013**, *117* (51), 26957–26963.

(62) Tian, G.; Gu, Z.; Zhou, L.; Yin, W.; Liu, X.; Yan, L.; Jin, S.; Ren, W.; Xing, G.; Li, S.; et al. Mn^{2+} Dopant-Controlled Synthesis of $NaYF_4$:Yb/Er Upconversion Nanoparticles for in Vivo Imaging and Drug Delivery. *Adv. Mater.* **2012**, *24* (9), 1226–1231.

(63) Zeng, S.; Yi, Z.; Lu, W.; Qian, C.; Wang, H.; Rao, L.; Zeng, T.; Liu, H.; Liu, H.; Fei, B.; et al. Simultaneous Realization of Phase/Size Manipulation, Upconversion Luminescence Enhancement, and Blood Vessel Imaging in Multifunctional Nanoprobes through Transition Metal Mn^{2+} Doping. *Adv. Funct. Mater.* **2014**, *24* (26), 4051–4059.

(64) Wang, J.; Wang, F.; Wang, C.; Liu, Z.; Liu, X. Single-Band Upconversion Emission in Lanthanide-Doped $KMnF_3$ Nanocrystals. **2011**, *50*, 10369–10372.

(65) Xie, M.; Peng, X.; Fu, X.; Zhang, J. Synthesis of Yb^{3+}/Er^{3+} Co-Doped MnF_2 Nanocrystals with Bright Red up-Converted Fluorescence. *Scr. Mater.* **2009**, *60* (3), 66–69.

(66) Yi, M.; Liu, Y.; Gao, H.; Huang, Z.; Liang, J.; Mao, Y. Upconversion Effective Enhancement of $NaYF_4$:Yb^{3+}/Er^{3+} Nanoparticles by Ni^{2+} Doping. *J. Mater. Sci.* **2018**, *53* (2), 1395–1403.

(67) Yu, H.; Cao, W.; Huang, Q.; Ma, E.; Zhang, X.; Yu, J. Upcoversion Performance Improvement of $NaYF_4$:Yb,Er by Sn Codoping: Enhanced Emission Intensity and Reduced Decay Time. *J. Solid State Chem.* **2013**, *207*, 170–177.

(68) Yang, M.; Sui, Y.; Wang, S.; Wang, X.; Wang, Y.; Lü, S.; Zhang, Z.; Liu, Z.; Lü, T.; Liu, W. Effects of Bi^{3+} doping on the Optical Properties of Er^{3+}:Y_2O_3. *J. Alloys Compd.* **2011**, *509* (3), 827–830.

(69) Jiang, L.; Xiao, S.; Yang, X.; Ding, J.; Dong, K. Enhancement of Up-Conversion Luminescence in Zn_2SiO_4:Yb^{3+},Er^{3+} by Co-Doping with Li^+ or Bi^{3+}. *Appl. Phys. B* **2012**, *107* (2), 477–481.

(70) Han, S.; Deng, R.; Xie, X.; Liu, X. Enhancing Luminescence in Lanthanide-Doped Upconversion Nanoparticles. *Angew. Chemie - Int. Ed.* **2014**, *53* (44), 11702–11715.

(71) Park, W.; Lu, D.; Ahn, S. Plasmon Enhancement of Luminescence Upconversion. *Chem. Soc. Rev.* **2015**, *44* (10), 2940–2962.

(72) Zhang, H.; Xu, D.; Huang, Y.; Duan, X. Highly Spectral Dependent Enhancement of Upconversion Emission with Sputtered Gold Island Films. **2012**, *47* (3), 979–981.

(73) Paudel, H. P.; Zhong, L.; Bayat, K.; Baroughi, M. F.; Smith, S.; Lin, C.; Jiang, C.; Berry, M. T.; May, P. S. Enhancement of Near-Infrared-to-Visible Upconversion Luminescence Using Engineered Plasmonic Gold Surfaces. *J. Phys. Chem. C* **2011**, *115* (39), 19028–19036.

(74) Saboktakin, M.; Ye, X.; Oh, S. J.; Hong, S. H.; Fafarman, A. T.; Chettiar, U. K.; Engheta, N.; Murray, C. B.; Kagan, C. R. Metal-Enhanced Upconversion Luminescence Tunable through Metal Nanoparticle-Nanophosphor Separation. *ACS Nano* **2012**, *6* (10), 8758–8766.

(75) Lu, D.; Cho, S. K.; Ahn, S.; Brun, L.; Summers, C. J.; Park, W. Plasmon Enhancement Mechanism for the Upconversion Processes in $NaYF_4$:Yb^{3+},Er^{3+} nanoparticles: Maxwell versus Förster. *ACS Nano* **2014**, *8* (8), 7780–7792.

(76) Schietinger, S.; Aichele, T.; Wang, H. Q.; Nann, T.; Benson, O. Plasmon-Enhanced Upconversion in Single $NaYF_4$:Yb^{3+}/Er^{3+} codoped Nanocrystals. *Nano Lett.* **2010**, *10* (1), 134–138.

(77) Zhang, W.; Ding, F.; Chou, S. Y. Large Enhancement of Upconversion Luminescence of $NaYF_4$:Yb^{3+}/Er^{3+} Nanocrystal by 3D Plasmonic Nano-Antennas. *Adv. Mater.* **2012**, *24* (35).

(78) Wazen, R. M.; Kuroda, S.; Nishio, C.; Sellin, K.; Brunski, J. B.; Nanci, A. Upconversion in $NaYF_4$:Yb,Er Nanoparticles Amplified by Metal Nanostructures. *Nanotechnology* **2011**, *22*, 325604.

(79) Zhang, H.; Li, Y.; Ivanov, I. A.; Qu, Y.; Huang, Y.; Duan, X. Plasmonic Modulation of the Upconversion Fluorescence in $NaYF_4$:Yb/Tm Hexaplate Nanocrystals Using Gold Nanoparticles or Nanoshells. *Angew. Chemie - Int. Ed.* **2010**, *49* (16), 2865–2868.

(80) Ge, W.; Zhang, X. R.; Liu, M.; Lei, Z. W.; Knize, R. J.; Lu, Y. Distance Dependence of Gold-Enhanced Upconversion Luminescence in Au/SiO_2/Y_2O_3:Yb^{3+},Er^{3+} nanoparticles. *Theranostics* **2013**, *3* (4), 282–288.

(81) Wurth, C.; Kaiser, M.; Wilhelm, S.; Graudel, B.; Hirsch, T.; Resch-Genger, U. Excitation Power Dependent Population Pathways and Absolute Quantum Yields of Upconversion Nanoparticles in Different Solvents. *Nanoscale* **2017**, *9* (12), 4283–4294.

(82) Wang, F.; Wang, J.; Liu, X. Direct Evidence of a Surface Quenching Effect on Size-Dependent Luminescence of Upconversion Nanoparticles. *Angew. Chemie - Int. Ed.* **2010**, *49* (41), 7456–7460.

(83) Sudarsan, V.; Veggel, F. C. J. M. Van; Herring, R. A.; Raudsepp, M. Surface Eu^{3+} Ions Are Different than '" Bulk "' Eu^{3+} Ions in Crystalline Doped. *J. Mater. Chem.* **2005**, *15*, 1332–1342.

(84) Chen, G.; Ågren, H.; Ohulchanskyy, T. Y.; Prasad, P. N. Light Upconverting Core-Shell Nanostructures: Nanophotonic Control for Emerging Applications. *Chem. Soc. Rev.* **2015**, *44* (6), 1680–1713.

(85) Yi, G. S.; Chow, G. M. Water-Soluble $NaYF_4$:Yb,Er(Tm)/$NaYF_4$/Polymer Core/Shell/Shell Nanoparticles with Significant Enhancement of Upconversion Fluorescence. *Chem. Mater.* **2007**, *19* (3), 341–343.

(86) Wang, Y. F.; Sun, L. D.; Xiao, J. W.; Feng, W.; Zhou, J. C.; Shen, J.; Yan, C. H. Rare-Earth Nanoparticles with Enhanced Upconversion Emission and Suppressed Rare-Earth-Ion Leakage. *Chem. - A Eur. J.* **2012**, *18* (18), 5558–5564.

(87) Chen, G.; Shen, J.; Ohulchanskyy, T. Y.; Patel, N. J.; Kutikov, A.; Li, Z.; Song, J.; Pandey, R. K.; Agren, H.; Prasad, P. N.; et al. (α-$NaYbF_4$:Tm^{3+})/CaF_2 core/Shell Nanoparticles with Efficient near-Infrared to near-Infrared Upconversion for High-Contrast Deep Tissue Bioimaging. *ACS Nano* **2012**, *6* (9), 8280–8287.

(88) Vetrone, F.; Naccache, R.; Mahalingam, V.; Morgan, C. G.; Capobianco, J. A. The Active-Core/Active-Shell Approach: A Strategy to Enhance the Upconversion Luminescence in Lanthanide-Doped Nanoparticles. *Adv. Funct. Mater.* **2009**, *19* (18), 2924–2929.

(89) Chen, G.; Damasco, J.; Qiu, H.; Shao, W.; Ohulchanskyy, T. Y.; Valiev, R. R.; Wu, X.; Han, G.; Wang, Y.; Yang, C.; et al. Energy-Cascaded Upconversion in an Organic Dye-Sensitized Core/Shell Fluoride Nanocrystal. *Nano Lett.* **2015**, *15* (11), 7400–7407.

(90) Zou, W.; Visser, C.; Maduro, J. A.; Pshenichnikov, M. S.; Hummelen, J. C. Broadband Dye-Sensitized Upconversion of near-Infrared Light. *Nat. Photonics* **2012**, *6* (8), 560–564.

(91) Stouwdam, J. W.; Veggel, F. C. J. M. Van. Near-Infrared Emission of Redispersible Er^{3+}, Nd^{3+}, and Ho^{3+} Doped LaF_3 Nanoparticles. *Nano Lett.* **2002**, *2*, 733–737.

(92) Yi, G.; Lu, H.; Zhao, S.; Ge, Y.; Yang, W.; Chen, D.; Guo, L. H. Synthesis, Characterization, and Biological Application of Size-Controlled Nanocrystalline $NaYF_4$:Yb,Er Infrared-to-Visible up-Conversion Phosphors. *Nano Letters*. 2004, pp 2191–2196.

(93) Vermelho, M. V.D.; Dos Santos, P. V.; De Araújo, M. T.; Gouveia-Neto, A. S.; Cassanjes, F. C.; Ribeiro, S. J. L.; Messaddeq, Y. Thermally Enhanced Cooperative Energy-Transfer Frequency Upconversion in Terbium and Ytterbium Doped Tellurite Glass. *J. Lumin.* **2003**, *102–103* (SPEC), 762–767.

(94) Zhang, J.; Wang, S.; Rong, T.; Chen, L. Upconversion Luminescence in Er^{3+} Doped and Yb^{3+}/Er^{3+} Codoped Yttria Nanocrystalline Powders. *J. Am. Ceram. Soc.* **2004**, *6*, 1072–1075.

(95) Liu, Y.; Tu, D.; Zhu, H.; Chen, X. Lanthanide-Doped Luminescent Nanoprobes: Controlled Synthesis, Optical Spectroscopy, and Bioapplications. *Chem. Soc. Rev.* **2013**, *42*, 6924–6958.

(96) Dacosta, M. V; Doughan, S.; Han, Y.; Krull, U. J. Lanthanide Upconversion Nanoparticles and Applications in Bioassays and Bioimaging : A Review. *Anal. Chim. Acta* **2014**, *832*, 1–33.

(97) Li, B. Z.; Zhang, Y.; Jiang, S. Multicolor Core / Shell-Structured Upconversion Fluorescent Nanoparticles. *Adv. Mater.* **2008**, *20*, 4765–4769.

(98) Jiang, G.; Pichaandi, J.; Johnson, N. J. J.; Burke, R. D.; Veggel, F. C. J. M. Van. An Effective Polymer Cross-Linking Strategy To Obtain Stable Dispersions of Upconverting $NaYF_4$ Nanoparticles in Buffers and Biological Growth Media for Biolabeling Applications. *Langmuir* **2012**, *28*, 3239–3247.

(99) Ptacek, P.; Eickmeier, H.; Haase, M.; Scha, B. H. Synthesis of Hexagonal Yb^{3+}, Er^{3+} -Doped $NaYF_4$ Nanocrystals at Low Temperature. *Adv. Funct. Mater.* **2009**, *19*, 3091–3097.

(100) Ptacek, B. P.; Schäfer, H.; Kömpe, K.; Haase, M. Crystal Phase Control of Luminescing $NaGdF_4$:Eu^{3+} Nanocrystals. *Adv. Funct. Mater.* **2007**, *17*, 3843–3848.

(101) Qian, H.; Zhang, Y. Synthesis of Hexagonal-Phase Core - Shell $NaYF_4$ Nanocrystals with Tunable Upconversion Fluorescence. *Langmuir* **2008**, *24*, 12123–12125.

(102) Chen, G.; Ohulchanskyy, T. Y.; Liu, S.; Law, W.-C.; Wu, F.; Swihart, M. T.; Ågren, H.; Prasad, P. N. Core/Shell $NaGdF_4:Nd^{3+}/NaGdF_4$ Nanocrystals with Efficient Near-Infrared to Near-Infrared Downconversion Photoluminescence for Bioimaging Applications. *ACS Nano* **2012**, *6* (4), 2969–2977.

(103) Li, C.; Quan, Z.; Yang, J.; Yang, P.; Lin, J. Highly Uniform and Monodisperse -$NaYF_4:Ln^{3+}$ (Ln = Eu , Tb , Yb / Er , and Yb / Tm) Hexagonal Microprism Crystals : Hydrothermal Synthesis and Luminescent Properties. *Inorg. Chem.* **2007**, *46* (16), 6329–6337.

(104) Roh, J.; Yu, H.; Jang, J. Hexagonal β-$NaYF_4:Yb^{3+},Er^{3+}$ Nanoprism-Incorporated Upconverting Layer in Perovskite Solar Cells for Near-Infrared Sunlight Harvesting. *ACS Appl. Mater. Interfaces* **2016**, *8* (31), 19847–19852.

(105) Zhang, Y.; Sun, X.; Si, R.; You, L.; Yan, C. Single-Crystalline and Monodisperse LaF_3 Triangular Nanoplates from a Single-Source Precursor. *J. Am. Ceram. Soc.* **2005**, *127*, 3260–3261.

(106) Boyer, J.; Vetrone, F.; Cuccia, L. A.; Capobianco, J. A. Synthesis of Colloidal Upconverting $NaYF_4$ Nanocrystals Doped with Er^{3+}, Yb^{3+} and Tm^{3+} , Yb^{3+} via Thermal Decomposition of Lanthanide Trifluoroacetate Precursors. *J. Am. Chem. Soc.* **2006**, *128*, 7444–7445.

(107) Quan, Z.; Yang, D.; Yang, P.; Zhang, X.; Lian, H.; Liu, X.; Lin, J. Uniform Colloidal Alkaline Earth Metal Fluoride Nanocrystals : Nonhydrolytic Synthesis and Luminescence Properties. *Inorg. Chem.* **2008**, *47* (20), 9509–9517.

(108) Chen, J.; Zhao, J. X. Upconversion Nanomaterials: Synthesis, Mechanism, and Applications in Sensing. *Sensors* **2012**, *12*, 2414–2435.

(109) Xu, W.; Dai, S.; Toth, L. M.; Del Cul, G. D.; Peterson, J. R. Green Upconversion Emission from Er^{3+} ion Doped into Sol-Gel Silica Glasses under Red Light (647.1 nm) Excitation. *J. Phys. Chem.* **1995**, *99* (13), 4447–4450.

(110) Ting, C.; Chiu, Y.; Chang, C.; Chuang, L. Visible and Infrared Luminescence Properties of Er^{3+} -Doped $Y_2Ti_2O_7$ Nanocrystals. *J. Solid State Chem.* **2011**, *184* (3), 563–571.

(111) Du, P.; Lim, J. H.; Kim, S. H.; Yu, J. S. Facile Synthesis of $Gd_2O_3:Ho^{3+}/Yb^{3+}$ Nanoparticles: An Efficient Upconverting Material for Enhanced Photovoltaic Performance of Dye-Sensitized Solar Cells. *Opt. Mater. Express* **2016**, *6* (6), 1896.

(112) Silver, J.; Martinez-Rubio, M. I.; Ireland, T. G.; Fern, G. R.; Withnall, R. The Effect of Particle Morphology and Crystallite Size on the Upconversion Luminescence Properties of Erbium and Ytterbium Co-Doped Yttrium Oxide Phosphors. *J. Phys. Chem. B* **2001**, *105* (5), 948–953.

(113) Wang, H.; Nann, T. Monodisperse Upconverting Nanocrystals by Microwave-Assisted Synthesis. *ACS Nano* **2009**, *3* (11), 3804–3808.

(114) Wang, H.; Nann, T. Monodisperse Upconversion GdF_3:Yb,Er Rhombi by Microwave-Assisted Synthesis. *Nanoscale Res. Lett.* **2011**, *6*, 267.

(115) Chen, X.; Xu, W.; Song, H.; Chen, C.; Xia, H.; Zhu, Y.; Zhou, D.; Cui, S.; Dai, Q.; Zhang, J. Highly Efficient $LiYF_4$:Yb^{3+},Er^{3+} Upconversion Single Crystal under Solar Cell Spectrum Excitation and Photovoltaic Application. *ACS Appl. Mater. Interfaces* **2016**, *8* (14), 9071–9079.

(116) Krämer, K. W.; Güdel, H. U.; Schwartz, R. N. Infrared-to-Visible Upconversion in $LaCl_3$:1% Er^{3+}: Energy-Level and Line-Strength Calculations. *Phys. Rev. B* **1997**, *56* (21), 830–840.

(117) Hömmerich, U.; Nyein, E. E.; Trivedi, S. B. Crystal Growth, Upconversion, and Infrared Emission Properties of Er^{3+} -Doped KPb_2Br_5. *J. Lumine* **2005**, *113*, 100–108.

(118) Martín-Rodríguez, R.; Fischer, S.; Ivaturi, A.; Froehlich, B.; Krämer, K. W.; Goldschmidt, J. C.; Richards, B. S.; Meijerink, A. Highly Efficient IR to NIR Upconversion in Gd_2O_2S: Er^{3+} for Photovoltaic Applications. *Chem. Mater.* **2013**, *25* (9), 1912–1921.

(119) Lin, H.-Y.; Chen, H.-N.; Wu, T.-H.; Wu, C.-S.; Su, Y.-K.; Chu, S.-Y. Investigation of Green Up-Conversion Behavior in $Y_6W_2O_{15}$:Yb^{3+},Er^{3+} Phosphor and Its Verification in 973-nm Laser-Driven GaAs Solar Cell. *J. Am. Ceram. Soc.* **2012**, *95* (10), 3172–3179.

(120) Andriamiadamanana, C.; Ibanez, A.; Ferrier, A.; Joudrier, A. L.; Lombez, L.; Liotaud, M.; Guillemoles, J. F.; Pellé, F. Erbium-Doped Yttria Thin Films Prepared by Metal Organic Decomposition for up-Conversion. *Thin Solid Films* **2013**, *537*, 42–48.

(121) Mattsson, B.; Brodin, A.; Torell, A.; Torell, L. M. Spin Coated Polymer Films as Hosts for Er^{3+} with Blue and Green Upconversion Radiation. *Electrochim. Acta* **1995**, *40* (13), 2393–2395.

(122) Huang, W.; Lu, C.; Jiang, C.; Wang, W.; Song, J.; Ni, Y.; Xu, Z. Controlled Synthesis of $NaYF_4$ nanoparticles and Upconversion Properties of $NaYF_4$: Yb, Er (Tm)/FC Transparent Nanocomposite Thin Films. *J. Colloid Interface Sci.* **2012**, *376* (1), 34–39.

(123) Orignac, X.; Barbier, D.; Min, X.; Almeida, R. M.; Mccarthy, O.; Yeatman, E. Sol ± Gel Silica / Titania-on-Silicon Er / Yb-Doped Waveguides for Optical Amplification at 1 . 5 l M. *Opt. Mater. (Amst).* **1999**, *12*, 1–18.

(124) Yu, M.; Lin, J.; Wang, Z.; Fu, J.; Wang, S.; Zhang, H. J.; Han, Y. C. Fabrication, Patterning, and Optical Properties of Nanocrystalline YVO_4:A (A = Eu^{3+}, Dy^{3+}, Sm^{3+}, Er^{3+}) Phosphor Films via Sol-Gel Soft Lithography. *Chem. Mater.* **2002**, *14* (5), 2224–2231.

(125) Pandey, A.; Kumar, V.; Kroon, R. E.; Swart, H. C. Temperature Induced Upconversion Behaviour of Ho^{3+}-Yb^{3+} codoped Yttrium Oxide Films Prepared by Pulsed Laser Deposition. *J. Alloys Compd.* **2016**, *672*, 190–196.

(126) Su, Z. P.; Teo, K. L.; Yu, P. Y.; Uchida, K. Mechanisms of Photoluminescence Upconversion at the GaAs/(Ordered) $GaInP_2$ interface. *Solid State Commun.* **1996**, *99* (12), 933–936.

(127) Van, T. T.; Van de Sanden, M. C. M.; Ostroumov, R.; Bargar, J. R.; Hoex, B.; Sawkar-Mathur, M.; Hoang, J.; Chang, J. P.; Wang, K. L.; Kessels, W. M. M. Optical Properties of Y_2O_3 Thin Films Doped with Spatially Controlled Er^{3+} by Atomic Layer Deposition. *J. Appl. Phys.* **2007**, *101* (12), 123116.

(128) Hoang, J.; Schwartz, R. N.; Wang, K. L.; Chang, J. P. Er^{3+} Interlayer Energy Migration as the Limiting Photoluminescence Quenching Factor in Nanostructured Er^{3+}:Y_2O_3 Thin Films. *J. Appl. Phys.* **2012**, *112*, 023116.

(129) Hoang, J.; Schwartz, R. N.; Wang, K. L.; Chang, J. P. The Effects of Energy Transfer on the Er^{3+} 1.54 Mm Luminescence in Nanostructured Y_2O_3 Thin Films with Heterogeneously Distributed Yb^{3+} and Er^{3+} Codopants. *J. Appl. Phys.* **2012**, *112*, 063117.

(130) Choy, K. L. Chemical Vapour Deposition of Coatings. *Prog. Mater. Sci.* **2003**, *48* (2), 57–170.

(131) Kamat, P. V.; Tvrdy, K.; Baker, D. R.; Radich, J. G. Beyond Photovoltaics: Semiconductor Nanoarchitectures for Liquid-Junction Solar Cells. *Chem. Rev.* **2010**, *110* (11), 6664–6688.

(132) Meng, X.; Wang, X.; Geng, D.; Ozgit-Akgun, C.; Schneider, N.; Elam, J. W. Atomic Layer Deposition for Nanomaterial Synthesis and Functionalization in Energy Technology. *Mater. Horiz.* **2017**, *4* (2), 133–154.

(133) Hu, L.; Qi, W.; Li, Y. Coating Strategies for Atomic Layer Deposition. *Nanotechnol. Rev.* **2017**, *6* (6), 527–547.

(134) Johnson, R. W.; Hultqvist, A.; Bent, S. F. A Brief Review of Atomic Layer Deposition: From Fundamentals to Applications. *Mater. Today* **2014**, *17* (5), 236–246.

(135) Sundberg, P.; Karppinen, M. Organic and Inorganic-Organic Thin Film Structures by Molecular Layer Deposition: A Review. *Beilstein J. Nanotechnol.* **2014**, *5* (1), 1104–1136.

(136) King, D. M.; Liang, X.; Weimer, A. W. Functionalization of Fine Particles Using Atomic and Molecular Layer Deposition. *Powder Technol.* **2012**, *221*, 13–25.

(137) Gregorczyk, K.; Knez, M. Hybrid Nanomaterials through Molecular and Atomic Layer Deposition: Top down, Bottom up, and in-between Approaches to New Materials. *Prog. Mater. Sci.* **2016**, *75*, 1–37.

(138) Liang, X.; Weimer, A. W. An Overview of Highly Porous Oxide Films with Tunable Thickness Prepared by Molecular Layer Deposition. *Curr. Opin. Solid State Mater. Sci.* **2015**, *19* (2), 115–125.

(139) Feng, J.; Zhang, H. Hybrid Materials Based on Lanthanide Organic Complexes: A Review. *Chem. Soc. Rev.* **2013**, *42*, 387–410.

(140) Tsukube, H.; Shinoda, S. Lanthanide Complexes in Molecular Recognition and Chirality Sensing of Biological Substrates. *Chem. Rev.* **2002**, *102*, 2389–2403.

(141) Bünzli, J.-C. . G.; Piguet, C. Taking Advantage of Luminescent Lanthanide Ions. *Chem. Soc. Rev.* **2005**, *34*, 1048–1077.

(142) Buono-Core, G. E.; Li, H. QUENCHING OF EXCITElD STATES BY LANTHANIDE IONS AND CHELATES IN SOLUTION. *Coord. Chem. Rev.* **1990**, *99*, 55–87.

(143) Escribano, P.; Julián-López, B.; Planelles-Aragó, J.; Cordoncillo, E.; Viana, B.; Sanchez, C. Photonic and Nanobiophotonic Properties of Luminescent Lanthanide-Doped Hybrid Organic-Inorganic Materials. *J. Mater. Chem.* **2008**, *18* (1), 23–40.

(144) Latva, M.; Takalo, H.; Mukkala, V.; Matachescu, C.; Rodriguez-ubis, J. C.; Kankare, J. Correlation between the Lowest Triplet State Energy Level of the Ligand and Lanthanide(II1) Luminescence Quantum Yield. *J. Lumin.* **1997**, *75*, 149–169.

(145) Selvin, P. R. Lanthanide-Based Resonance Energy Transfer. *IEEE J. Sel. Top. Quantum Electron.* **1996**, *2* (4), 1077–1087.

(146) Aboshyan-sorgho, L.; Besnard, C.; Pattison, P.; Kittilstved, K. R.; Aebischer, A.; Bünzli, J. G.; Hauser, A.; Piguet, C. Near-Infrared - Visible Light Upconversion in a Molecular Trinuclear d – f – d Complex. *Angew. Chemie - Int. Ed.* **2011**, *50*, 4108–4112.

(147) Hyppänen, I.; Lahtinen, S.; Ääritalo, T.; Mäkelä, J.; Kankare, J.; Soukka, T. Photon Upconversion in a Molecular Lanthanide Complex in Anhydrous Solution at Room Temperature. *ACS Photonics* **2014**, *1*, 394–397.

(148) Suffren, Y.; Golesorkhi, B.; Zare, D.; Guénée, L.; Nozary, H.; Eliseeva, S. V.; Petoud, S.; Hauser, A.; Piguet, C. Taming Lanthanide- Centered Upconversion at the Molecular Level. *Inorg. Chem.* **2016**, *55*, 9964–9972.

(149) Nonat, A.; Chan, C. F.; Liu, T.; Platas-Iglesias, C.; Liu, Z.; Wong, W. T.; Wong, W. K.; Wong, K. L.; Charbonnière, L. J. Room Temperature Molecular up Conversion in Solution. *Nat. Commun.* **2016**, *7* (May).

(150) Souri, N.; Tian, P.; Platas-iglesias, C.; Wong, K.; Nonat, A.; Charbonniere, L. Upconverted Photosensitization of Tb Visible Emission by NIR Yb Excitation in Discrete Supramolecular Heteropolynuclear Complexes. *J. Am. Chem. Soc.* **2017**, *139*, 1456–1459.

(151) Nonat, A.; Bahamyirou, S.; Lecointre, A.; Przybilla, F.; Mély, Y.; Platas-iglesias, C.; Camerel, F.; Jeannin, O.; Charbonnière, L. J. Molecular Upconversion in Water in Heteropolynuclear Supramolecular Tb/Yb Assemblies. *J. Am. Chem. Soc.* **2019**, *141*, 1568–1576.

(152) Beeby, A.; Clarkson, I. M.; Dickins, R. S.; Faulkner, S.; Parker, D.; Royle, L.; Sousa, A. S. De; Williams, J. A. G.; Woods, M. Non-Radiative Deactivation of the Excited States of Europium , Terbium and Ytterbium Complexes by Proximate Energy-Matched OH , NH and CH Oscillators : An Improved Luminescence Method for Establishing Solution Hydration States. **1999**, *2* (5), 493–503.

(153) Li, Y.; Tang, J.; He, L.; Liu, Y.; Liu, Y.; Chen, C. Core – Shell Upconversion Nanoparticle @ Metal – Organic Framework Nanoprobes for Luminescent / Magnetic Dual-Mode Targeted Imaging. *Adv. Mater.* **2015**, *27*, 4075–4080.

(154) Deng, K.; Hou, Z.; Li, X.; Li, C.; Zhang, Y.; Deng, X.; Cheng, Z.; Lin, J. Aptamer-Mediated Up-Conversion Core/ MOF Shell Nanocomposites for Targeted Drug Delivery and Cell Imaging. *Sci. Rep.* **2015**, *5*, 7851.

(155) Yaghi, O. M.; O'Keeffe, M.; Ockwig, N. W.; Chae, H. K.; Eddaoudi, M.; Kim, J. Reticular Synthesis and the Design of New Materials. *Nature* **2003**, *423* (6941), 705–714.

(156) Nguyen, T. N.; Ebrahim, F. M.; Stylianou, K. C. Photoluminescent , Upconversion Luminescent and Nonlinear Optical Metal-Organic Frameworks : From Fundamental Photophysics to Potential Applications. *Coord. Chem. Rev.* **2018**, *377*, 259–306.

(157) Yang, J.; Yue, Q.; Li, G. D.; Cao, J. J.; Li, G. H.; Chen, J. S. Structures, Photoluminescence, up-Conversion, and Magnetism of 2D and 3D Rare-Earth Coordination Polymers with Multicarboxylate Linkages. *Inorg. Chem.* **2006**, *45* (7), 2857–2865.

(158) Mahata, P.; Ramya, K. V.; Natarajan, S. Pillaring of $CdCl_2$-like Layers in Lanthanide Metal-Organic Frameworks: Synthesis, Structure, and Photophysical Properties. *Chem. - A Eur. J.* **2008**, *14* (19), 5839–5850.

(159) Zhang, X.; Li, B.; Ma, H.; Zhang, L.; Zhao, H. Metal-Organic Frameworks Modulated by Doping Er^{3+} for Up-Conversion Luminescence. *ACS Appl. Mater. Interfaces* **2016**, *8* (27), 17389–17394.

(160) Zhao, J.; Zheng, X.; Schartner, E. P.; Ionescu, P.; Zhang, R.; Nguyen, T. L.; Jin, D.; Ebendorff-Heidepriem, H. Upconversion Nanocrystal-Doped Glass: A New Paradigm for Photonic Materials. *Adv. Opt. Mater.* **2016**, *4* (10), 1507–1517.

(161) Sooraj Hussain Nandyala; José Domingos da Silva Santos. *Physics and Chemistry of Rare-Earth Ions Doped Glasses*; Trans Tech Publications, 2008.

(162) Masayuki Yamane; Yoshiyuki Asahara. *Glasses for Photonics*; Cambridge University Press, 2000.

(163) Lopez-Iscoa, P.; Petit, L.; Massera, J.; Janner, D.; Boetti, N. G.; Pugliese, D.; Fiorilli, S.; Novara, C.; Giorgis, F.; Milanese, D. Effect of the Addition of Al_2O_3, TiO_2 and ZnO on the Thermal, Structural and Luminescence Properties of Er^{3+}-Doped Phosphate Glasses. *J. Non. Cryst. Solids* **2017**, *460*, 161–168.

(164) Zheng, X.; Wen, G.; Song, L.; Huang, X. X. Effects of P_2O_5 and Heat Treatment on Crystallization and Microstructure in Lithium Disilicate Glass Ceramics. *Acta Mater.* **2008**, *56* (3), 549–558.

(165) Ballato, J.; Ebendorff-Heidepriem, H.; Zhao, J.; Petit, L.; Troles, J. Glass and Process Development for the Next Generation of Optical Fibers: A Review. *Fibers* **2017**, *5* (1), 11.

(166) Jiang, S.; Zeng, P.; Liao, L.; Tian, S.; Guo, H.; Chen, Y.; Duan, C.; Yin, M. Optical Thermometry Based on Upconverted Luminescence in Transparent Glass Ceramics Containing $NaYF_4$:Yb^{3+}/Er^{3+} Nanocrystals. *J. Alloys Compd.* **2014**, *617*, 538–541.

(167) Montiel i Ponsoda, J. J.; Norin, L.; Ye, C.; Bosund, M.; Söderlund, M. J.; Tervonen, A.; Honkanen, S. Ytterbium-Doped Fibers Fabricated with Atomic Layer Deposition Method. *Opt. Express* **2012**, *20* (22), 25085.

(168) Su, F.; Deng, Z. Indirect Sensitization Blue-Upconversion Wavelength Vary in Tm^{3+}/Yb^{3+} Co-Doped TeO_2-TiO_2-K_2O Glasses. *Opt. Mater. (Amst).* **2007**, *29* (11), 1452–1455.

(169) Wang, N. Q.; Zhao, X.; Li, C. M.; Pun, E. Y. B.; Lin, H. Upconversion and Color Tunability in $Tm^{3+}/Ho^{3+}/Yb^{3+}$ Doped Low Phonon Energy Bismuth Tellurite Glasses. *J. Lumin.* **2010**, *130* (6), 1044–1047.

(170) Dousti, M. R.; Sahar, M. R.; Amjad, R. J.; Ghoshal, S. K.; Awang, A. Surface Enhanced Raman Scattering and Up-Conversion Emission by Silver Nanoparticles in Erbium-Zinc-Tellurite Glass. *J. Lumin.* **2013**, *143*, 368–373.

(171) Rivera, V. A. G.; Ledemi, Y.; Osorio, S. P. A.; Manzani, D.; Ferri, F. A.; Ribeiro, S. J. L.; Nunes, L. A. O.; Marega, E. Tunable Plasmon Resonance Modes on Gold Nanoparticles in Er^{3+}-Doped Germanium-Tellurite Glass. *J. Non. Cryst. Solids* **2013**, *378*, 126–134.

(172) Morena, R. Phosphate Glasses as Alternatives to Pb-Based Sealing Frits. *Journal of Non-Crystalline Solids*. 2000, pp 382–387.

(173) Ming, C.; Song, F.; Liu, H. Intense Blue Up-Conversion Emission in Tm^{3+}/ Yb^{3+} Co-Doped Phosphate Glass. *J. Non. Cryst. Solids* **2013**, *360*, 1–3.

(174) Fedorov, P. P.; Luginina, A. A.; Popov, A. I. Transparent Oxyfluoride Glass Ceramics. *J. Fluor. Chem.* **2015**, *172*, 22–50.

(175) Chen, Z.; Wu, G.; Jia, H.; Sharafudeen, K.; Dai, W.; Zhang, X.; Zeng, S.; Liu, J.; Wei, R.; Lv, S.; et al. Improved Up-Conversion Luminescence from Er^{3+}:LaF_3 nanocrystals Embedded in Oxyfluoride Glass Ceramics via Simultaneous Triwavelength Excitation. *J. Phys. Chem. C* **2015**, *119* (42), 24056–24061.

(176) Gorni, G.; Balda, R.; Fernández, J.; Pascual, L.; Durán, A.; Pascual, M. J. Effect of the Heat Treatment on the Spectroscopic Properties of Er^{3+}-Yb^{3+}-Doped Transparent Oxyfluoride Nano-Glass-Ceramics. *J. Lumin.* **2018**, *193* (May 2017), 51–60.

(177) Huang, J.; Huang, Y.; Wu, T.; Huang, Y.; Zhang, P. High Efficiency White Luminescence in $Tm^{3+}/Er^{3+}/Yb^{3+}$ tri-Doped Oxyfluoride Glass Ceramic Microsphere Pumped by 976 Nm Laser. *J. Lumin.* **2015**, *157*, 215–219.

(178) Chen, Q. J.; Zhang, W. J.; Huang, X. Y.; Dong, G. P.; Peng, M. Y.; Zhang, Q. Y. Efficient Down- and up-Conversion of Pr^{3+}-Yb^{3+} co-Doped Transparent Oxyfluoride Glass Ceramics. *J. Alloys Compd.* **2012**, *513*, 139–144.

(179) Liu, F.; Ma, E.; Chen, D.; Yu, Y.; Wang, Y. Tunable Red-Green Upconversion Luminescence in Novel Transparent Glass Ceramics Containing Er:$NaYF_4$ Nanocrystals. *J. Phys. Chem. B* **2006**, *110* (42), 20843–20846.

(180) Gao, Y.; Hu, Y.; Zhou, D.; Qiu, J. Effect of Heat Treatment Mechanism on Upconversion Luminescence in Er^{3+}/Yb^{3+} co-Doped $NaYF_4$ oxyfluoride Glass-Ceramics. *J. Alloys Compd.* **2017**, *699*, 303–307.

(181) Liu, F.; Ma, E.; Chen, D.; Wang, Y.; Yu, Y.; Huang, P. Infrared Luminescence of Transparent Glass Ceramic Containing Er^{3+}:$NaYF_4$ nanocrystals. *J. Alloys Compd.* **2009**, *467* (1–2), 317–321.

(182) Chen, D.; Wan, Z.; Zhou, Y.; Huang, P.; Ji, Z. Ce^{3+} Dopants-Induced Spectral Conversion from Green to Red in the Yb/Ho:$NaLuF_4$ Self-Crystallized Nano-Glass-Ceramics. *J. Alloys Compd.* **2016**, *654*, 151–156.

(183) Shang, Y.; Hao, S.; Yang, C.; Chen, G. Enhancing Solar Cell Efficiency Using Photon Upconversion Materials. *Nanomaterials* **2015**, *5* (4), 1782–1809.

(184) Richards, B. S. Enhancing the Performance of Silicon Solar Cells via the Application of Passive Luminescence Conversion Layers. *Sol. Energy Mater. Sol. Cells* **2006**, *90* (15), 2329–2337.

(185) Huang, X.; Han, S.; Huang, W.; Liu, X. Enhancing Solar Cell Efficiency: The Search for Luminescent Materials as Spectral Converters. *Chem. Soc. Rev.* **2013**, *42* (1), 173–201.

(186) Green, M.; Emery, K.; Hishikawa, Y.; Warta, W.; Dunlop, E. Solar Cell Efficiency Tables (Version 48). *Prog. Photovoltaics Res. Appl.* **2016**, *24*, 905–913.

(187) Shalav, A.; Richards, B. S.; Trupke, T.; Krämer, K. W.; Güdel, H. U. Application of $NaYF_4$:Er^{3+} up-Converting Phosphors for Enhanced near-Infrared Silicon Solar Cell Response. *Appl. Phys. Lett.* **2005**, 013505.

(188) Fischer, S.; Goldschmidt, J. C.; Löper, P.; Bauer, G. H.; Brüggemann, R.; Krämer, K.; Biner, D.; Hermeie, M.; Glunz, S. W. Enhancement of Silicon Solar Cell Efficiency by Upconversion: Optical and Electrical Characterization. *J. Appl. Phys.* **2010**, *108*, 6831–6847.

(189) Boccolini, A.; Faoro, R.; Favilla, E.; Veronesi, S.; Tonelli, M. BaY_2F_8 Doped with Er^{3+}: An Upconverter Material for Photovoltaic Application. *Journall Appl. Phys.* **2013**, *114*, 64904.

(190) Fischer, S.; Favilla, E.; Tonelli, M.; Goldschmidt, J. C. Record Efficient Upconverter Solar Cell Devices with Optimized Bifacial Silicon Solar Cells and Monocrystalline BaY_2F_8:30% Er^{3+} upconverter. *Sol. Energy Mater. Sol. Cells* **2015**, *136*, 127–134.

(191) Goldschmidt, J. C.; Fischer, S.; Löper, P.; Krämer, K. W.; Biner, D.; Hermle, M.; Glunz, S. W. Experimental Analysis of Upconversion with Both Coherent Monochromatic Irradiation and Broad Spectrum Illumination. *Sol. Energy Mater. Sol. Cells* **2011**, *95* (7), 1960–1963.

(192) Hernández-Rodríguez, M. A.; Imanieh, M. H.; Martín, L. L.; Martín, I. R. Experimental Enhancement of the Photocurrent in a Solar Cell Using Upconversion Process in Fluoroindate Glasses Exciting at 1480 nm. *Sol. Energy Mater. Sol. Cells* **2013**, *116*, 171–175.

(193) Lee, T. D.; Ebong, A. U. A Review of Thin Film Solar Cell Technologies and Challenges. *Renew. Sustain. Energy Rev.* **2017**, *70* (December 2016), 1286–1297.

(194) Zhang, X. D.; Jin, X.; Wang, D. F.; Xiong, S. Z.; Geng, X. H.; Zhao, Y. Synthesis of $NaYF_4$:Yb,Er Nanocrystals and Its Application in Silicon Thin Film Solar Cells. *Phys. Status Solidi Curr. Top. Solid State Phys.* **2010**, *7* (3–4), 1128–1131.

(195) De Wild, J.; Rath, J. K.; Meijerink, A.; Van Sark, W. G. J. H. M.; Schropp, R. E. I. Enhanced Near-Infrared Response of a-Si:H Solar Cells with β-$NaYF_4$:Yb^{3+}(18%), Er^{3+}(2%) Upconversion Phosphors. *Sol. Energy Mater. Sol. Cells* **2010**, *94* (12), 2395–2398.

(196) Zhao, S.; Xu, S.; Jia, G.; Deng, D.; Huang, L.; Wang, H. Er^{3+}/Yb^{3+} Codoped Oxyfluoride Borosilicate Glass Ceramic Containing $NaYF_4$ Nanocrystals for Amorphous Silicon Solar Cells. *Mater. Lett.* **2011**, *65* (15–16), 2407–2409.

(197) Xin, F.; Zhao, S.; Huang, L.; Deng, D.; Jia, G.; Wang, H.; Xu, S. Up-Conversion Luminescence of Er^{3+} -Doped Glass Ceramics Containing β -$NaGdF_4$ Nanocrystals for Silicon Solar Cells. *Mater. Lett.* **2012**, *78*, 75–77.

(198) Yang, F.; Liu, C.; Wei, D.; Chen, Y.; Lu, J.; Yang, S. E. Er^{3+}-Yb^{3+} co-Doped TeO_2-PbF_2 oxyhalide Tellurite Glasses for Amorphous Silicon Solar Cells. *Opt. Mater. (Amst).* **2014**, *36* (6), 1040–1043.

(199) O'Regan, B.; Gratzel, M. A Low-Cost, High-Efficiency Solar-Cell Based on Dye-Sensitized Colloidal TiO_2 Films. *Nature* **1991**, *353* (6346), 737–740.

(200) Shan, G. Bin; Demopoulos, G. P. Near-Infrared Sunlight Harvesting in Dye-Sensitized Solar Cells via the Insertion of an Upconverter-TiO_2 Nanocomposite Layer. *Adv. Mater.* **2010**, *22* (39), 4373–4377.

(201) Wang, J.; Lin, J.; Wu, J.; Huang, M.; Lan, Z.; Chen, Y.; Tang, S.; Fan, L.; Huang, Y. Application of Yb^{3+}, Er^{3+} -Doped Yttrium Oxyfluoride Nanocrystals in Dye-Sensitized Solar Cells. *Electrochim. Acta* **2012**, *70*, 131–135.

(202) Zhang, J.; Shen, H.; Guo, W.; Wang, S.; Zhu, C.; Xue, F.; Hou, J.; Su, H.; Yuan, Z. An Upconversion $NaYF_4$:Yb^{3+},Er^{3+}/TiO_2 Core e Shell Nanoparticle Photoelectrode for Improved Efficiencies of Dye-Sensitized Solar Cells. *J. Power Sources* **2013**, *226*, 47–53.

(203) Akihiro Kojima, Kenjiro Teshima, Yasuo Shirai, and T. M. Organometal Halide Perovskites as Visible- Light Sensitizers for Photovoltaic Cells. *J Am Chem Soc* **2009**, *131* (October), 6050–6051.

(204) Yang, W. S.; Park, B.; Jung, E. H.; Jeon, N. J. Iodide Management in Formamidinium-Lead-Halide – Based Perovskite Layers for Efficient Solar Cells. *Science* **2017**, *356* (6345), 1376–1379.

(205) Manser, J. S.; Saidaminov, M. I.; Christians, J. A.; Bakr, O. M.; Kamat, P. V. Making and Breaking of Lead Halide Perovskites. *Acc. Chem. Res.* **2016**, *49* (2), 330–338.

(206) Qiao, Y.; Li, S.; Liu, W.; Ran, M.; Lu, H.; Yang, Y. Recent Advances of Rare-Earth Ion Doped Luminescent Nanomaterials in Perovskite Solar Cells. *Nanomaterials* **2018**, *8* (1), 43.

(207) He, M.; Pang, X.; Liu, X.; Jiang, B.; He, Y.; Snaith, H.; Lin, Z. Monodisperse Dual-Functional Upconversion Nanoparticles Enabled Near-Infrared Organolead Halide Perovskite Solar Cells. *Angew. Chemie - Int. Ed.* **2016**, *55* (13), 4280–4284.

(208) Liang, J. W.; Gao, H. P.; Yi, M. J.; Shi, W. J.; Liu, Y. F.; Zhang, Z. L.; Mao, Y. L. Beta-$NaYF_4$:Yb^{3+},Tm^{3+} @ TiO_2 Core-Shell Nanoparticles Incorporated into the Mesoporous Layer for High Efficiency Perovskite Solar Cells. *Electrochim. Acta* **2018**, *261*, 14–22.

(209) Tang, J.; Zhang, Y.; Zheng, G.; Gou, J.; Wu, F. Improving the NIR Light-Harvesting of Perovskite Solar Cell with Upconversion Fluorotellurite Glass. *J. Am. Ceram. Soc.* **2018**, *101* (5), 1923–1928.

(210) Wang, H. Q.; Stubhan, T.; Osvet, A.; Litzov, I.; Brabec, C. J. Up-Conversion Semiconducting MoO_3:Yb/Er Nanocomposites as Buffer Layer in Organic Solar Cells. *Sol. Energy Mater. Sol. Cells* **2012**, *105*, 196–201.

(211) Ahvenniemi, E.; Karppinen, M. Atomic/Molecular Layer Deposition: A Direct Gas-Phase Route to Crystalline Metal- Organic Framework Thin Films. *Chem. Commun.* **2016**, *52*, 1139–1142.

(212) Eisentraut, K. J.; Sievers, R. E. *Volatile Rare-Earth Chelates of 2,2,6,6-Tetramethylheptane-3,5-Dione. Inorganic Syntheses*; John Wiley & Sons, 1968; Vol. 11.

(213) Monguzzi, A.; Tubino, R.; Meinardi, F. Multicomponent Polymeric Film for Red to Green Low Power Sensitized Up-Conversion. *J. Phys. Chem. A* **2009**, *113* (7), 1171–1174.

(214) Zheng, X. J.; Ablet, A.; Ng, C.; Wong, W. T. Intensive Upconversion Luminescence of Na-Codoped Rare-Earth Oxides with a Novel RE-Na Heterometallic Complex as Precursor. *Inorg. Chem.* **2014**, *53* (13), 6788–6793.

(215) Hölsä, J.; Laamanen, T.; Laihinen, T.; Lastusaari, M.; Pihlgren, L.; Rodrigues, L. C. V. White Up-Conversion Luminescence of $NaYF_4$:Yb^{3+},Pr^{3+},Er^{3+}. *Opt. Mater. (Amst).* **2014**, *36*, 162–1630.

(216) Hölsä, J.; Laihinen, T.; Laamanen, T.; Lastusaari, M.; Pihlgren, L.; Rodrigues, L. C. V.; Soukka, T. Enhancement of the Up-Conversion Luminescence from $NaYF_4$:Yb^{3+},Tb^{3+}. *Phys. B* **2014**, *439*, 20–23.

(217) Massera, J.; Gaussiran, M.; Głuchowski, P.; Lastusaari, M.; Petit, L.; Hölsä, J.; Hupa, L. Effect of the Glass Melting Condition on the Processing of Phosphate-Based Glass-Ceramics with Persistent Luminescence Properties. *Opt. Mater. (Amst).* **2016**, *52*, 56–61.

(218) Massera, J.; Głuchowski, P.; Lastusaari, M.; Rodrigues, L. C. V; Petit, L.; Hölsä, J.; Hupa, L.; Hupa, M. New Alternative Route for the Preparation of Phosphate Glasses with Persistent Luminescence Properties. *J. Eur. Ceram. Soc.* **2015**, *35* (4), 1255–1261.

UNIVERSITY
OF TURKU

Punamusta Oy, Finland 2019

ISBN 978-951-29-7877-9 (PRINT)
ISBN 978-951-29-7878-6 (PDF)
ISSN 0082-7002 (Painettu/Print)
ISSN 2343-3175 (Sähköinen/Online)